INFORMATION TO USERS

.

RICE UNIVERSITY

NMR Relaxation and Diffusion Characterization of Hydrocarbon Gases and Liquids
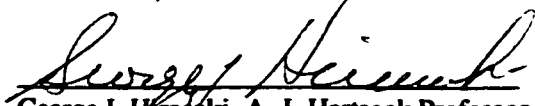
by

Ying Zhang

A THESIS SUBMITTED
IN PARTIAL FULFILLMENT OF THE
REQUIREMENTS FOR THE DEGREE

Doctor of Philosophy

APPROVED, THESIS COMMITTEE:

George J. Hirasaki, A. J. Hartsook Professor, Chair
Chemical Engineering

Walter G. Chapman, Professor
Chemical Engineering

Waylon V. House, Adjunct Professor
Chemical Engineering

Stanley A. Dodds, Associate Professor
Physics and Astronomy

Harold J. Vinegar
Shell International Exploration & Production Inc.

HOUSTON, TEXAS

APRIL, 2002

UMI Number: 3047384

UMI®

ABSTRACT

NMR Relaxation and Diffusion Characterization of Hydrocarbon Gases and

Liquids

by

Ying Zhang

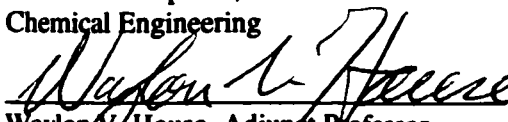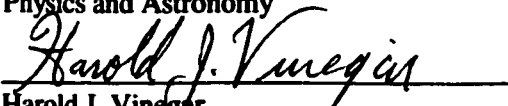The proton nuclear spin-lattice relaxation times and self-diffusion coefficients of ethane and propane were measured at elevated temperatures and pressures. It is found that pure ethane and propane depart from the linear correlations between relaxation time and viscosity/temperature and diffusivity found for pure higher alkanes and dead crude oils. The inverse relationship between the diffusion coefficient and viscosity/temperature for pure methane, pure higher alkanes, and methane-higher alkane mixtures holds for pure ethane and propane.

The proton relaxation times were calculated and compared with the experimental data for ethane. The governing relaxation mechanism is shown to be the spin rotation interaction in gaseous ethane. At liquid densities, intra- and intermolecular dipole-dipole interactions and the spin rotation interaction all have significant contributions. A mixing rule was developed to estimate T_1 of gas mixtures. The estimated results by the mixing rule compared closely with experimental results for CH_4-CO_2 and CH_4-N_2 gas mixtures.

T_1, and T_2 relaxation times of about 30 heavy crude oils were measured with different frequency NMR spectrometers. In addition, relaxation times of some oil samples were measured at various temperatures. Light oils have equal T_1 and T_2 relaxation times.

However, heavy or asphaltene crude oils have different T_1 and T_2 with the ratio of T_1/T_2 increasing with increasing viscosity, Larmor frequency, asphaltene content and free radical content. For heavy oils, apparent T_2 time constants increase and the signal amplitude decreases with increasing echo spacing. Apparent hydrogen index of heavy crude oils increases with increasing temperature. With increasing echo spacing, apparent hydrogen index of heavy oils decreases.

ACKNOWLEDGEMENTS

TABLE OF CONTENTS

LIST OF TABLES

LIST OF FIGURES

NOMENCLATURE

a	Molecular radius
A_i	Constant defined by Equation (7.2.6)
B_0	Static magnetic field
B_1	Radio-frequency magnetic field
ΔB_0	Inhomogeneity of B_0
C	Spin rotation coupling tensor
C_{av}	Spin rotation constant defined by Equation (3.2.11)
ΔC	Spin rotation constant defined by Equation (3.2.12)
C_{eff}	Effective spin rotation constant
$C_\parallel$	Spin rotation constant along parallel axis
$C_\perp$	Spin rotation constant along perpendicular axis
d	Distance of protons from the center of the molecule
D	Diffusion coefficient
Dr	Rotational diffusion coefficient
$D_\parallel$	Rotational diffusion constant along parallel axis
$D_\perp$	Rotational diffusion constant along perpendicular axis
E	Energy of a magnetic moment μ in a magnetic field B_0
ΔE	Energy difference between adjacent energy levels
f_i	Resonant nucleus fraction
g	Gradient strength

g	Nuclear g factor
$g(\sigma)$	Radial distribution function
G	Gradient strength
G_{ij}	Coefficient defined by Equation (7.2.11)
h	Planck's constant
$\hbar$	Planck's constant divided by 2π
h_{peak}	Peak height of free radical signal
H_{sr}	Hamiltonian for the spin rotation interaction
HI	Hydrogen index
I	Spin quantum number
I	Spin angular momentum operator of the resonant spin
I_{av}	Average moment of inertia of the molecule
$I_\parallel$	Moment of inertia of the molecule along parallel axis
$I_\perp$	Moment of inertia of the molecule along perpendicular axis
$j(\omega)$	Spectral density
J	Rotational quantum number
J	Molecular rotational angular momentum
ΔJ	Change in the rotational angular momentum vector of the molecule by a collision
k	Boltzmann's constant
K	Rotational quantum number
m	Magnetic quantum number

m_1	Molecular mass of molecule 1
m_2	Molecular mass of molecule 2
m_e	Mass of the electron
m_i	Molecular mass of molecule i
m_j	Molecular mass of molecule j
m_p	Mass of the proton
m_{sample}	Sample weight
M	Magnetization vector
M_0	Total magnetization
MW	Molecular weight
n	Number density
N_A	Avogadro number
N_{lower}	Number of nuclei in the lower energy state at equilibrium
N_{upper}	Number of nuclei in the upper energy state at equilibrium
P	Probability function
r	Distance between two nuclei in the same molecule
r_{ij}	Distance between two nuclei in the same molecule
$<r^2>$	Root mean square distance of the random flight
R	Total relaxation rate
R_{intra}	Relaxation rate by intramolecular dipole-dipole interaction
R_{inter}	Relaxation rate intermolecular dipole-dipole interaction
R_{sr}	Relaxation rate by spin rotation interaction

s	Paramter defined in Equation (3.2.16)
S	Coefficient defined in Equation (8.1.10)
t_p	Pulse length
T	Temperature
T_1	Spin-lattice relaxation time
T_2	Spin-spin relaxation time
T_2^*	Apparent spin-spin relaxation time
TE	Echo spacing
$\bar{v}$	Mean relative velocity
V	Molar volume
W_2	Parameter defined by Equation (8.1.3)
x	x axis in the rotating frame
x_j	Mole fraction
y	y axis in the rotating frame
y	Parameter defined by Equation (3.2.14)
$Y_{2m}(\Omega)$	Spherical harmonic
z	z axis in the rotating frame
α	Parameter defined by Equation (3.2.13)
α'	Factor in Equation (7.1.15)
β'	Factor in Equation (7.1.15)
δ	Duration of gradient
Δ	Duration between two gradient pulses

η	Viscosity
γ	Gyromagnetic ratio
κ	Correction factor for slip boundary conditions compared with stick boundary conditions
μ	Reduced mass
μ	Magnetic moment
μ_z	z component of μ
ν	Number of protons per molecule
ν_0	Angular frequency
θ	Precessing angle
θ	Angle defined in Equation (3.2.38)
θ_p	Tip angle
ρ	Molar density
σ	Molecular diameter
σ_J	Cross section for angular momentum transfer
σ_d'	Atomic diamagnetic shielding
σ_p'	Average paramagnetic shielding
τ^0	Zero-viscosity intercept in Equation (3.2.5)
τ	Half of the echo spacing
τ_{12}	Correlation time related with the cross term between J and JY_{2m}
τ_c	Rotational correlation time

τ_J Angular momentum correlation time

$\tau_{J\parallel}$ Angular momentum correlation time along parallel axis

$\tau_{J\perp}$ Angular momentum correlation time along perpendicular axis

τ'_{12} Correlation time related with the tensor of rank one formed by the product

of J and $Y_{2m}(\Omega)$

ω_0 Larmor frequency

Ω' Parameter defined in Equation (7.1.14)

I. Introduction

The petroleum industry uses NMR well logging to evaluate rock and fluid properties of formations immediately after a well is drilled. This includes quantitatively distinguishing the amounts of water, oil, and gas present in the formation and estimating the viscosity of the oil (Freedman et al., 2001; Kleinberg and Vinegar, 1996). The NMR logging tool measures the relaxation due to surface relaxation (in the case of water), bulk fluid relaxation, and diffusion in the presence of a magnetic field gradient. The bulk fluid relaxation is a function of viscosity, temperature, and dissolved gas content.

The relaxation time and diffusivity of crude oils are often correlated with viscosity/temperature (Morriss et al., 1997) and those for natural gas with density and temperature (Akkurt et al., 1996). In gas mixtures and gas-oil mixtures, the respective components contribute to the overall relaxation time distributions and diffusivity distributions. For example, it has been shown that the relaxation times of live oils are a function of the solution's gas/oil ratio (Lo, 1999; Lo et al., 2000). Also, the relaxation time distribution is related to the diffusivity distribution (Freedman et al., 2001).

Figure 1.1 is the plot of relaxation time versus viscosity/temperature for pure alkanes (Gerritsma et al., 1971; Kashaev et al., 1964; Muller and Noble, 1963; Zega, 1987) and alkane mixtures (Lo, 1999). Previous work shows that pure higher alkanes, higher alkane mixtures, viscosity standards and stock tank crude oils, which relax by dipole-dipole interactions, have NMR relaxation times that are inversely proportional to viscosity/temperature (Kashaev et al., 1964; Morriss et al., 1997; Zega, 1987, 1990). However, methane gas, which relaxes predominantly by the spin rotation interaction, has

a NMR relaxation time that is approximately directly proportional to viscosity/temperature (Bloom et al., 1967; Gerritsma et al., 1971; Johnson and Waugh, 1961; Lo, 1999; Lo et al., 2000; Oosting and Trappeniers, 1971). Live oils at reservoir conditions contain methane, ethane and propane. The work by this laboratory (Lo, 1999; Lo et al., 2000) shows that higher alkanes containing dissolved methane depart from the straight line relationship because of the relaxation of methane. The existence of methane in live oils makes interpretation of NMR logging data more complicated. The straight line of cryogenic liquid ethane (Muller and Noble, 1963) in Figure 1.1 departs from the linear correlation of higher alkanes as well. It is interesting to note that the curve of liquid methane converges to the curve of cryogenic liquid ethane with increasing viscosity/temperature.

Ethane and propane like methane also are common components of natural gas associated with oils at reservoir conditions. In spite of this fact, the NMR relaxation times of these materials have not been published at conditions typical of petroleum reservoirs. Their contributions to the relaxation of live oils are not known. It is not certain if ethane and propane will relax by the spin rotation mechanism like methane or by dipole-dipole interactions as other higher alkanes.

Pure higher alkanes and stock tank oils, which relax by dipole-dipole interactions, have diffusion coefficients that are proportional to relaxation times. However, for live oils with dissolved methane, ethane and propane, this correlation may not hold because these light alkanes may relax by spin rotation interactions.

So the first objective of this work was to measure NMR relaxation times and self-diffusion coefficients of pure ethane and propane at conditions typical of petroleum

reservoirs and to determine the contributions of three relaxation mechanisms to the relaxation of light hydrocarbons. A mixing rule was developed to estimate T_1 of gas mixtures, which are representative of natural gas.

At the other extreme, heavy crude oils also depart from the viscosity correlation of intermediate viscosity dead oils. It is well known that the presence of heavy components in an oil complicates analysis and interpretation. Vinegar, et al. (Vinegar et al., 1991) measured the T_1 of a number of crude oils with an 80 MHz NMR spectrometer and found that the log mean T_1 had a minimum value of about 100 msec for crude oils with viscosity greater than about 100 cP. McCann et al. (McCann et al., 1999) and LaTorraca et al. (LaTorraca et al., 1998) measured both T_1 and T_2 of viscous oils with the 2 MHz NMR spectrometers and found that T_1 and T_2 had significant deviation above a viscosity of about 1,000 cP.

The T_1 and T_2 relaxation times for a number of crude oils and pure hydrocarbons are plotted as a function of viscosity and Larmor frequency in Figure 1.2. The correlation of Morriss et al. (Morriss et al., 1997) is shown as the straight line. Pure alkanes differ from the low viscosity crude oils. However, if the alkanes remain saturated with air, the relaxation times of the alkanes reduce to values that are consistent with those of the light crude oils as shown in Figure 1.3. The interesting aspects of Figure 1.2 are the difference between T_1 and T_2 for the viscous oils and the frequency dependence of this difference.

So the second objective of this work was to measure T_1, T_2 relaxation times of crude oils with different frequency NMR spectrometers and at various temperatures. Then the dependence of the ratio of the logarithmic mean T_1/T_2 on oil viscosity,

asphaltene content, the Larmor frequency of the NMR spectrometer, and the free radical content was investigated.

This thesis is divided into nine chapters. The basic NMR theory and relaxation mechanisms as well as relaxation and diffusion measurements are given in Chapters II-IV. The NMR equipment and experimental procedures are described in Chapter V. The experimental results and discussion for light components are presented in Chapters VI and VII. Chapter VIII deals with the crude oils. Finally, Chapter IX concludes this work and proposes further relevant studies.
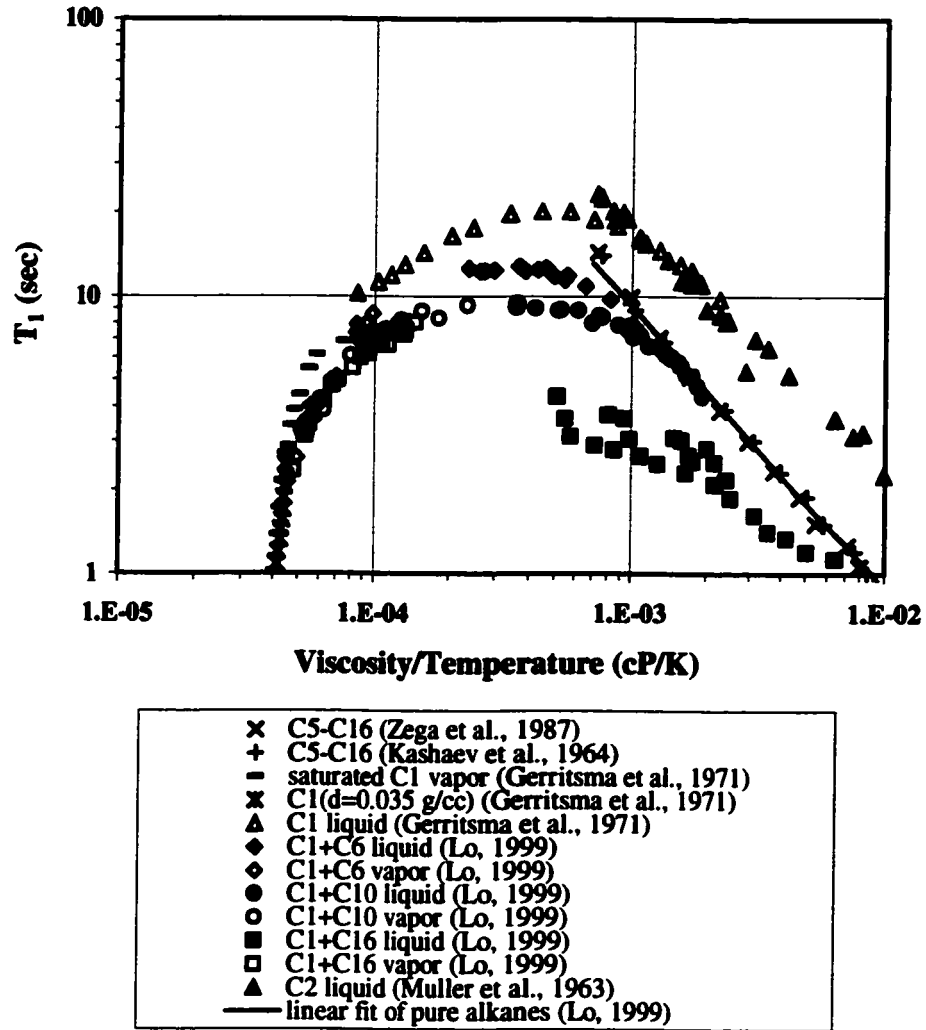
Figure 1.1 T_1 versus viscosity/temperature plot. Pure higher alkanes, which relax by dipole-dipole interactions, have NMR relaxation times that are inversely proportional to viscosity/temperature. Methane gas, which relaxes predominantly by the spin rotation interaction, has a NMR relaxation time that is approximately directly proportional to viscosity/temperature. Higher alkanes containing dissolved methane depart from the straight line relationship because of the relaxation of methane.
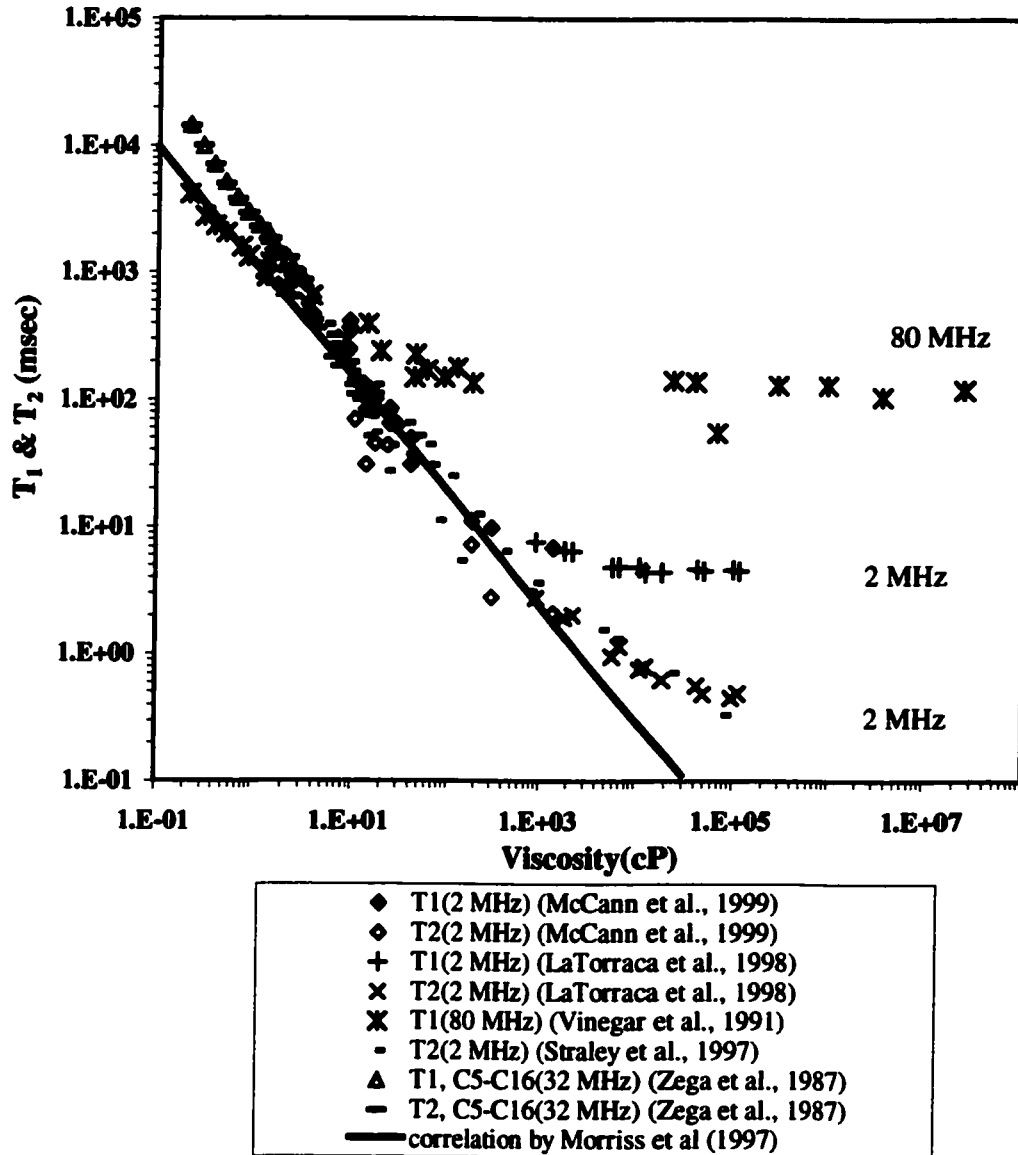
Figure 1.2 T_1 and T_2 relaxation times as a function of viscosity and Larmor frequency. The log mean T_1 measured by the 80 MHz spectrometer had a minimum value of about 100 ms for crude oils with viscosity greater than about 100 cP. T_1 and T_2 of viscous oils with the 2 MHz NMR spectrometers had significant deviation above a viscosity of about 1,000 cP. Pure alkanes differ from the low viscosity crude oils.

$y = 2669.2x^{-1.0475}$
$R^2 = 0.9974$

Legend:
+ T1, C5-C16(32 MHz)(deoxygenated) (Zega, 1987)
o T2, C5-C16(32 MHz)(deoxygenated) (Zega, 1987)
X T1, C5-C16(2 MHz)(air saturated) (Lo, 1999)
——— linear fit for T1 of pure alkanes
- - - - T2 correlation by Morriss et al. (1997)

Axis labels: Relaxation Time(msec) vs Viscosity(cP)
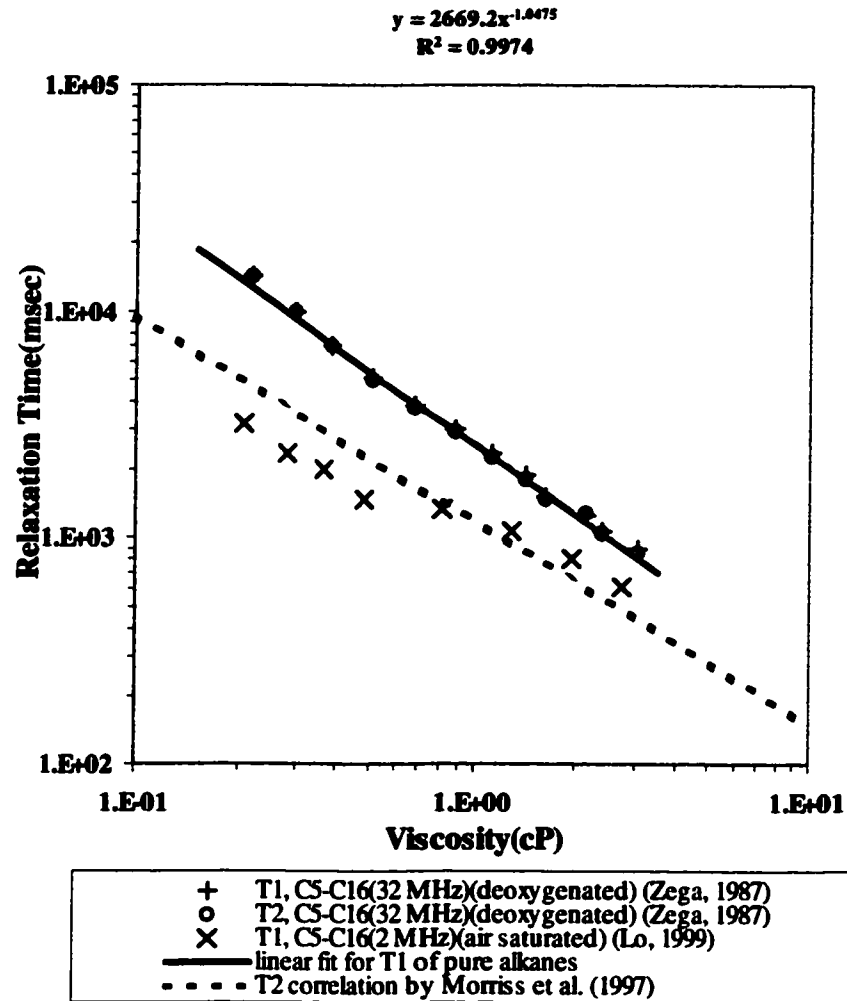
Figure 1.3 The effect of oxygen on relaxation times of alkanes. If the alkanes remain saturated with air, the relaxation times of the alkanes reduce to values that are consistent with those of the light crude oils

II. Basic Theory of Nuclear Magnetic Resonance

Many excellent reviews (Abragam, 1961; Cowan, 1997; Farrar and Becker, 1971; Hore, 1995; McConnell, 1987) of NMR theory have been published. This chapter will explain NMR phenomena using both classical and quantum descriptions. The classical description is adequate for the treatment of many NMR phenomena. The quantum description can give insight into NMR phenomena, particularly relaxation.

2.1 Classical Description of NMR

A simple vector model of magnetic resonance in classical mechanics provides a convenient way to understand the behavior of nuclei in a magnetic field. In NMR experiments, two kinds of magnetic fields are important. One is the strong static magnetic field B_0 along the z axis, and the other is a weak radio-frequency (RF) magnetic field B_1 which rotates in the x-y plane. Thus the total magnetic field B is tilted slightly away from the z axis. When a sample containing a large number of spin-½ nuclei is placed under the static magnetic field B_0, the total magnetization M will precess around B_0 as shown in Figure 2.1.1. M precesses at an angular frequency v_0 (radians per second),

$$v_0 = \gamma B_0,\tag{2.1.1}$$

where γ is the gyromagnetic ratio. γ is constant , which has different values for different nuclei. For the proton, the value of γ is 2.675×10^8 radian Tesla^{-1} sec^{-1}.

The potential energy of the precessing particle with the precessing angle θ is given by

$$E = -\mu_z B_0 = -\mu B_0 \cos\theta,\tag{2.1.2}$$

where μ_z is the z-direction magnetic moment of the spin. If a radio-frequency field rotating at the Larmor frequency, B_1, is applied perpendicular to B_0 and absorbed by the spin, the spin will be excited and the angle θ will change. The flip angle θ_p of the net magnetization M after the radio-frequency pulse is applied is

$$\theta_p = \gamma t_p B_1, \tag{2.1.3}$$

where t_p is the duration of the radio-frequency pulse and θ_p is in radians. When B_1 is removed, radio-frequency energy will be re-emitted and the spin will return to its equilibrium state. This process is called relaxation. Figure 2.1.2 illustrates the absorption and emission processes. In NMR instruments, the RF field B_1 is produced by the coil of a radio-frequency tank circuit. The discussion in this thesis is based exclusively on the rotating frame that rotates about B_0 in the same direction in which the nuclear moments precess.
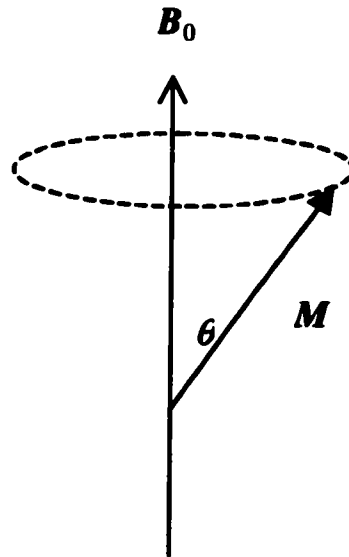
Figure 2.1.1 Precession of magnetization. When spin-1/2 nuclei are placed under the static magnetic field B_0, the total magnetization M will precess around B_0.
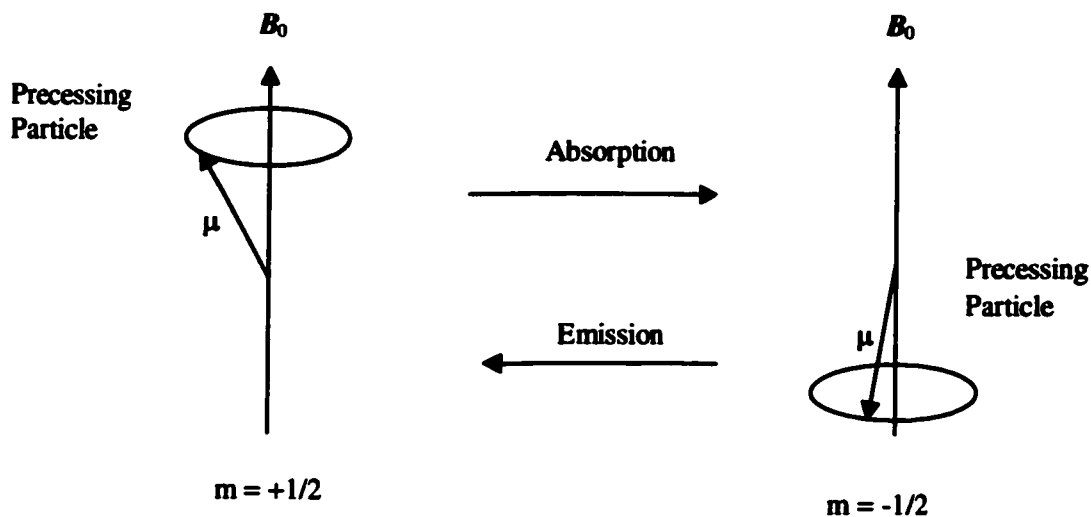
Figure 2.1.2 Absorption and emission processes of a precessing particle. The radio-frequency field rotating at the Larmor frequency, B_1, is applied perpendicular to B_0 and absorbed by the spin, the spin will be excited. When B_1 is removed, radio-frequency energy will be re-emitted and the spin will return to its equilibrium state.

Conversely, after B_1 is switched off, the decaying transverse magnetization M will induce an oscillating sinusoidal current in a receiver coil, which can be detected. This is the NMR signal. The recovery of the z magnetization to its equilibrium state requires spins to flip so as to re-establish the Boltzmann population distribution. The xy magnetization will decay to zero. After a 90° pulse is applied and the spin is flipped 90°, M will return to its equilibrium state in a spiral motion. The oscillating, decaying transverse magnetization is detected by the NMR spectrometer via the voltage induced in the receiver coil. This signal is called the free induction decay (FID). Figure 2.1.3(a) shows the returning process of M after a 90° pulse, and 2.2.3(b) is the signal detected through the x axis and the z axis.
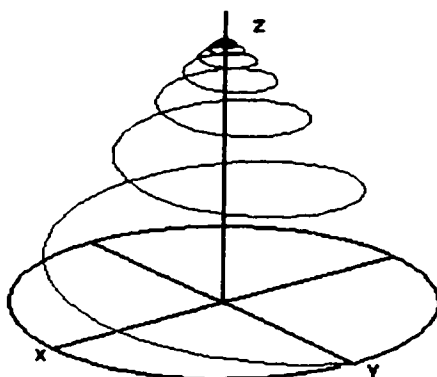
Figure 2.1.3 (a) Following a 90° pulse, the magnetization returns to its equilibrium state in a spiral motion.
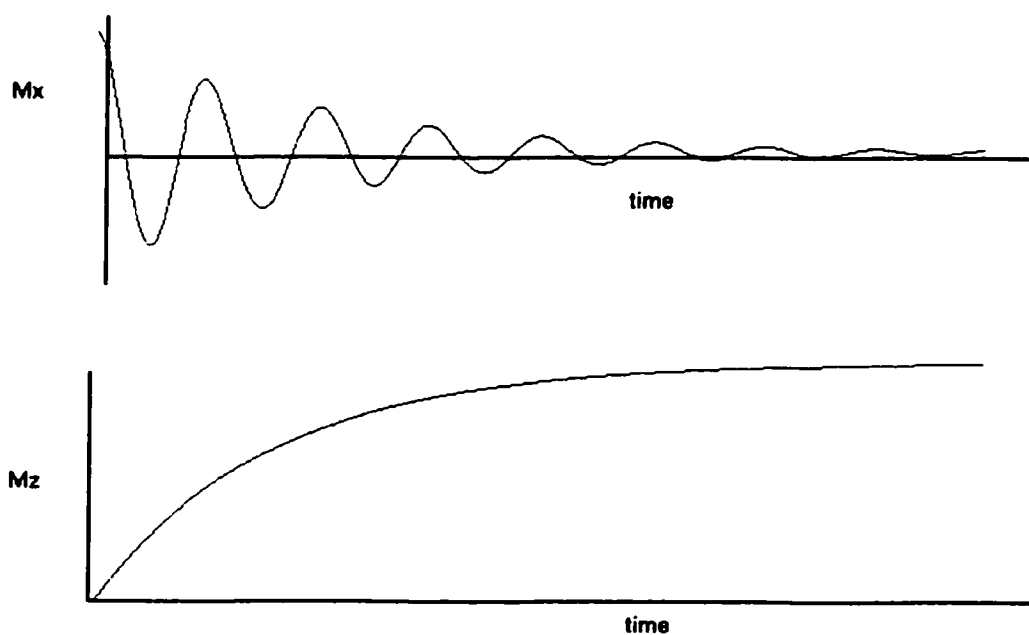
Figure 2.1.3 (b) The signal detected from the x-axis and the z-axis. The transverse components of M decay to zero with a characteristic time constant T_2. The z component goes back to M_0 with the characteristic time constant T_1. T_1 and T_2 will be discussed in Section 3.1.

2.2 Quantum Description of NMR

A magnetic nucleus possesses an intrinsic angular momentum known as spin and it has angular momentum I, which is a vector quantity. The direction and magnitude of I are quantized. The spin quantum number I of a nucleus may be zero, a positive integer or half integer. I is determined by the number of protons and neutrons. I is zero when the number of protons and neutrons are both even, and I is an integer when they are both odd. I is a half integer when one of the two numbers is even and the other one is odd.

When a nucleus with spin quantum number I is placed in a magnetic field, it will have $(2I+1)$ discrete states. The components of angular momentum for these states will have values of $I, I-1, I-2, ..., -I$.

The nucleus that is of interest here is the proton, ^1H, which has spin quantum number ½. For the proton, there are two quantum states which correspond to $I = $ ½ and $I = $ -½.

The magnetic moment μ of a nucleus is associated with its spin angular momentum. It is defined

$$\mu = \gamma I. \tag{2.2.1}$$

When ^1H is placed in an external magnetic field B_0, two magnetic quantum states m appear, $m = 1/2$ and $m = -1/2$. The energy E of the nucleus at the m quantum state is

$$E = \gamma m \hbar B_0, \tag{2.2.2}$$

where $\hbar$ is Planck's constant h divided by 2π. Thus, the energy difference ΔE between states is

$$\Delta E = \gamma \hbar B_0. \tag{2.2.3}$$

Figure 2.2.1 shows the two energy levels of the nucleus under magnetic field B_0.

For ^{1}H, there are only two energy levels; Thus the transitions are between adjacent energy levels. The resonance condition for $I = \frac{1}{2}$ is

$$\Delta E = h\omega_0 . \tag{2.2.4}$$

Here ω_0 is the resonance frequency and is also called the Larmor frequency. Substituting Equation (2.2.3) into Equation (2.2.4), we obtain the expression for the Larmor frequency ω_0

$$\omega_0 = \frac{\gamma B_0}{2\pi} . \tag{2.2.5}$$

The Larmor frequency is the angular frequency ν_0 divided by 2π,

$$\omega_0 = \frac{\nu_0}{2\pi} . \tag{2.2.6}$$

When nuclei are not under the magnetic field, they will be equally distributed between the two quantum states. However, when the magnetic field is present, the populations of nuclei in the two states will rearrange and the lower energy state ($m = \frac{1}{2}$) will predominate, according to the Boltzmann relation. The ratio of populations on the two states is given by

$$\frac{N_{upper}}{N_{lower}} = e^{\frac{-\Delta E}{kT}} , \tag{2.2.7}$$

where N_{upper} is the number of nuclei in the upper energy state and N_{lower} is the number of nuclei in the lower energy state. The unequal distribution give rises to a bulk magnetization M in the direction of the magnetic field B_0. When the magnetic field is not disturbed (equilibrium state), M is denoted as M_0.
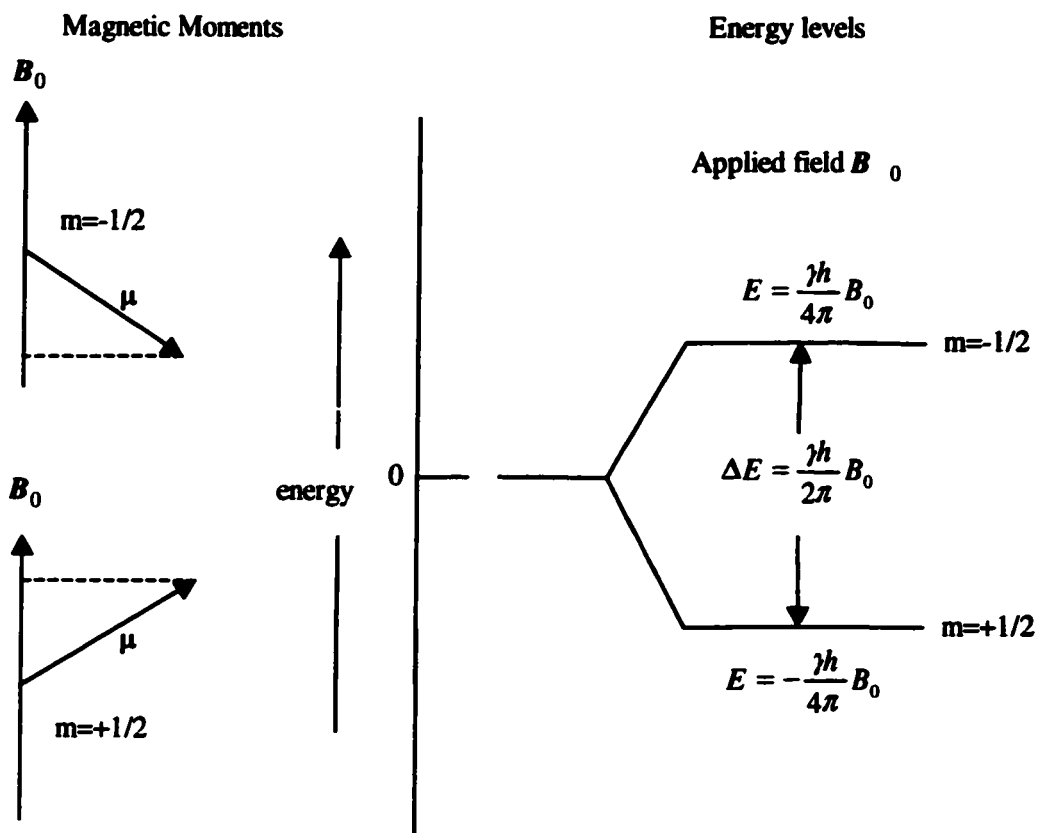
Figure 2.2.1 Energy levels for a nucleus with I = ½. When a nucleus with I = ½ is placed in an external magnetic field B_0, two magnetic quantum states m appear, m = 1/2 and m = -1/2. In addition, two energy levels appear.

III. NMR Relaxation

NMR relaxation processes and mechanisms have been discussed in many reviews (Abragam, 1961; Blicharski, 1963; Cowan, 1997; Farrar and Becker, 1971; Fukushima and Roeder, 1993; Gordon, 1966; Hubbard, 1963; McConnell, 1987; Wang, 1973). Therefore, this chapter will summarize the concepts that are relevant to this thesis.

3.1. NMR Relaxation Processes

NMR relaxation describes the return of the magnetization to equilibrium following the disturbance of the Boltzmann population of oriented magnetic moments. NMR relaxation processes can be classified into two main types. The first type is the spin-lattice (longitudinal) relaxation associated with dispersion of irradiated energy. The second type is the spin-spin (transverse) relaxation associated with the loss of phase coherence of spin groups caused by local variations of the Larmor frequency.

As it has been mentioned in the previous chapter, if a group of spin-$\frac{1}{2}$ nuclei are placed in the static magnetic field B_0, they would distribute themselves between the two energy states according to the Boltzmann relation. As a result, more spins will stay in lower energy state than in the upper state. The population difference results in a net bulk magnetization M_0. If this equilibrium state is disturbed by applying a RF field B_1, the nuclei will absorb the energy and the population of nuclei in the two states will be redistributed. When B_1 is removed, the excess population is restored to the lower energy level and the energy observed is transferred to the surrounding (lattice). This process is called the spin-lattice relaxation. For a sample with identical spins, this spin-lattice relaxation process is generally the exponential decay characterized with a time constant,

the spin-lattice relaxation time T_1. The return of z-component of magnetization can be expressed as:

$$\frac{dM_z}{dt} = -\frac{M_z - M_0}{T_1}.$$

(3.1.1)

When the magnetization is flipped, x and y components of the magnetization also exists, and they will also restore to the equilibrium value zero. This decay is referred to as the spin-spin relaxation and is a result of the spins redistributing energy among themselves. The characteristic time constant T_2 for the exponential decay process is defined from the equations governing the return of transverse magnetizations

$$\frac{dM_x}{dt} = -\frac{M_x}{T_2},$$

(3.1.2)

$$\frac{dM_y}{dt} = -\frac{M_y}{T_2}.$$

(3.1.3)

In contrast, the spin-spin relaxation process does not require energy transitions but depends on local variations of the magnetic field strength. Figures 3.1.1 (a) and (b) show the recoveries of longitudinal and transverse of magnetization respectively.

$M_z(0) = -M_0$ $\qquad\qquad$ $M_z(t)$ $\qquad\qquad$ $M_z = M_0$

t = 0 $\qquad\qquad\qquad$ t $\qquad\qquad\qquad$ t = infinity
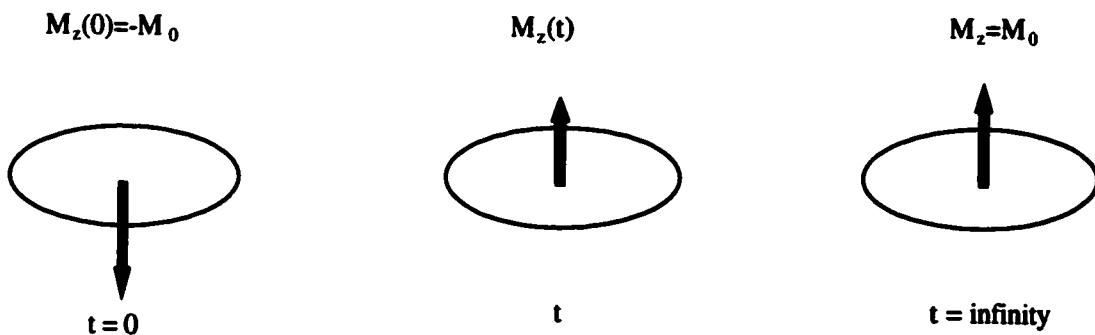
Figure 3.1.1 (a) Recovery of the longitudinal magnetization
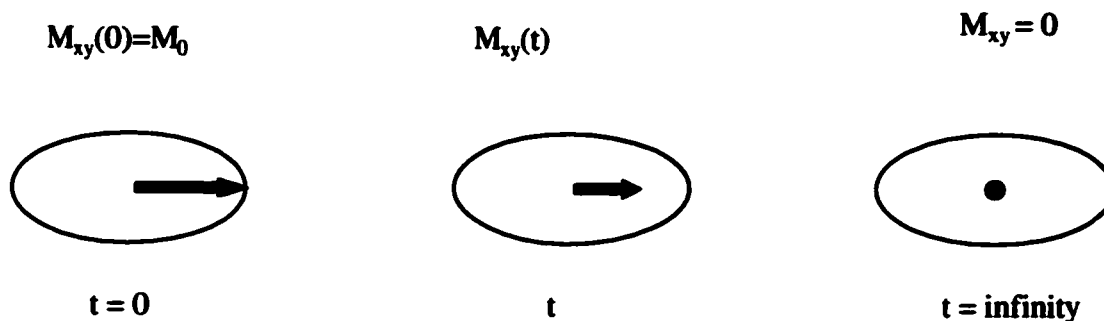
Figure 3.1.1 (b) Recovery of the transverse magnetization

T_2 can be affected by inhomogeneity of the static magnetic field B_0. If the spins are placed in an inhomogeneous field B_0, spins at different locations will precess at different frequencies according to their surrounding field strength. This will result in phase incoherence of the nuclei's transverse magnetization. An additional transverse decay with a time constant $1/(\gamma \Delta B_0)$ will occur. The net transverse relaxation rate arises from both of these mechanisms and has a time constant $1/T_2^*$,

$$\frac{1}{T_2^*} \cong \frac{1}{T_2} + \gamma \Delta B_0,$$

(3.1.4)

where ΔB_0 is the inhomogeneity of the static field B_0.

3.2. NMR Relaxation Mechanisms

In general, three mechanisms, viz. the intra- and intermolecular dipole-dipole interactions and the spin rotation interaction contribute to the total relaxation rate for most spin ½ nuclei. If these interactions are independent, the total relaxation rate may be given by (Abragam, 1961; McConnell, 1987)

$$\frac{1}{T_1} = R = R_{intra} + R_{inter} + R_{sr},$$ (3.2.1)

where R_{intra} is the relaxation rate by the <u>intra</u>molecular dipole-dipole interaction, R_{inter} is the relaxation rate by the <u>inter</u>molecular dipole-dipole interaction, and R_{sr} is the relaxation rate by the spin rotation interaction.

The theoretical calculation of different contributions will be briefly discussed in the following.

3.2.1. <u>Intermolecular Dipole-Dipole Interaction</u>

The dipole-dipole interaction mechanism is caused by the interaction of the magnetic dipoles of the nuclei. For the interaction with nuclei in neighboring molecules, it is the <u>inter</u>molecular dipole-dipole interaction. The relaxation will in general arise from the relative translational motion of the molecules.

McConnell (McConnell, 1987) described the molecular motion with a Langevin equation assuming that the molecular motion can be described as translational and rotational diffusions and then derived the relation for the dipole-dipole interaction

$$\frac{1}{T_1} = I(I+1)\left\{\frac{4}{3}j(\omega_0) + \frac{16}{3}j(2\omega_0)\right\},$$ (3.2.2)

where $j(\omega)$ is the spectral density.

The evaluation of the spectral density will depend on whether the dipole-dipole interaction is <u>inter</u>molecular or <u>intra</u>molecular, and also on the particular model chosen to describe the thermal motion. For <u>inter</u>molecular dipole-dipole interaction, the Brownian motion model in the extreme narrowing limit gives (McConnell, 1987)

$$\frac{1}{T_{1,inter}} = R_{inter} = \frac{8\pi n v \gamma^4 \hbar^2 I(I+1)}{15 D \sigma},$$ (3.2.3)

where n is the number density, v is the number of resonant nuclei in a given molecule, σ is the molecular diameter, and D is the translational diffusion coefficient.

3.2.2. Intramolecular Dipole-Dipole Interaction

Intramolecular dipole-dipole interaction mechanism is due to the interaction of nuclei in the same molecule. If the molecule is regarded as rigid, the relaxation results from the rotational motion of the molecule.

It is assumed that the autocorrelation function is exponential. If the rotational molecular motion can be described by the diffusion equation, Equation (3.2.2) in the extreme narrowing limit will be expressed as (Abragam, 1961; McConnell, 1987)

$$\frac{1}{T_{1,intra}} = R_{intra} = 2I(I+1)\gamma^4 \hbar^2 \tau_c \sum_{j=1} r_{ij}^{-6},$$ (3.2.4)

where r_{ij} is distance between two nuclei in the same molecule, and τ_c is the rotational correlation time.

Numerous studies of rotational molecular motion have shown that the rotational correlation time can be given by the Stokes-Einstein-Debye equation (Alms et al., 1973a, b, c; Bartoli and Litovitz, 1972; Bauer et al., 1975; Debye, 1929; Einstein, 1956; Evans and Kivelson, 1986)

$$\tau_c = Q\eta/T + \tau^0,$$ (3.2.5)

where η is the viscosity, T is the temperature, τ^0 is the zero-viscosity intercept, and Q is related to the volume and geometry of the rotating particle and the drag that the particle experiences from the surrounding fluid. Alm et al. (Alms et al., 1973b, c) suggested that

the intercept was related to free rotation correlation time τ_{FR} and that it could be described as

$$\tau^0 = \tau_{FR} = \left(\frac{2\pi}{9}\right)^{1/2}\left(\frac{I_{av}}{kT}\right)^{1/2}, \tag{3.2.6}$$

where k is Boltzmann's constant and I_{av} is given by

$$\frac{1}{I_{av}} = \frac{1}{3}\left(\frac{2}{I_\perp} + \frac{1}{I_\parallel}\right). \tag{3.2.7}$$

$I_\parallel$, $I_\perp$ are moments of inertia of the molecule along parallel and perpendicular axes.

Substituting Equations (3.2.5), (3.2.6) and (3.2.7) into Equation (3.2.4), we obtain

$$\frac{1}{T_{1,intra}} = R_{intra} = 2I(I+1)\gamma^4\hbar^2\left[Q\frac{\eta}{T} + \left(\frac{2\pi}{9}\right)^{1/2}\left(\frac{1}{kT}\cdot\frac{3I_\parallel I_\perp}{2I_\parallel + I_\perp}\right)^{1/2}\right]\sum_{j=1}r_{ij}^{-6}. \tag{3.2.8}$$

3.2.3. Spin Rotation Interaction

It has been shown that the spin rotation interaction is the dominant mechanism for spin ½ in a gas (Armstrong and Courtney, 1969, 1972a, b; Armstrong and Hanrahan, 1968; Armstrong and Tward, 1967; Courtney and Armstrong, 1970; Gerritsma et al., 1971; Johnson and Waugh, 1961; Oosting and Trappeniers, 1971). The spin rotation interaction is due to magnetic fields generated at a nucleus by a molecular magnetic moment which arises from the motion of the electron distribution in a molecule. Molecular collisions cause the magnetic moment to fluctuate. This can result in fluctuating magnetic fields which are felt by the nucleus. The magnitude of the effect is proportional to the rotational velocity and inversely proportional to the moment of inertia. Thus the spin rotation interaction will be the strongest in small spherical molecules. The

Hamiltonian for the interaction of molecular and nuclear magnetic moment is (Abragam, 1961; McConnell, 1987)

$$H_{sr} = -hI \cdot C \cdot J,$$
(3.2.9)

where C is the spin rotation coupling tensor, I is the spin angular momentum operator of the resonant spin, and J is the molecular rotational angular momentum of the molecule. For symmetric top molecules, the spin rotation coupling tensor is a symmetric tensor.

Theoretical predictions concerning the spin rotation interaction can be categorized to two cases, the kinetic model for low densities and the diffusion model for high densities. The two models differ in the assumed model for the rotation molecular motion.

3.2.3.1. Kinetic Model

In dilute gases, T_1 can be connected to the thermal average of the binary collision cross sections for angular momentum transfer for spin rotation interaction. The kinetic model can adequately describe the spin rotation interaction in dilute gases. Gordon (Gordon, 1966) developed the kinetic model of the spin rotation interaction for the case of linear molecules. Then Bloom et al. (Bloom et al., 1967; Dong and Bloom, 1970) extended theoretical treatment to spherical and symmetric top molecules. The basic assumptions underlying the kinetic model are as follows

(a) "High frequency" transitions associated with changes in the energy of rigid rotation and centrifugal distortion are neglected.

(b) The Larmor period is much longer than interaction times during which the molecules reorient.

(c) The free molecule correlation functions (in the absence of collisions) are independent of time. The effect of molecular collisions is to limit the lifetime of the molecule in any state and to cause the free molecule correlation functions to decay to zero exponentially.

(d) The oscillating terms in the free molecule correlation functions are negligible.

(e) The rotational angular momentum J_1 and the rotation matrix for frame transformation $D_{0-1}{}^2$ are not statistically independent in the dilute gases.

For symmetric top molecules with the resonant nuclei on the principal symmetry axis (e. g., ^{13}C in ethane), the relaxation time in the extreme narrowing limit may be expressed as

$$\frac{1}{T_{1,sr}} = 4\pi^2 \left\{ \frac{2}{3}C_{av}^2 \left\langle J(J+1) \right\rangle^{J,K} \tau_J - \frac{4}{9}\Delta C C_{av} \left\langle 2K^2 - J(J+1) \right\rangle^{J,K} \tau_{12}' \right.$$

$$\left. + \frac{2}{27}(\Delta C)^2 \left\langle \frac{[3K^2 - J(J+1)]^2}{J(J+1)} \right\rangle^{J,K} \tau_{12} \right\}, \tag{3.2.10}$$

where J, K are rotational quantum numbers, τ_J is the correlation time related with the angular momentum operator J, τ_{12}' is the correlation time related with the tensor of rank one formed by the product of J and the spherical harmonic $Y_{2m}(\Omega)$, τ_{12} is the correlation time related with the cross term between J and JY_{2m}, and

$$C_{av} = \frac{1}{3}(C_{\parallel} + 2C_{\perp}), \tag{3.2.11}$$

$$\Delta C = C_{\perp} - C_{\parallel}, \tag{3.2.12}$$

where $C_{\parallel}$, $C_{\perp}$ are spin rotation constants describing the coupling of the nuclear and molecular angular momenta along parallel and perpendicular axes. Armstrong et al.

(Armstrong and Courtney, 1972a, b) calculated the rotational averages in Equation (3.2.10) using the method of Birnbaum in terms of α and y, defined as

$$\alpha = \frac{\hbar^2}{2I_\perp kT},$$
(3.2.13)

$$y = \left(1 - \frac{I_\parallel}{I_\perp}\right)^{1/2}.$$
(3.2.14)

Then we obtain

$$\frac{1}{T_{1,sr}} = \frac{4\pi^2}{\alpha}\left\{\left(1 - \frac{y^2}{3}\right)C_{av}^2\tau_J + \frac{4}{9}y^2\Delta C C_{av}\tau_{12}'\right.$$

$$\left. + (\Delta C)^2\left[9\left(\frac{1-y^2}{y^2}\right)^2\left(-1 - \frac{1}{3}y^2 + s\right) - 1 + \frac{5}{3}y^2\right]\tau_{12}\right\},$$
(3.2.15)

where

$$s = \frac{1}{2y}\ln\left(\frac{1+y}{1-y}\right) \qquad for I_\perp > I_\parallel$$

$$= \frac{1}{|y|}\tan^{-1}|y| \qquad for I_\perp < I_\parallel.$$
(3.2.16)

The averages in Equation (3.2.10) are inversely proportional to α, and α is inversely proportional to temperature. It turns out that the averages in Equation (3.2.10) are proportional to temperature.

Armstrong et al. (Armstrong and Courtney, 1972b) investigated the kinetic model for the resonant nuclei off the symmetry axis of the symmetric-top molecules (e. g., ^{1}H in ethane). In this case, the C tensor is not diagonal and can be expressed by Equation (3.2.37) in the molecular frame. The complete Hamiltonian for the spin rotation interaction is expressed as

$$H_{sr} = -hI^A \cdot C^A \cdot J - \frac{1}{6}hI^{E_1} \cdot C^{E_1} \cdot J - \frac{1}{2}hI^{E_2} \cdot C^{E_2} \cdot J, \qquad (3.2.17)$$

where

$$C^A = \frac{1}{2}\begin{pmatrix} C_{xx} + C_{yy} & 0 & 0 \\ 0 & C_{xx} + C_{yy} & 0 \\ 0 & 0 & 2C_{zz} \end{pmatrix}, \qquad (3.2.18)$$

$$C^{E_1} = \frac{3}{2}\begin{pmatrix} C_{xx} - C_{yy} & 0 & 0 \\ 0 & -(C_{xx} - C_{yy}) & 0 \\ 0 & 0 & 0 \end{pmatrix}, \qquad (3.2.19)$$

$$C^{E_2} = -\frac{\sqrt{3}}{2}\begin{pmatrix} 0 & C_{xx} - C_{yy} & 0 \\ C_{xx} - C_{yy} & 0 & 0 \\ 0 & 0 & 0 \end{pmatrix}, \qquad (3.2.20)$$

with C_{xx}, C_{yy}, C_{zz} the diagonal components of the spin rotation tensor.

Armstrong (Armstrong and Courtney, 1972b) argued that it was reasonable to neglect the contribution of the last two terms to Hamiltonian. Equation (3.2.15) and Equation (3.2.16) can also be used for the resonant nuclei off the symmetry axis of the symmetric-top molecules. However, for the resonant nuclei off the symmetry axis, Equation (3.2.12) becomes

$$\Delta C = (C_\perp - C_\parallel)(1 - \frac{3}{2}\sin^2 \theta), \qquad (3.2.21)$$

where θ is the angle defined by Equation (3.2.38).

For spherical top molecules, y is equal to 0 and τ_J, τ_{12}', and τ_{12} are equal. Equation (3.2.15) simplifies to

$$\frac{1}{T_{1,sr}} = \frac{8\pi^2 I_{av} kT}{\hbar^2}\left(C_{av}^2 + \frac{4}{45}\Delta C^2\right)\tau_J \quad \text{(spherical top molecules)}. \qquad (3.2.22)$$

For linear molecules, only the perpendicular component, $C_\perp$, is nonzero. Thus C

tensor reduces to a scalar and Gordon's Kinetic theory (Gordon, 1966) gives

$$\frac{1}{T_{1,sr}} = \frac{16\pi^2 C_\perp^2 I_{av} kT}{3\hbar^2} \tau_J \qquad \text{(linear molecules)}. \qquad (3.2.23)$$

It is important to note that both Armstrong's and Gordon's calculation gives the

same temperature dependence to the pre-factor in the relaxation rate by the spin rotation

interaction. τ_J represents the average time between collisions that cause angular

momentum transfer and is given by Gordon's theory (Gordon, 1966) as follows

$$\tau_J = (n\bar{v}\sigma_J)^{-1} = \frac{1}{n\sigma_J}\sqrt{\frac{\pi\mu}{8kT}}, \qquad (3.2.24)$$

where $\bar{v}$ is the mean relative velocity $(8kT/\pi\mu)^{1/2}$, μ is the reduced mass for a collision

pair of molecules, and σ_J is the cross section for transfer of angular momentum by a

collision. The reduced mass μ is given by

$$\frac{1}{\mu} = \frac{1}{m_1} + \frac{1}{m_2}, \qquad (3.2.25)$$

where m_1 and m_2 are the mass of two colliding molecules respectively.

The cross section $\sigma_J(T)$ is interpreted classically as (Gordon, 1966)

$$\sigma_J(T) = \frac{1}{4I_{av}kT} \int_0^\infty \left\langle (\Delta J)^2 \right\rangle 2\pi b\,db, \qquad (3.2.26)$$

where ΔJ is the change in the rotational angular momentum vector of the molecule by a

collision and < > denotes the average over the initial distribution of internal states before

a collision and the initial distribution of relative velocities. If the collision integral is

temperature independent, the cross section is inversely proportional to temperature. Then

the angular momentum correlation time τ_J is expected to be proportional to $T^{1/2}$. It is assumed that the molecular motion is governed by a single correlation time. Substituting Equation (3.2.24) and Equation (3.2.26) into Equation (3.2.15), we obtain

$$\frac{T_{1,sr}}{n} = \frac{\hbar^2}{8\pi^2 C_{\text{eff}}^2 I_{av} I_\perp k^2} \cdot \sqrt{\frac{k}{2\pi\mu}} \cdot \left(\int_0^\infty \langle (\Delta J)^2 \rangle 2\pi b \, db \right) \cdot \frac{1}{T^{3/2}}, \qquad (3.2.27)$$

with

$$C_{\text{eff}}^2 = \left(1 - \frac{y^2}{3}\right) C_{av}^2 + \frac{4}{9} y^2 \Delta C C_{av} + (\Delta C)^2 \left[9\left(\frac{1-y^2}{y^2}\right)^2 \left(-1 - \frac{1}{3}y^2 + s\right) - 1 + \frac{5}{3}y^2 \right].$$

$$(3.2.28)$$

And we would expect that T_1/n has a $T^{-3/2}$ temperature dependence for the symmetrical top molecules. Apparently, this conclusion is also valid for spherical top and linear molecules.

At dense gases, the assumptions underlying the kinetic model may not be valid. We may estimate the main correction at dense gases by analogy with Enskog's theory of transport in dense gases (Gordon, 1968). For nuclear spin relaxation in compressed polyatomic gases, the collision frequency effect is important (Gordon, 1968). Then the only modification is the replacement of n with $ng(\sigma)$ where $g(\sigma)$ is Enskog's correction to the collision frequency. The radial distribution function $g(\sigma)$ can be given by Carnahan-Starling equation (Carnahan and Starling, 1969; Dymond, 1985):

$$g(\sigma) = \frac{(1 - 0.5\xi)}{(1-\xi)^3}, \qquad (3.2.29)$$

where $\xi = b/4V$ for a molar volume V and $b = 2\pi N_A \sigma^3 /3$ (N_A is the Avogadro number). In dense fluids, Equation (3.2.24) becomes

$$\tau_J = \left[n g(\sigma) \bar{v} \sigma_J \right]^{-1} = \frac{1}{n \sigma_J} \cdot \frac{(1-\xi)^3}{(1-0.5\xi)} \cdot \sqrt{\frac{\pi \mu}{8kT}} .$$

(3.2.30)

Since $g(\sigma)$ is independent of temperature, τ_J is still proportional to $T^{1/2}$ in dense gases. In general, we would expect

$$T_{1,sr} \propto n T^{-3/2}$$

(3.2.31)

in the kinetic model. This temperature dependence has in fact been used as a reassuring indication of the dominance of the spin rotation interaction in relaxation (Johnson and Waugh, 1961).

3.2.3.2. Diffusion Model

The binary collision theory may not be useful in treating dense gases or liquids. Calculations of T_1 in dense fluids have often been based upon the diffusion model, which describes the rotational motion of molecules with a diffusion equation (Blicharski, 1963; Hubbard, 1963; McClung, 1972; Wang, 1973). The diffusion process can be regarded as a random walk over points in phase space caused by collisions interrupting the free motion of the molecules. The diffusion model is appropriate when the angular momentum correlation time is small compared to the mean period of rotation of the free rotor.

The diffusion model for the spin rotation contribution to T_1 derived by Wang et al (Blicharski, 1963; Hubbard, 1963; McClung, 1972; Wang, 1973) will be summarized in the next paragraphs. In the liquid, the anisotropic intermolecular interactions are large. The restriction (e) in the kinetic model might be removed and the assumption of statistical independence may be reasonable for the liquid. The correlation functions can

be evaluated by a Langevin equation for the molecular angular velocity. If the resonant nuclei are on the symmetry axis of symmetrical top molecules, the coordinate system chosen for diagonalizing the diffusion tensor will simultaneously diagonalize the C tensor. The expression for the spin rotation contribution to the relaxation time is given as

$$\frac{1}{T_{1,sr}} = R_{sr} = \frac{8\pi^2}{3\hbar^2}\int_0^\infty dt \cos(\omega_0 t)\left\{e^{-D_{\perp}t}C_{\parallel}\left\langle J_z(0)J_z(t)\right\rangle\right.$$

$$\left. + e^{-2(D_{\parallel}+D_{\perp})t}C_{\perp}^2\left\langle J_x(0)J_x(t)+J_y(0)J_y(t)\right\rangle\right\}, \tag{3.2.32}$$

where $D_{\parallel}$, $D_{\perp}$ are rotational diffusion constants parallel and perpendicular to the symmetry axis (Wang, 1973). Generally, the angular momentum correlation function is expected to decay over a time short to the Larmor period. It is reasonable for us to assume

$$\left\langle J_i(0)J_i(t)\right\rangle = I_i^2\left\langle\omega_i^2\right\rangle e^{-t/\tau_{Ji}} = kTI_i e^{-t/\tau_{Ji}} \quad i=x,\,y,\,z, \tag{3.2.33}$$

where ω_i is the component of the angular velocity along the i-th principal axis, I_i is the component of moment of inertia along the i-th principal axis and τ_{Ji} is the angular momentum correlation time along the i-th principal axis and is given by

$$\tau_{Ji} = \frac{1}{\left\langle\omega_i^2\right\rangle}\int_0^\infty\left\langle\omega_i(0)\omega_i(t)\right\rangle dt . \tag{3.2.34}$$

Substituting Equation (3.2.33) into Equation (3.2.32), we obtain the expression for the relaxation time due to spin rotation interaction in the extreme narrowing limit as

$$\frac{1}{T_{1,sr}} = \frac{8\pi^2 kT}{3\hbar^2}\left(I_{\parallel}C_{\parallel}^2(\frac{\tau_{J\parallel}}{1+2D_{\perp}\tau_{J\parallel}})+2I_{\perp}C_{\perp}^2(\frac{\tau_{J\perp}}{1+(D_{\perp}+D_{\parallel})\tau_{J\perp}})\right), \tag{3.2.35}$$

where $\tau_{J\parallel}$, $\tau_{J\perp}$ are angular momentum correlation times along parallel and perpendicular axes.

Equation (3.2.35) reduces to

$$\frac{1}{T_{1,sr}} = \frac{8\pi^2 kT}{3\hbar^2}\left(I_\parallel\, C_\parallel^2 \tau_{J\parallel} + 2I_\perp C_\perp^2 \tau_{J\perp}\right) \tag{3.2.36}$$

in the limit $(D_\perp + D_\parallel)\tau_{J\perp} \ll 1, D_\perp \tau_{J\parallel} \ll 1$.

Equation (3.2.35) and (3.2.36) may not be applied to the resonant nuclei off the symmetry axis (e. g., ^1H in ethane). Wang (Wang, 1973) has derived the diffusion model for the spin rotation contribution to T_1 for the resonant nuclei off the symmetry axis. He first assumes that the C-H bond in a molecule such as ethane lies along the z axis with the proton along the z axis at which the C tensor for the proton is diagonalized. And he then relocates the proton to its final position at the y axis on the x-y plane by rotation about the carbon through an angle θ. As a result, the C tensor element for the proton after the transformation is given by

$$C = \begin{pmatrix} C_\perp - \Delta C\sin^2\theta & 0 & \Delta C\sin\theta\cos\theta \\ 0 & C_\perp & 0 \\ \Delta C\sin\theta\cos\theta & 0 & C_\parallel + \Delta C\sin^2\theta \end{pmatrix}, \tag{3.2.37}$$

$$\theta = \frac{180° - \angle H - C - C}{2}. \tag{3.2.38}$$

Wang (Wang, 1973) then obtains the expression for the spin rotation contribution to the relaxation time

$$\frac{1}{T_{1,sr}} = R_{sr} = \frac{8\pi^2 kT}{3\hbar^2}\left\{ I_\parallel\,(C_\parallel + \Delta C\sin^2\theta)^2 \frac{\tau_{J\parallel}}{1+2D_\perp\tau_{J\parallel}} + I_\perp(\Delta C)^2\sin^2\theta\cos^2\theta\left[\frac{\tau_{J\perp}}{1+2D_\perp\tau_{J\perp}}\right.\right.$$

$$+\frac{\tau_{_{\!/\!|}}}{1+(D_\perp+D_{_{\!|}})\tau_{_{\!/\!|}}}\Bigg]+I_\perp\Big[(C_\perp-\Delta C\sin^2\theta)^2+C_\perp^2\Big]\frac{\tau_{_{\!J\!\perp}}}{1+(D_\perp+D_{_{\!|}})\tau_{_{\!J\!\perp}}}\Bigg\}\qquad(3.2.39)$$

which reduces to

$$\frac{1}{T_{1,sr}}=R_{sr}=\frac{8\pi^2kT}{3\hbar^2}\Big\{I_{_{\!|}}\,(C_{_{\!|}}+\Delta C\sin^2\theta)^2\tau_{_{\!J\!|}}+I_\perp(\Delta C)^2\sin^2\theta\cos^2\theta[\tau_\perp+\tau_{_{\!J\!|}}\,/(1+D_{_{\!|}}\tau_{_{\!J\!|}})]$$

$$+I_\perp[(C_\perp-\Delta C\sin^2\theta)^2+C_\perp^2]\tau_{_{\!J\!\perp}}\Big\}\qquad(3.2.40)$$

in the limit $D_\perp\tau_{_{\!J\!\perp}}\ll1,D_\perp\tau_{_{\!J\!|}}\ll1$. Note that Equation (3.2.40) reduces to Equation (3.2.36) for $\theta=0$.

For spherical top molecules, Equation (3.2.36) reduces to

$$\frac{1}{T_{1,sr}}=\frac{8\pi^2I_{av}kT}{\hbar^2}\Big(C_{av}^2+\frac{2}{9}\Delta C^2\Big)\tau_J\qquad\text{(spherical top molecules).}\qquad(3.2.41)$$

For linear molecules, T_1 may be deduced from Equation (3.2.41) by putting $C_{_{\!|}}$ equal to 0. That is

$$\frac{1}{T_{1,sr}}=\frac{16\pi^2C_\perp^2I_{av}kT}{3\hbar^2}\tau_J\qquad\text{(linear molecules).}\qquad(3.2.42)$$

From hydrodynamics theory (Alms et al., 1973a; Debye, 1929; McConnell, 1980), the angular momentum correlation time may be related to viscosity η as following

$$\tau_{Ji}=\frac{I_i}{8\pi a^3\eta}\kappa\qquad i=x,\,y,\,z,\qquad(3.2.43)$$

where a is the molecular radius and κ is the correction factor for slip boundary conditions compared with stick boundary conditions (Hu and Zwanzig, 1974; McClung and Kivelson, 1968). In general, the theoretical prediction using slip boundary conditions may agree well with the experimental measurement for small molecular fluids.

From substitution of Equation (3.2.43) into Equation (3.2.40), we obtain

$$\frac{1}{T_{1,sr}} = R_{sr} = \frac{\pi \kappa kT}{3\hbar^2 a^3 \eta} \left\{ I_1^2 (C_{\parallel} + \Delta C \sin^2 \theta)^2 + I_{\perp}(\Delta C)^2 \sin^2 \theta \cos^2 \theta [I_{\perp} + I_{\parallel} /(1 + D_{\parallel} \tau_{J\parallel})] \right.$$

$$\left. + I_{\perp}^2 [(C_{\perp} - \Delta C \sin^2 \theta)^2 + C_{\perp}^2] \right\}. \tag{3.2.44}$$

It is to be expected that

$$T_{1,sr} \propto \frac{\eta}{T} \tag{3.2.45}$$

if the diffusion model is appropriate.

Table 3.2.1 summarizes the theoretical equations for spherical top molecules and linear molecules by two models. Note that for spherical top molecules the coefficient for the "ΔC^2" term given by the kinetic model differs from that given by the diffusion model by a factor of 2/5. Bloom's explanation (Bloom et al., 1967) is that a factor of 1/5 is accounted for by dropping of the oscillating contribution to correlation functions and that the remaining factor of 2 is due to the fact that J_1 and D_{0-1}^2 are not statistically independent for the gases. It might be noted that both models lead to the same result in the limit of linear molecules. In the diffusion model, Equation (3.2.42) can be obtained from Equation (3.2.41). However, we cannot derive Equation (3.2.23) directly from Equation (3.2.22).

Table 3.2.1 Theoretical equations of relaxation times by the spin rotation interaction based on the kinetic model and the diffusion model

	Kinetic model	Diffusion model
Spherical top	$\dfrac{1}{T_{1,sr}} = \dfrac{8\pi^2 I_{av} kT}{\hbar^2} \left(C_{av}^2 + \dfrac{4}{45} \Delta C^2 \right) \tau_J$	$\dfrac{1}{T_{1,sr}} = \dfrac{8\pi^2 I_{av} kT}{\hbar^2} \left(C_{av}^2 + \dfrac{2}{9} \Delta C^2 \right) \tau_J$
Linear	$\dfrac{1}{T_{1,sr}} = \dfrac{16\pi^2 C_{\perp}^2 I_{av} kT}{3\hbar^2} \tau_J$	$\dfrac{1}{T_{1,sr}} = \dfrac{16\pi^2 C_{\perp}^2 I_{av} kT}{3\hbar^2} \tau_J$

3.3 Measurements of Relaxation

In this section, the methods of measuring T_1 and T_2 will be discussed. The methods are based on the use of spin echoes, which involve dephasing and rephrasing of magnetic moments precessing in inhomogeneous magnetic fields.

There are several methods for measuring T_1. In this work, the inversion recovery (IR) method (Farrar and Becker, 1971; Fukushima and Roeder, 1993) was used since it is the most convenient and is generally applicable. The pulse sequence is shown in Figure 3.3.1. The pulse sequence of the inversion-recovery method consists of a 180° pulse followed by a 90° pulse. The 180° pulse flips the equilibrium magnetization M to the negative z axis. After delay t, a 90° pulse is applied to tip the magnetization to the y axis, and the free induction decay is recorded to get the initial amplitude of the FID, which is proportional to M. For each T_1 experiment, this process is repeated 40 to 50 times with different delay time t. With the initial condition $M_z = -M_0$ at $t = 0$, T_1 for a single type of protons can be described as a function of t,

$$M_z = M_0\left(1 - 2e^{\frac{-t}{T_1}}\right).$$
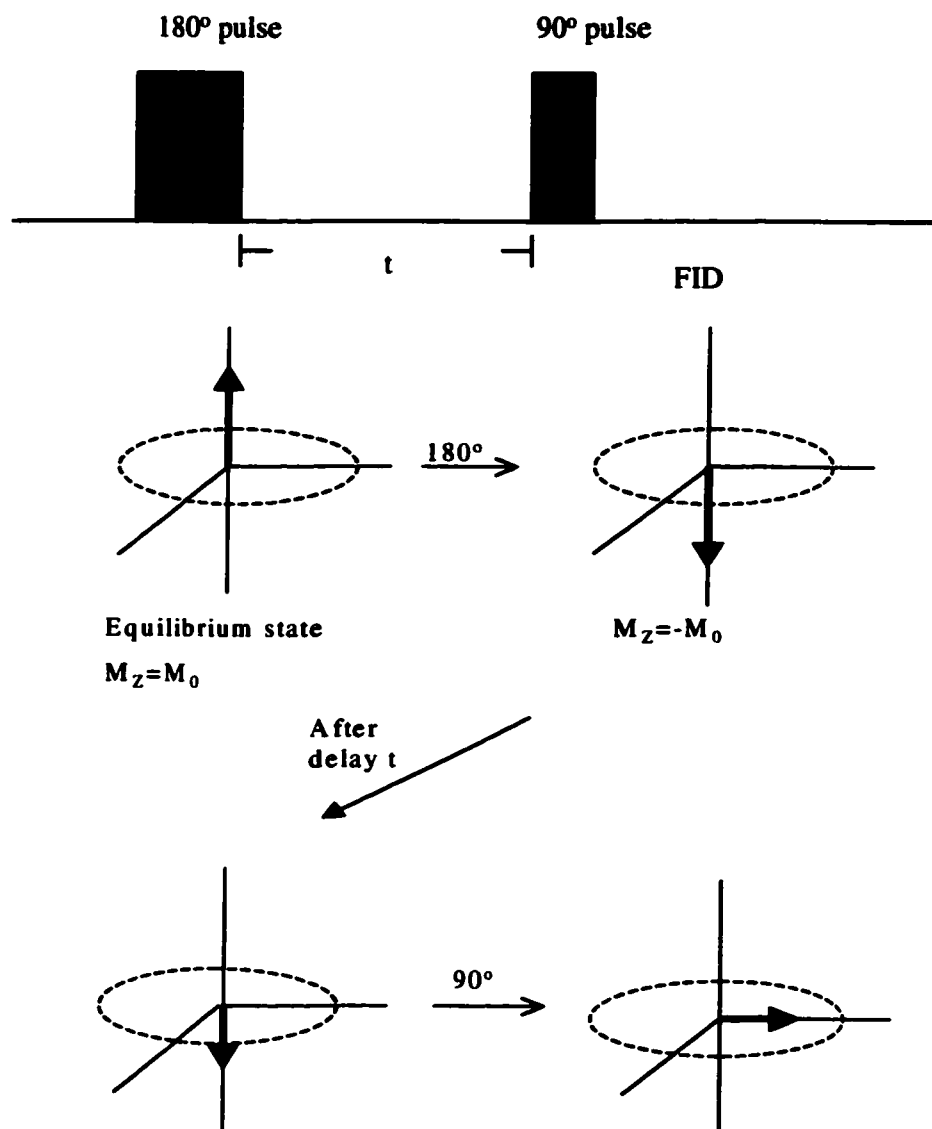
Figure 3.3.1 The inversion recovery pulse sequence for the T_1 measurement. The 180° pulse flips the equilibrium magnetization M to the negative z axis. After delay t, a 90° pulse is applied to tip the magnetization to the y axis.

The Mieboom-Gill variation of the Carr-Purcell pulse sequence (Farrar and Becker, 1971; Fukushima and Roeder, 1993) is the most convenient method for T_2 measurement. The sequence is illustrated in Figure 3.3.2. The Carr-Purcell-Mieboom-Gill (CPMG) sequence consists of a 90° pulse and a series of 180° pulses. The 90° pulse is first applied to flip the magnetization to the y axis, and then the spin isochromats dephase due to the inhomogeneity of the static magnetic field. The spins in higher fields (spin type R) precess faster than the ones at lower fields (spin type S). After time τ, a 180° pulse is applied along the y axis and the spin echo occurs at time 2τ. 180° pulses are applied again at time $3\ \tau,\ 5\ \tau,\ 7\ \tau$, ..., and spin echoes occur at $2\ \tau,\ 4\ \tau,\ 6\ \tau$, ... The time spacing between the 180° pulses is 2τ and is called echo spacing. The amplitude of each spin echo is measured. For a sample with a single type of spins, the magnetization can be described as a function of real time t,

$$M(t) = M_0 e^{-\frac{t}{T_2} - \gamma^2 G^2 D \tau^2 \frac{t}{3}}.$$

(3.3.2)

In Equation (3.3.2), G is the magnetic field gradient due to the inhomogeneity of the static magnetic field. The relationship between the apparent T_2 $(T_2{}^*)$ and the intrinsic T_2 is

$$\frac{1}{T_2^*} = \frac{1}{T_2} + \gamma^2 G^2 D \frac{\tau^2}{3}.$$

(3.3.3)

For a slow diffusing sample, the diffusion term can be eliminated by making τ very small. In this case,

$$M(t) = M_0 e^{-\frac{t}{T_2}}.$$

(3.3.4)

Equilibrium state

$M_Z = M_0$

90°

Dephase

$0 < t < \tau$

180°

$t = \tau$
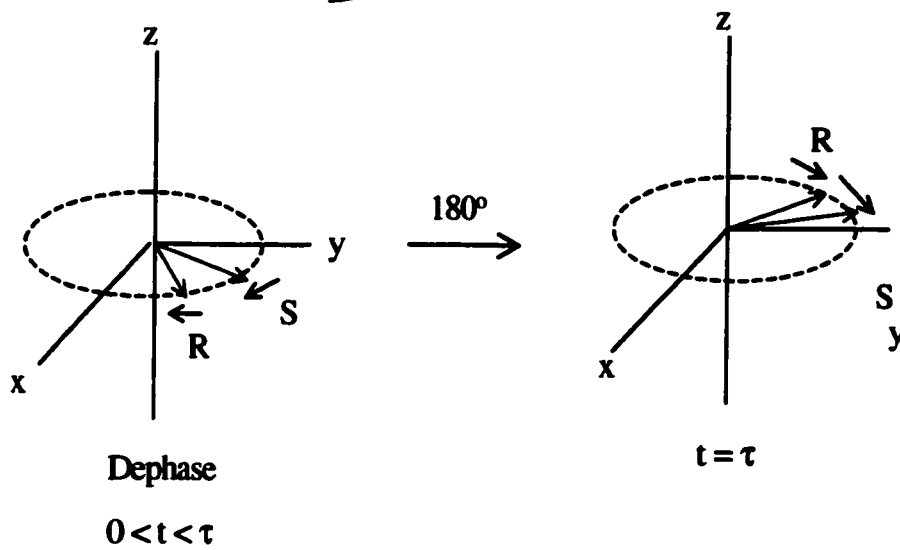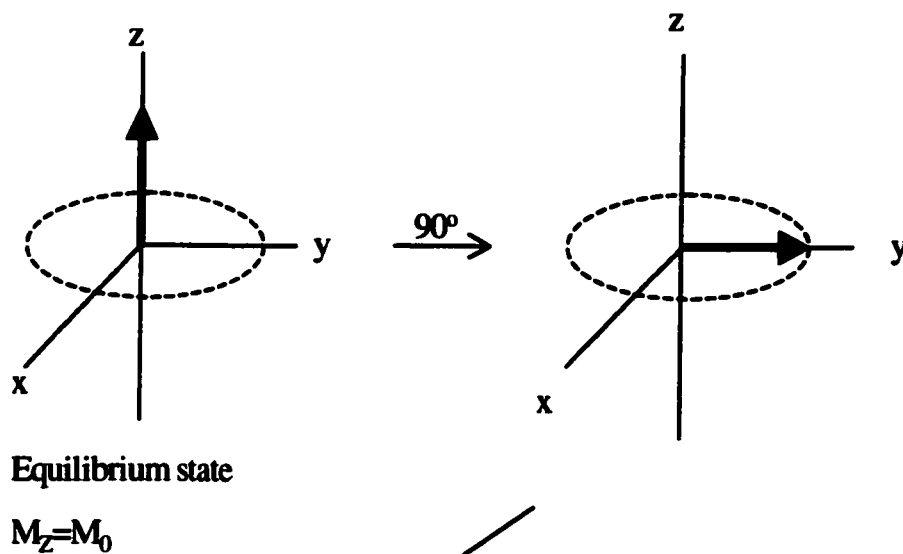
(Continue on next page)
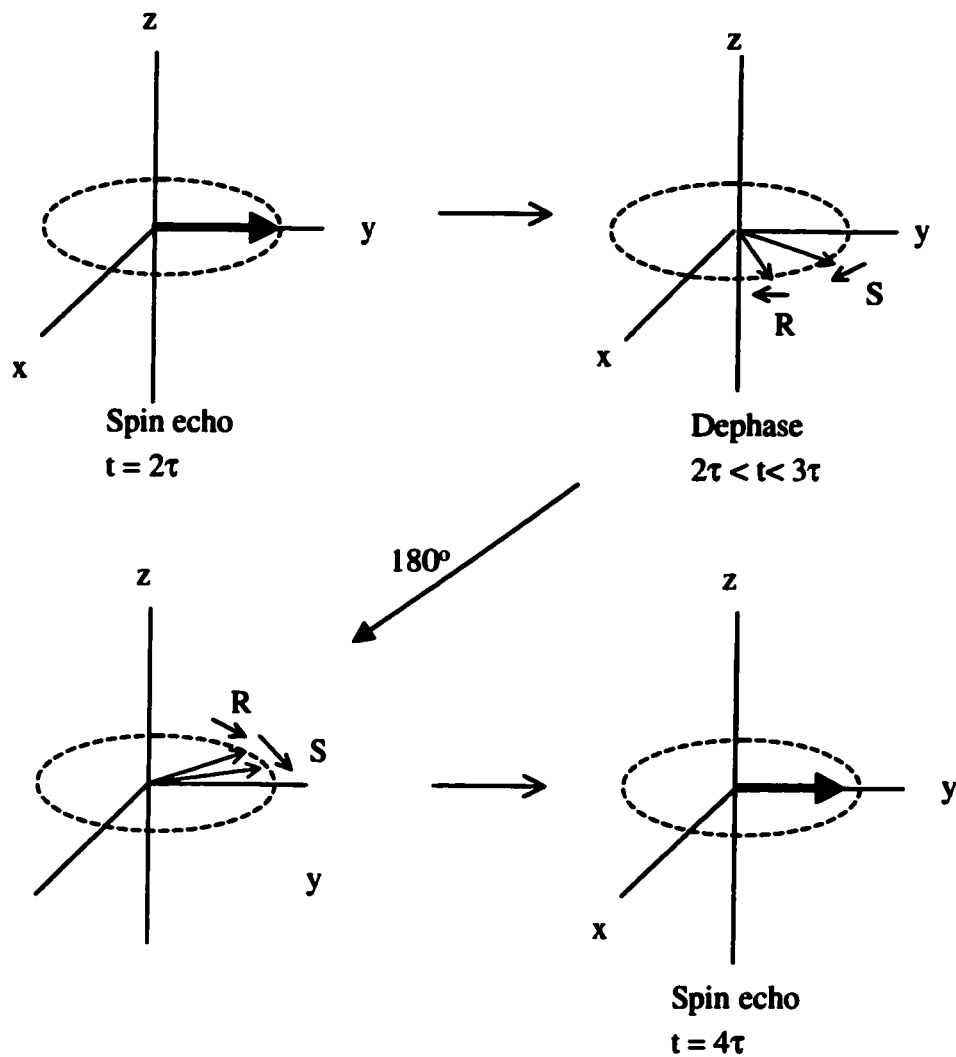
Figure 3.3.2 The CPMG pulse sequence for the T_2 measurement. The 90° pulse is first applied to flip the magnetization to the y axis, and then the spin isochromats dephase due to the inhomogeneity of the static magnetic field. After time τ, a 180° pulse is applied along the y axis and the spin echo occurs at time 2τ.

IV. Molecular Diffusion

In the uniform, homogeneous fluid, molecules undergo random translational motion driven by kinetic energy. This is the self-diffusion characterized by the self-diffusion coefficient, D. The Stokes-Einstein equation (Einstein, 1956) is the most important relation between diffusion and viscosity in liquids. According to the Stokes-Einstein Equation, the self-diffusion coefficient is defined in terms of the velocity autocorrelation function, $\langle U(0)U(t) \rangle$,

$$D = \int_0^\infty \langle U(0)U(t) \rangle dt = \frac{kT}{4\pi a \eta}. \tag{4.1}$$

The self-diffusion coefficient is related to the thermal energy kT and the viscous drag on a sphere.

The determination of the self-diffusion coefficient can be based either on measurements of the flux density and the concentration gradients or on measurements of the particle distribution at different times. Molecular concentrations can be determined by chemical and various physical methods. Consequently, a variety of experimental techniques have been developed to determine the self-diffusion coefficient of systems. NMR provides a convenient method for measuring self-diffusion coefficients. The early NMR self-diffusion measurement used the Carr and Purcell (CP) method (Carr and Purcell, 1954). A 90° pulse is first applied to flip the magnetization to the y axis. Then the spin isocromats dephase for a time duration τ, due to the inhomogeneity of the magnetic field. At time τ, a 180° pulse is applied along the x axis to flip the spins. At a time 2τ, the spins converge, creating an echo. The echo amplitude at time 2τ, $M(2\tau)$, is expressed as

$$M(2\tau) \propto e^{-\frac{2\tau}{T_2} - \frac{2\gamma^2 G^2 D\tau^3}{3}} \quad . \tag{4.2}$$

Through the application of a sufficiently large gradient, G, the self-diffusion coefficient can be determined by repeating the sequence for different τ values,

$$\ln R' = \ln \frac{M(2\tau)}{M(0)} = -\frac{2\gamma^2 G^2 D\tau^3}{3} . \tag{4.3}$$

In Equation (4.3), $M(0)$ is the echo amplitude when the gradient is turned off. When $\ln$ (R') is plotted as a function of τ^3, the slope of the straight line is $-2\gamma^2 G^2 D/3$.

However, the CP method for measuring self-diffusion coefficients has several limitations. In the CP method, the magnetic field gradient must be turned on throughout the whole experiment, which has several negative consequences. The NMR linewidth is broadened by the gradient particularly with the gradient strength needed for the measurements of very small diffusion coefficients. Thus the FID becomes short and the echo amplitude decreases.

The broadening of the linewidth may cause the incomplete focus of magnetization in the x-y plane if the RF pulse is not short enough. To avoid this problem, the power output of the pulse transmitter must be increased in order to keep B_1 greater than the linewidth. When the gradient field is strong, the bandwidth of the detection system has to be large to improve its transient response, and the increase of bandwidth will admit more noise.

Furthermore, the CP method has a lower limit of about 10^{-7} cm^2/sec. In addition, the CP method does not allow the determination of restricted diffusion. The restricted diffusion happens when the time for the molecule to reach the boundary is shorter than

the time the molecule is monitored. The apparent diffusion coefficient is dependent on the spatial restriction.

The pulse gradient spin-echo method developed by Tanner and Stejskal (Tanner and Stejskal, 1968) overcomes some of these limitations. The sequence of the pulse gradient spin-echo method is shown in Figure 4.1. The magnetic field gradient of strength g and duration δ is applied twice. The 90° pulse flips the magnetization to the y axis, and the spin isochromats start to dephase due to the inhomogeneity of the magnetic field. Then the first gradient pulse is applied, followed by a 180° pulse. The gradient causes the spins to dephase more rapidly, with the normal rate of dephasing resuming after the gradient pulse. The 180° pulse serves to effectively reverse the direction of dephasing. The second identical gradient pulse is applied after the 180° RF pulse to affect the dephasing rate. The time interval between two RF pulses is τ, and the time between two gradient pulses is Δ. A spin-echo occurs at time 2τ.

For unbounded diffusion, the random walk motion of molecules can be described as a probability function $P(r_0 \mid r, t)$. r_0 is the initial position of a molecule, and r is the position that it moves to after the time interval t. According to Fick's law, the probability can be described as

$$P(r_0 \mid r,t) = \left(4\pi Dt\right)^{-\frac{3}{2}} e^{-\frac{(r-r_0)^2}{4Dt}} . \tag{4.4}$$

This corresponds to a Gaussian distribution with variant $2Dt$. For a nuclear spin that diffuses according to the above equation, the spin echo amplitude attenuation R' for the pulse gradient experiment is given by

$$R' = \frac{M}{M(0)} = e^{-\gamma^2 \delta^2 g^2 (\Delta - \frac{1}{3}\delta)D} . \tag{4.5}$$

M is the echo amplitude with applied gradient, *g*, and *M*(0) is the echo amplitude when the gradient is off.

When measuring the diffusion coefficient with the pulse gradient spin-echo sequence, *g*, δ or Δ can be varied. If we take the natural logarithm of Equation (4.5), we obtain

$$\ln(R') = -\gamma^2 \delta^2 G^2 \left(\Delta - \frac{1}{3}\delta\right) D \qquad (4.6)$$

The diffusion coefficient can be calculated by plotting $\ln(R')$ against $-\gamma^2 \delta^2 G^2 \left(\Delta - \frac{1}{3}\delta\right)$. The slope is the diffusion coefficient.

Since the gradient does not have to be turned on all the time, the linewidth broadening problem is eliminated for the pulse gradient spin-echo sequence. Also the limit of the diffusion coefficient being measured is smaller. The lower limit is about 10^{-9} cm^2/sec. This method also has the ability of measuring restricted diffusion.
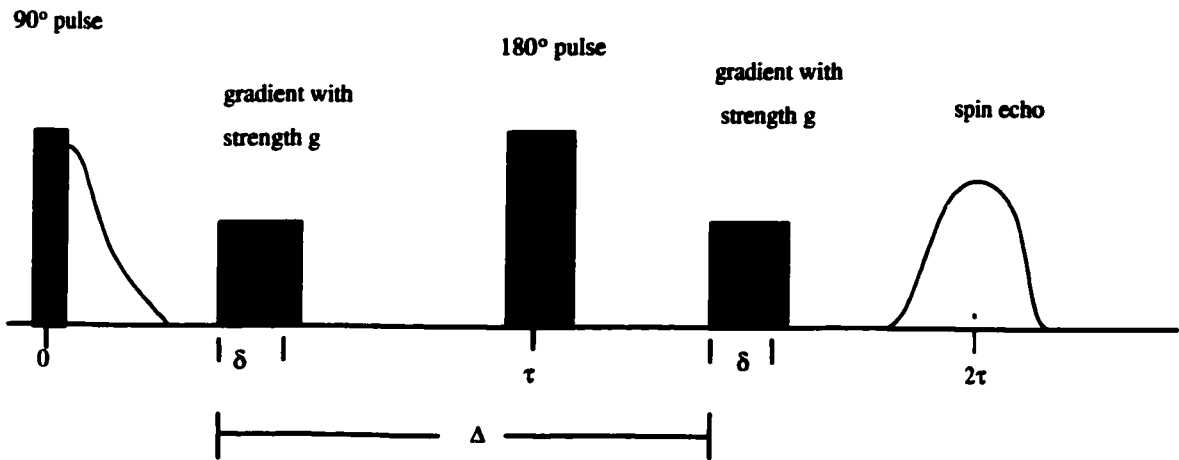
Figure 4.1 The sequence of the pulse gradient spin-echo method. The 90° pulse flips the magnetization to the y axis, and the spin isochromats start to dephase due to the inhomogeneity of the magnetic field. Then the first gradient pulse is applied, followed by a 180° pulse. The gradient causes the spins to dephase more rapidly, with the normal rate of dephasing resuming after the gradient pulse. The 180° pulse serves to effectively reverse the direction of dephasing. The second identical gradient pulse is applied after the 180° RF pulse to affect the dephasing rate. A spin-echo occurs at time 2τ.

V. Experimental Procedure

5.1 Equipment

Four NMR spectrometers were used to measure relaxation times of crude oils at ambient pressure. A Bruker minispec NMR spectrometer using a 20 MHz permanent magnet is coupled with a variable temperature controller unit. This 20 MHz NMR spectrometer is used to measure relaxation times of crude oils at 60 °C and 100 °C. The temperature of the magnet remained stabilized at 40 °C throughout the experiment. The other three spectrometers use permanent magnets operating at 2 MHz, 7.5 MHz and 20 MHz respectively. The 2 MHz spectrometer is the MARAN Ultra NMR spectrometer operating at 30°C while the 7.5 MHz and 20 MHz spectrometers are Bruker minispec NMR spectrometers operating at 40°C.

Relaxation times and self-diffusion of ethane and propane at elevated temperatures and pressures were measured using a NMR spectrometer with a 89 MHz super-conducting magnet that has been described earlier (Etesse, 1992; Lo, 1999). This spectrometer was connected with a high pressure vapor-liquid equilibrium apparatus and a temperature regulated air bath that maintains a constant temperature of the fluid as it is introduced to the NMR probe. A schematic diagram of the apparatus is shown in Figure 5.1.1. The super-conducting magnet was made by Oxford with the proton frequency of 89 MHz. It was kept at liquid helium temperature. The probe was suitable for high pressure fluids by constructing the sample chamber and sensing coils inside the pressure vessel.

The temperature was controlled by an air bath with an operating range of 20 °C to 60 °C. Eight coiled Nichrome heating elements were installed in the lower section of the air bath. Six of the heating elements were connected in series to a power stat to supply a baseline output. The others were connected to a Bayley Model 123 precision temperature controller. Figure 5.1.2 showed the actual NMR system. Four blowers circulated the air from the bath externally to the probe. Two of them were right below the heating elements and blew the hot air to the upper part of the air bath system. The top blower moved hot air to the probe through PVC pipes and the exhausted hot air was sucked out of the conduit by the bottom blower. Thus the return air went through the heater unit and was reheated. The temperatures were measured by three non-magnetic resistant temperature detectors (RTDs) installed in the closed air bath system, at the probe and at the magnet bore. The RTDs were connected to Omega Model CN77373-C2 temperature meters. The temperature accuracy was ± 0.2 °C. The reported temperature was the one taken at the sample probe. In addition, the cool air was blown between the magnet bore and the PVC liner during the higher (30 °C and above) temperature experiments. Using this technique, the magnet bore can be kept below 25 °C.

Two high pressure tubes were used to connect the sapphire cell and the sample probe. The samples were transferred to and from the probe by a magnetic pump.

The system pressure was generated by two HiP Model 62-6-10 high pressure hand pumps. For fluid experiments, a hand pump with bigger volume was introduced to the system, which can help achieve high pressure. The pressures were measured at three different locations. Two Setra Model 204 pressure transducers with pressure range 0 to 5000 psig were installed near the HiP high pressure pumps, and one Setra Model 280E

pressure transducer with pressure range 0 to 10000 psig was installed between the sapphire cell and the NMR probe. All of the pressure transducers were connected to the Omega Model DP41-S high performance strain gauge indicators for pressure readings.

The viscosity for crude oils was measured by an ARES rheometer with a circulating temperature bath and a Brookfield LVDV-III+ rheometer coupled to a Haake DC50-K35 thermostatic bath.

5.2. Sample Preparation

Pure ethane and propane gases were obtained from Matheson Gas Products. The quality of both ethane and propane was Matheson purity, 99.95% minimum. The oxygen content was less than 2 ppm. No further purification of ethane and propane was attempted except for further removal of oxygen.

Oxygen presence affects relaxation time significantly since it is paramagnetic (Johnson and Waugh, 1961). The oxygen contained in ethane and propane gases was further removed by passing the gases through an oxygen absorbing purifier, Matheson Model 6411. The oxygen content should be less than 0.1 ppm after purifying.

The apparatus was cleaned before introducing a new sample. The apparatus was filled with hexane for one day and then the hexane was flushed out. Then the apparatus was heated to 50 °C and evacuated for at least eight hours to ensure complete removal of hexane. The cleaning procedure was performed three times.

Thirty-one crude oils from various fields were used in this investigation. The crude oil samples analyzed included SMY, SMP, SMT, SM, M13, M11, SMID, M4, M14, CO, DB, SMP69, NB, M2, M1, SWCQ, M10, BP, BC1, BC2, BC3, CH1, CH2,

CH3, CH4, CH5, CH6, CH7, CH8, CH9 and CH10. For the 7.5 MHz and 20 MHz Bruker NMR spectrometers at 40 °C, the sample tubes were 13 mm in diameter. For the 20 MHz Bruker NMR spectrometer with the variable temperature controller unit, the sample tubes were 10 mm in diameter. Sample handling was performed only in clean glassware. First, the glassware was thoroughly cleaned with toluene and acetone. Then it was rinsed with tap water and deionized water. Using disposable pipettes, oil samples were transferred into the sample tubes to a height of about 1 cm. To remove oils that stuck to the column of the sample tubes, a chemwipe was wrapped around a pipette, which was then inserted and revolved within the sample tubes. The sample tubes were then capped, labeled, and saran-wrapped to prevent evaporation. The oil samples were preconditioned in a thermostat at the measurement temperature for at least 30 minutes before relaxation measurements were taken.

5.3 Spin-Lattice and Spin-Spin Relaxation Measurements

The spin-lattice relaxation time T_1 was measured by the standard inversion recovery sequence (Farrar and Becker, 1971; Fukushima and Roeder, 1993). For each measurement, 35 to 50 FIDs were acquired over duration time t up to six times the longest T_1. The data collected were $M(t)$ as a function of time t. The amplitude $M(0)$ was determined at least four times by taking the maximum point of the FID and the average was used. The $M(t)$-t curve can be converted to a T_1 distribution based on the following equation:

$$M(t) = \sum_i M_i(0)\left(1 - 2e^{\frac{-t}{T_{1i}}}\right).$$

(5.3.1)

The T_1 fitting algorithm used in this work was developed in previous work (Chuah, 1996; Huang, 1997).

The Carr-Purcell-Meiboom-Gill (CPMG) method (Farrar and Becker, 1971) described in Section 3.3 was used for the spin-spin relaxation measurements. The raw data were fitted to the multi-exponential decay equation

$$M(t) = \sum_i M_{0_i} e^{-\frac{t}{T_{2i}}}$$ (5.3.2)

to obtain a T_2 distribution. The fitting algorithm was developed in previous work. Regularization algorithm was used to obtain T_2 distributions (Chuah, 1996; Huang, 1997).

5.4.Self-Diffusion Measurements

The pulse gradient spin-echo sequence (Tanner and Stejskal, 1968) described in Chapter 4 is used for diffusion measurements. For each measurement, the gradient duration δ was changed. 30 to 40 data points were taken at different δ's, and the corresponding echo amplitude was recorded. All other variables (gradient strength g and the duration between two pulses Δ) were kept constant within one experiment. For each sample, a distribution of the diffusion coefficient can be obtained by fitting the raw data to

$$M = \sum_i M_{0i} e^{-\gamma^2 \delta^2 g^2 \left(\Delta - \frac{1}{3}\delta\right) D_i}.$$ (5.4.1)

The logarithmic mean diffusion coefficient was calculated from the distribution.

5.5. Estimation of Viscosity

Figure 5.5.1 compares the estimated viscosity by SUPERTRAPP with literature experimental data (Eakin et al., 1962) for pure ethane at 70, 100 and 130 °F in temperature, and 15 to 7000 psia in pressure. SUPERTRAPP is a software for thermodynamic and transport properties estimation (NIST, 1999). It turns out that SUPERTRAPP gives close estimations for ethane at temperature higher than 70 °F. For estimation at lower temperature (70 °F), the error increases with pressure. Therefore, interpolations of experimental data were used to estimate ethane viscosity.

Viscosity of pure propane was estimated by SUPERTRAPP. Estimated viscosity data by SUPERTRAPP were compared with literature experimental data (Starling et al., 1960) at 70, 100 and 130 °F in temperature, and 200 to 7000 psia in pressure. Figure 5.5.2 shows the results of the comparison. SUPERTRAPP can give good estimation at the temperature range from 70 °F to 130 °F. Since most of the measurements are in this temperature range, SUPERTRAPP estimations are adequate within experimental conditions.
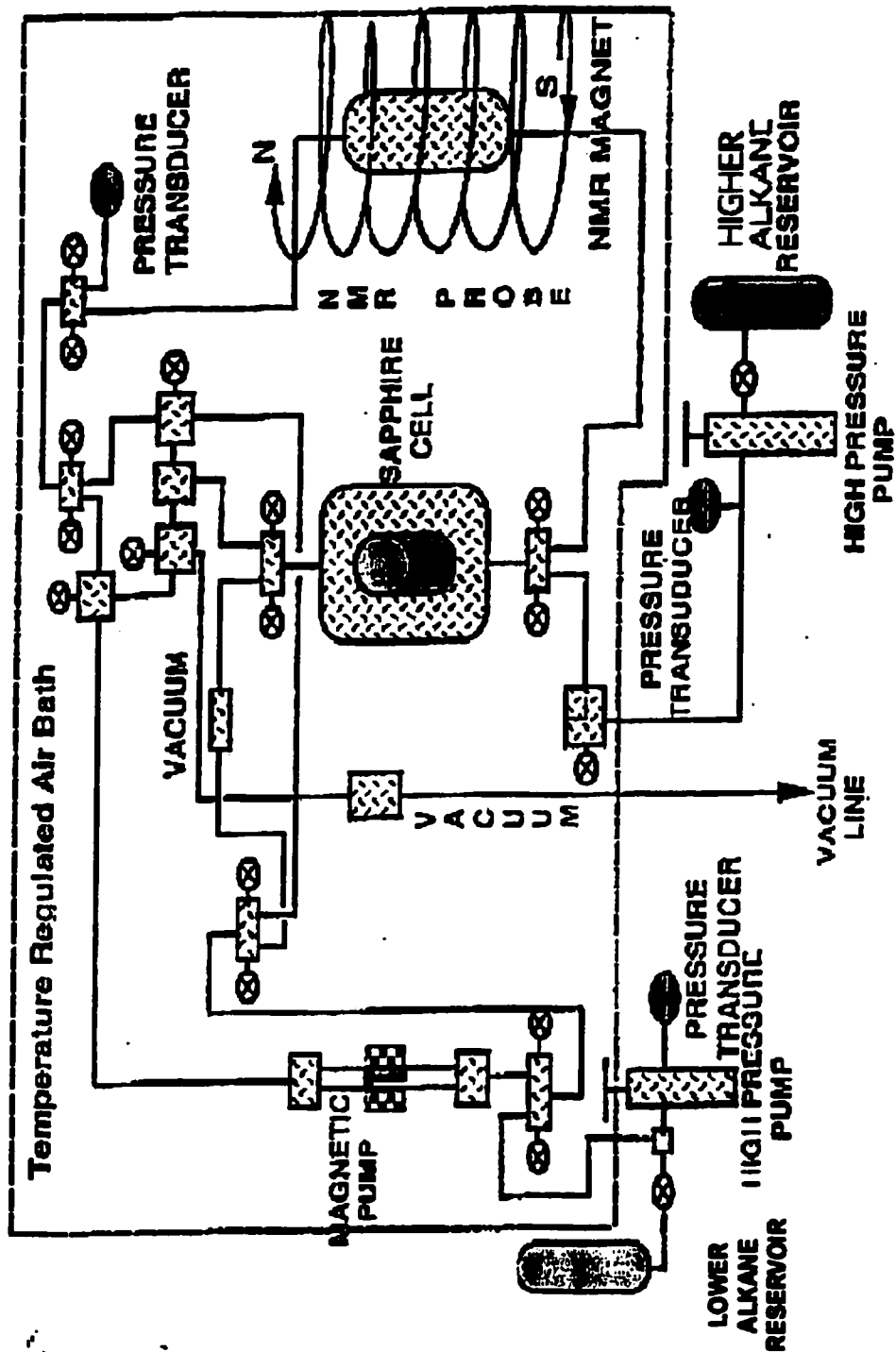
Figure 5.1.1 The schematic diagram of the high pressure NMR apparatus. The 89 MHz spectrometer was connected with a high pressure vapor-liquid equilibrium apparatus and a temperature regulated air bath.
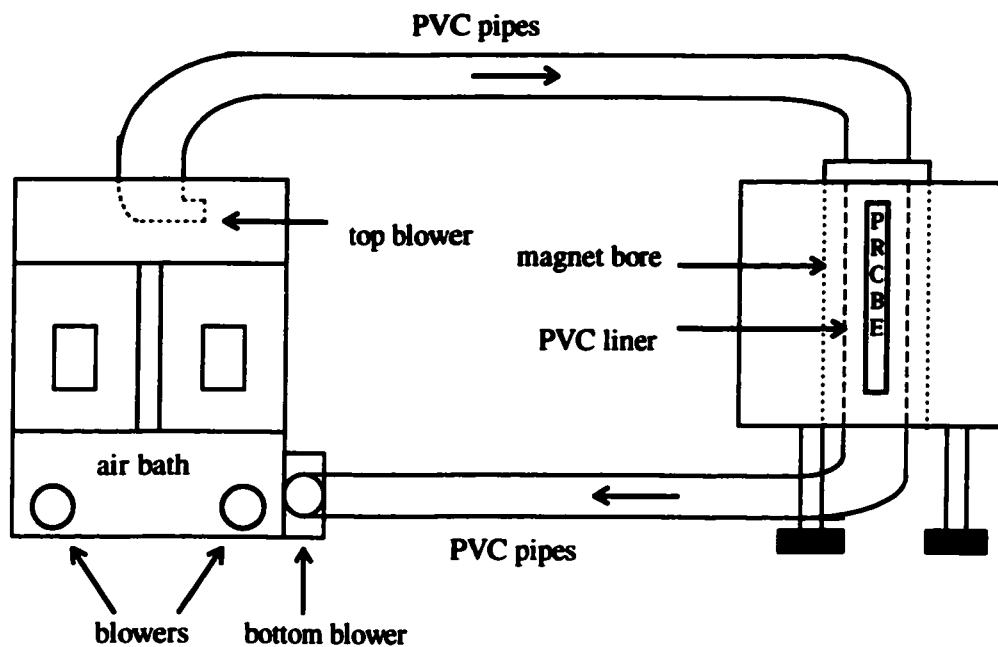
Figure 5.1.2 The NMR system (Lo, 1999). Two high pressure tubes were used to connect the sapphire cell and the sample probe. The samples were transferred to and from the probe by a magnetic pump.

(a)
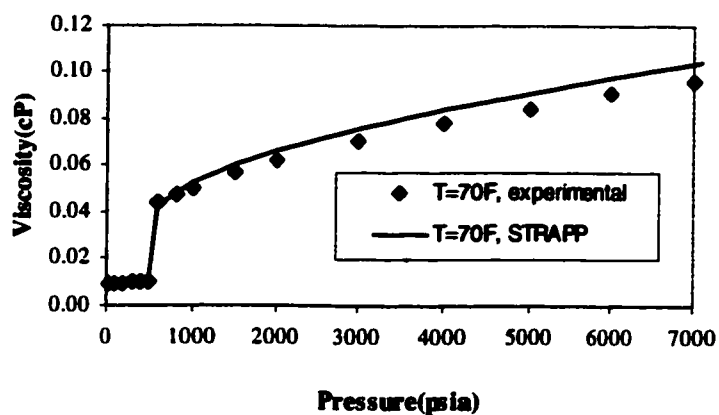
(b)
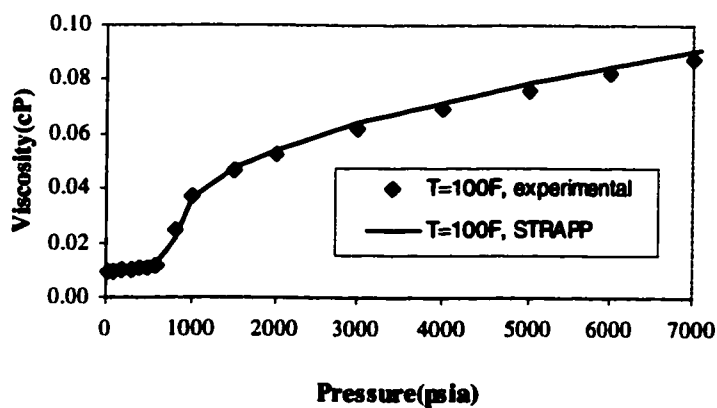
(c)
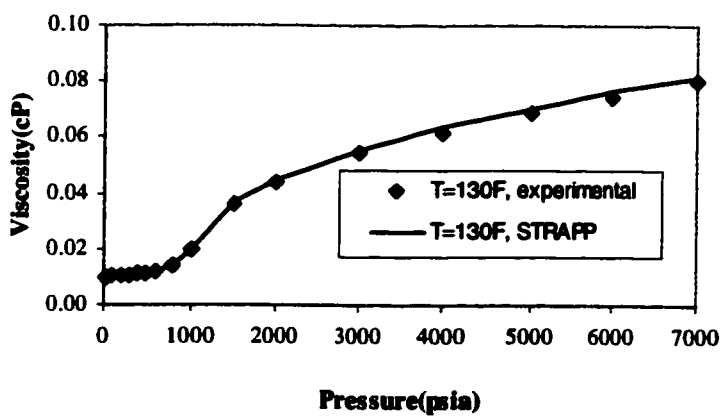
Figure 5.5.1 Comparison of viscosity for pure ethane – experimental (Eakin et al., 1962) and SUPERTRAPP. SUPERTRAPP gives close estimations for ethane at temperature higher than 70 °F. For estimation of lower temperature (70 °F), the error increases with pressure.

(a)
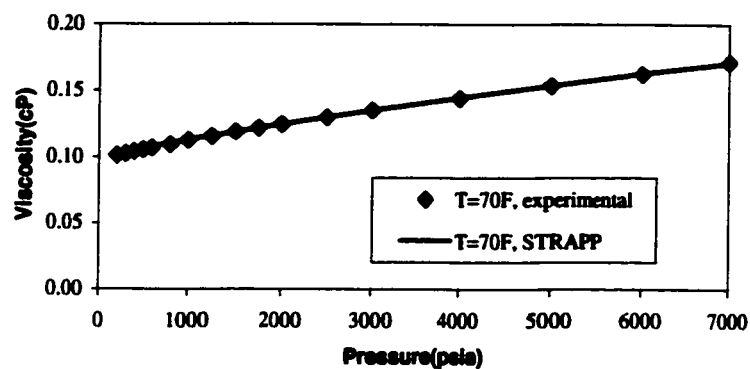
(b)
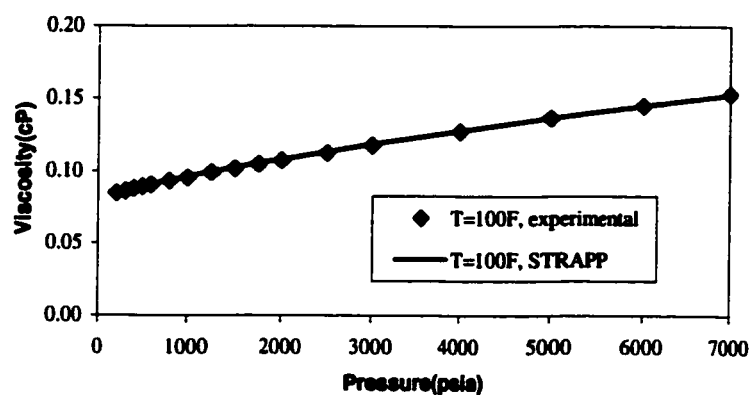
(c)
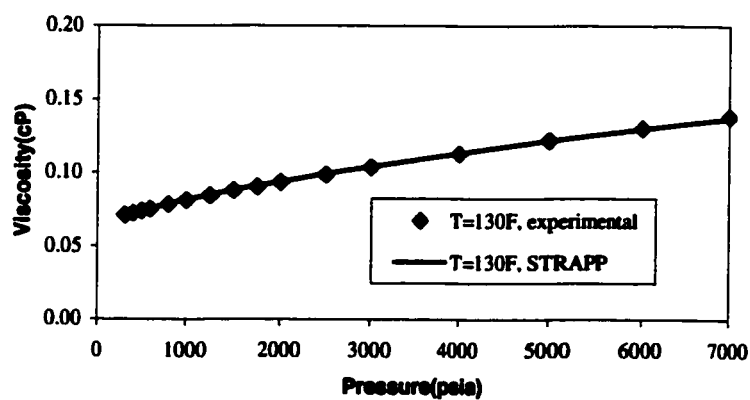
Figure 5.5.2 Comparison of viscosity for pure propane – experimental (Starling et al., 1960) and SUPERTRAPP. SUPERTRAPP can give good estimation for propane at the temperature range from 70 °F to 130 °F.

VI. Spin-Lattice Relaxation and Self-Diffusion in Ethane and Propane

6.1.Relaxation Times

Relaxation times of pure ethane and propane were measured at various temperatures and pressures. The results are shown in Table 6.1.1 and Table 6.1.2 respectively.

Figure 6.1.1 is the plot of relaxation time versus viscosity/temperature for pure ethane, pure propane, pure methane (Gerritsma et al., 1971), and other pure alkanes (Kashaev et al., 1964; Zega, 1987). The relaxation time of ethane as a function of viscosity/temperature departs significantly from the relationship that is common for higher alkanes. This indicates that both the spin rotation and the dipole-dipole relaxation are contributing to the relaxation process for ethane. Propane departs from the relationship that is common for higher alkanes only at elevated temperatures. This indicates that the relaxation of propane is dominated by the dipole-dipole mechanism but that the spin rotation mechanism has a contribution at higher temperatures.

Figure 6.1.2 shows the plot of T_1 versus viscosity based on the same data. It is interesting to note that the data points of methane, ethane, and propane fall on the same curve in this plot. In addition, the data points of propane converge to the straight line of higher alkanes with increasing viscosity. Liquid ethane follows the same correlation of pure alkanes. Currently, we have no satisfactory explanation for the better interpretation of data by eliminating the temperature term.

6.2. Diffusion Coefficients

Self-diffusion coefficients of ethane were also measured at various temperatures and pressures. The result is shown in Table 6.2.1. The attempt to measure diffusion coefficients for propane was not very successful. The power supply to the NMR spectrometer was changed due to the laboratory renovation in Abercrombie Laboratory. And the new power line introduced significant noise. For the propane gas, the spin echo signal is too small to be measurable. Diffusion coefficient measurement can be made for liquid propane, but the noise was still large although the scan number was doubled. The diffusion coefficient data obtained for the propane system may show greater error than the ethane system. Table 6.2.2 summarizes the diffusion coefficient data for propane.

T_1 dependence on diffusion coefficient is plotted. Figure 6.2.1 is the plot of log mean T_1 against diffusion coefficient for ethane, propane and other alkanes (Lo, 1999). Ethane and propane depart from the straight line of the pure higher alkanes.

Diffusion coefficient dependence on viscosity/temperature was plotted in Figure 6.2.2. The Stokes-Einstein equation (Einstein, 1956) as shown in Equation (4.1) relates the diffusion coefficient D to viscosity η and temperature T. Diffusion coefficients are proportional to T/η. And the curve shown in the Figure 6.2.2 is $D=5.05\times10^{-8}\times T/\eta$, where D is expressed in cm^2/sec, viscosity is expressed in cP and T is absolute temperature in K (Lo, 1999). The literature diffusion coefficient data for ethane and propane are also plotted here (Greiner-Schmid et al., 1991; Helbæk et al., 1996; Woessner et al., 1969). The data from this work agree with the literature data. The inverse relationship between the self-diffusion coefficient and viscosity/temperature for methane, higher alkanes, and methane-higher alkane mixtures also applies to ethane and propane. This result is

consistent with the Stokes-Einstein equation. This is to be expected as the self-diffusion

and viscosity are independent of the NMR relaxation mechanisms.

Table 6.1.1 Spin-lattice relaxation times of pure ethane

Temp. (°C)	Pressure (psia)	Viscosity (cP)	Visc./Temp. (cP/K)	Log mean T_1 (sec)
19.4	433	9.48E-03	3.24E-05	7.20
19.3	495	9.68E-03	3.31E-05	7.28
19.6	550	2.45E-02	8.38E-05	19.50
20.0	572	3.95E-02	1.35E-04	20.39
20.5	658	4.82E-02	1.64E-04	20.06
20.0	990	5.14E-02	1.75E-04	22.10
19.6	1612	5.85E-02	2.00E-04	21.24
19.9	2344	6.56E-02	2.24E-04	22.01
19.9	2948	7.07E-02	2.41E-04	19.52
20.3	2764	6.91E-02	2.35E-04	18.37
19.9	3825	7.76E-02	2.65E-04	19.40
20.0	4409	8.16E-02	2.78E-04	17.46
27.8	576	1.23E-02	4.09E-05	8.57
28.7	706	3.43E-02	1.14E-04	16.75
32.1	1336	4.78E-02	1.57E-04	18.28
33.4	761	2.87E-02	9.36E-05	17.64
34.9	1151	4.28E-02	1.39E-04	18.36
36.1	663	1.88E-02	6.08E-05	9.94
36.1	802	2.73E-02	8.82E-05	17.56
36.3	613	1.54E-02	4.98E-05	8.49
36.7	716	2.09E-02	6.76E-05	10.28
46.1	739	1.71E-02	5.36E-05	9.07

Table 6.1.2 Spin-lattice relaxation times of pure propane

Temp. (°C)	Pressure (psia)	Viscosity (cP)	Visc./Temp. (cP/K)	Log mean T_1 (sec)
18.7	114	8.48E-03	2.91E-05	3.93
29.0	150	8.91E-03	2.95E-05	5.66
33.0	160	9.05E-03	2.96E-05	3.79
20.2	211	1.04E-01	3.54E-04	21.69
20.7	403	1.06E-01	3.60E-04	21.11
19.4	639	1.21E-01	4.13E-04	19.86
20.4	971	1.14E-01	3.87E-04	21.71
20.8	1501	1.20E-01	4.07E-04	23.16
20.7	1994	1.25E-01	4.26E-04	22.65
20.7	2501	1.31E-01	4.44E-04	21.99
20.1	3026	1.37E-01	4.66E-04	20.99
20.4	4040	1.46E-01	4.98E-04	18.70
20.8	4569	1.51E-01	5.12E-04	20.91
20.8	5003	1.54E-01	5.26E-04	18.91
20.8	5940	1.63E-01	5.54E-04	18.72
52.5	304	7.22E-02	2.22E-04	26.85
52.3	604	7.75E-02	2.38E-04	26.42
51.8	1049	8.46E-02	2.60E-04	26.67
52.3	2023	9.60E-02	2.95E-04	25.49
52.5	2981	1.06E-01	3.25E-04	23.50
48.5	3960	1.18E-01	3.67E-04	23.24
52.5	3997	1.15E-01	3.53E-04	23.73
48.5	4987	1.27E-01	3.94E-04	21.58
52.5	5979	1.31E-01	4.03E-04	19.39

Table 6.2.1 Diffusion coefficients of pure ethane

Temp. (°C)	Pressure (psia)	Viscosity (cP)	Visc./Temp. (cP/K)	Log mean D (cm²/sec)
19.7	434	9.50E-03	3.24E-05	1.28E-03
19.2	483	1.13E-02	3.87E-05	6.05E-04
19.9	571	3.96E-02	1.35E-04	3.06E-04
20.1	722	4.91E-02	1.68E-04	2.56E-04
20.1	835	4.92E-02	1.68E-04	2.44E-04
20.2	925	5.04E-02	1.72E-04	2.35E-04
20.0	1560	5.80E-02	1.98E-04	2.38E-04
20.1	2233	6.46E-02	2.20E-04	2.32E-04
20.0	2929	7.04E-02	2.40E-04	2.05E-04
19.8	3791	7.71E-02	2.63E-04	1.98E-04
19.7	4557	8.27E-02	2.82E-04	1.87E-04
28.0	549	1.19E-02	3.96E-05	1.12E-03
28.0	577	1.23E-02	4.09E-05	1.40E-03
28.7	706	3.43E-02	1.14E-04	3.95E-04
32.0	1301	4.72E-02	1.55E-04	3.16E-04
33.4	761	2.87E-02	9.36E-05	5.30E-04
35.0	1137	4.20E-02	1.36E-04	3.40E-04
36.1	802	2.73E-02	8.82E-05	4.59E-04
36.3	614	1.54E-02	4.98E-05	9.02E-04
36.5	474	1.07E-02	3.46E-05	1.52E-03
36.7	715	2.09E-02	6.76E-05	7.84E-04
46.3	740	1.71E-02	5.36E-05	9.24E-04

Table 6.2.2 Diffusion coefficients of pure propane

Temp. (°C)	Pressure (psia)	Viscosity (cP)	Visc./Temp. (cP/K)	Log mean $D(cm^2/sec)$
18.4	124	1.04E-01	3.58E-04	1.77E-04
20.5	609	1.09E-01	3.71E-04	1.62E-04
20.6	986	1.14E-01	3.87E-04	1.19E-04
16.0	1967	1.30E-01	4.50E-04	1.04E-04
18.4	2988	1.38E-01	4.74E-04	1.10E-04
19.1	3958	1.47E-01	5.02E-04	1.11E-04
17.5	5027	1.59E-01	5.46E-04	1.04E-04
17.5	5943	1.67E-01	5.74E-04	8.56E-05
28.8	159	9.36E-02	3.10E-04	1.67E-04
40.0	219	8.30E-02	2.65E-04	2.17E-04
40.0	2161	1.08E-01	3.45E-04	1.32E-04
52.6	309	7.22E-02	2.21E-04	2.07E-04
52.5	5032	1.24E-01	3.80E-04	1.14E-04
52.5	6053	1.32E-01	4.05E-04	1.22E-04
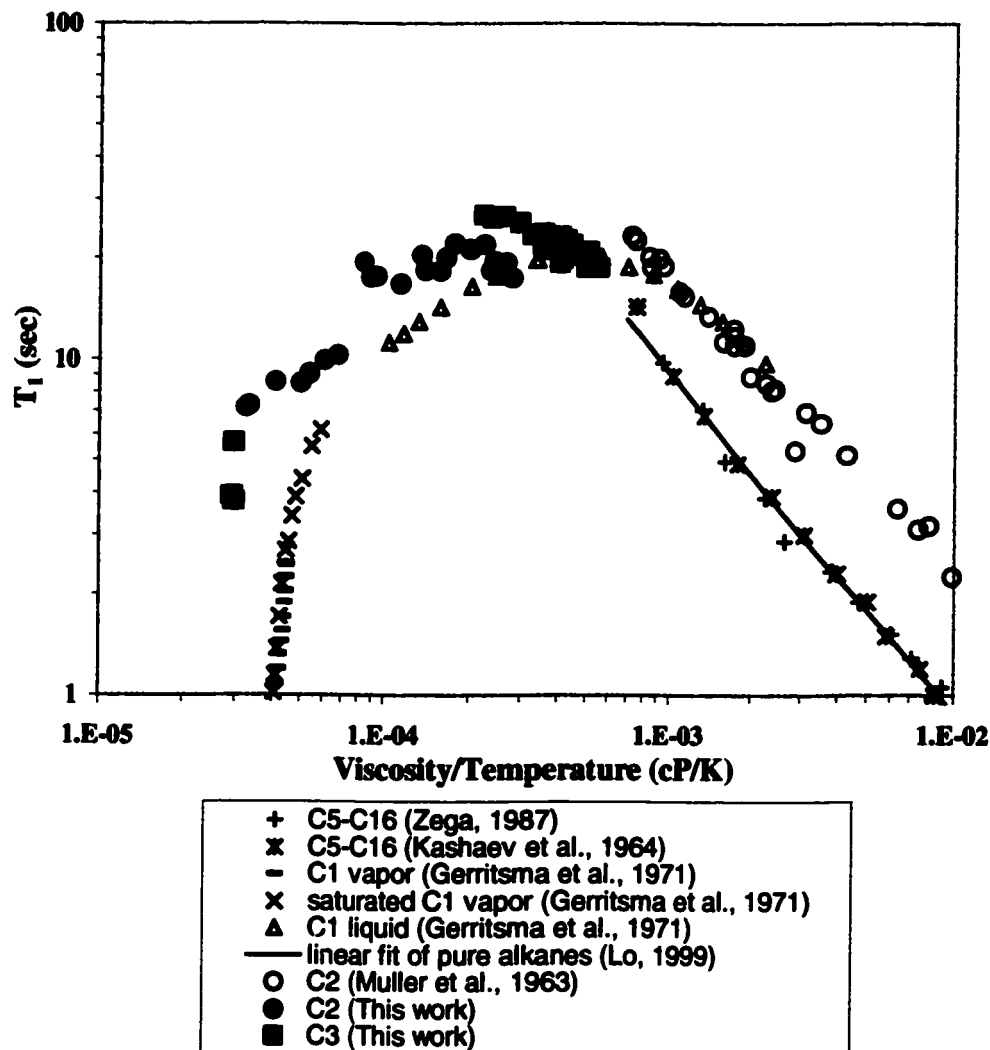
Figure 6.1.1 T_1 versus viscosity/temperature plot for pure alkanes. The relaxation time of ethane as a function of viscosity/temperature departs significantly from the relationship that is common for higher alkanes. Propane departs from the relationship that is common for higher alkanes only at elevated temperatures.

Legend:
+ C5-C16 (Zega et al., 1987)
✖ C5-C16 (Kashaev et al., 1964)
▲ C1 liquid (Gerritsma et al., 1971)
✗ saturated C1 vapor (Gerritsma et al., 1971)
○ C2 liquid (Muller et al., 1963)
● C2(T=20C-46C) (This work)
■ C3(T=20C-52C) (This work)
—— linear fit for pure higher alkanes (This work)
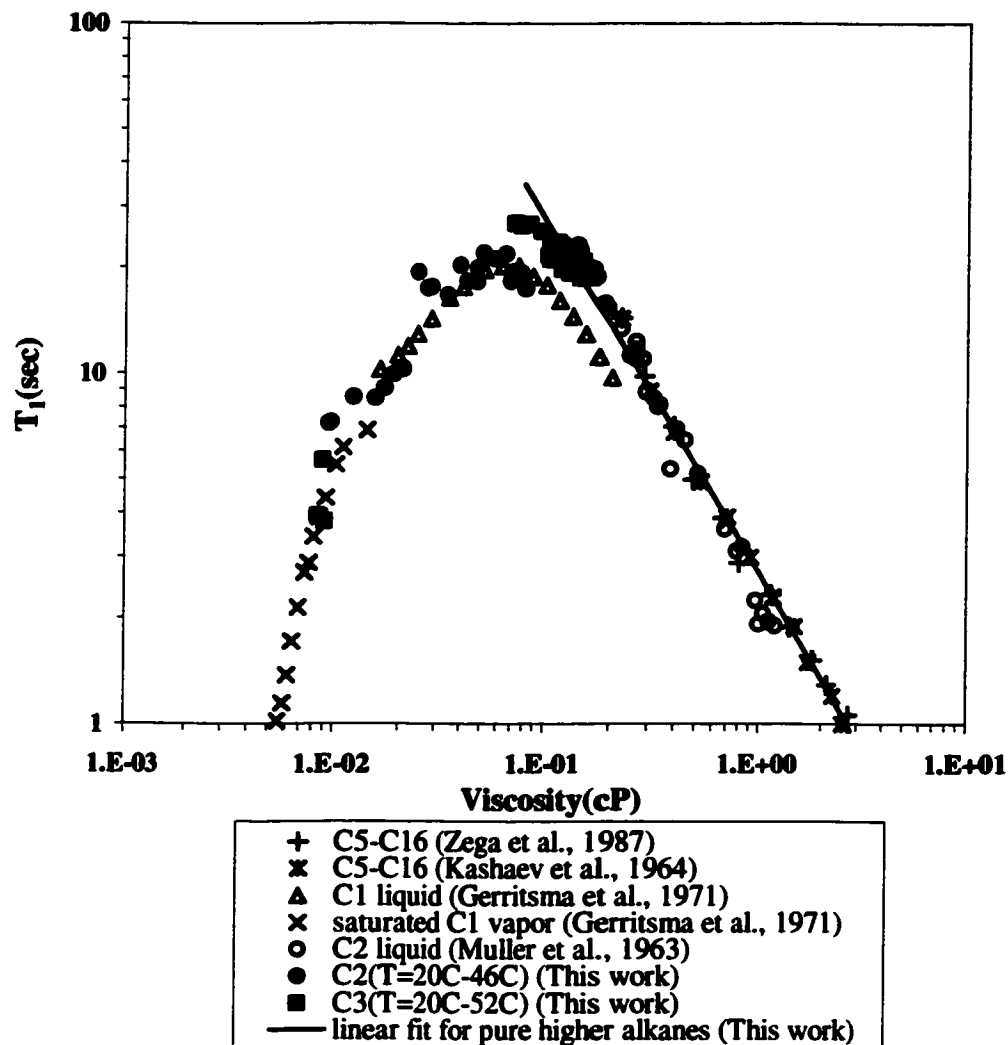
Figure 6.1.2 T_1 versus viscosity plot for pure alkanes. The data points of methane, ethane, propane and other alkanes fall on the same curve in this plot. In addition, the data points of propane converge to the straight line of higher alkanes with increasing viscosity. Liquid ethane follows the same correlation of pure alkanes.
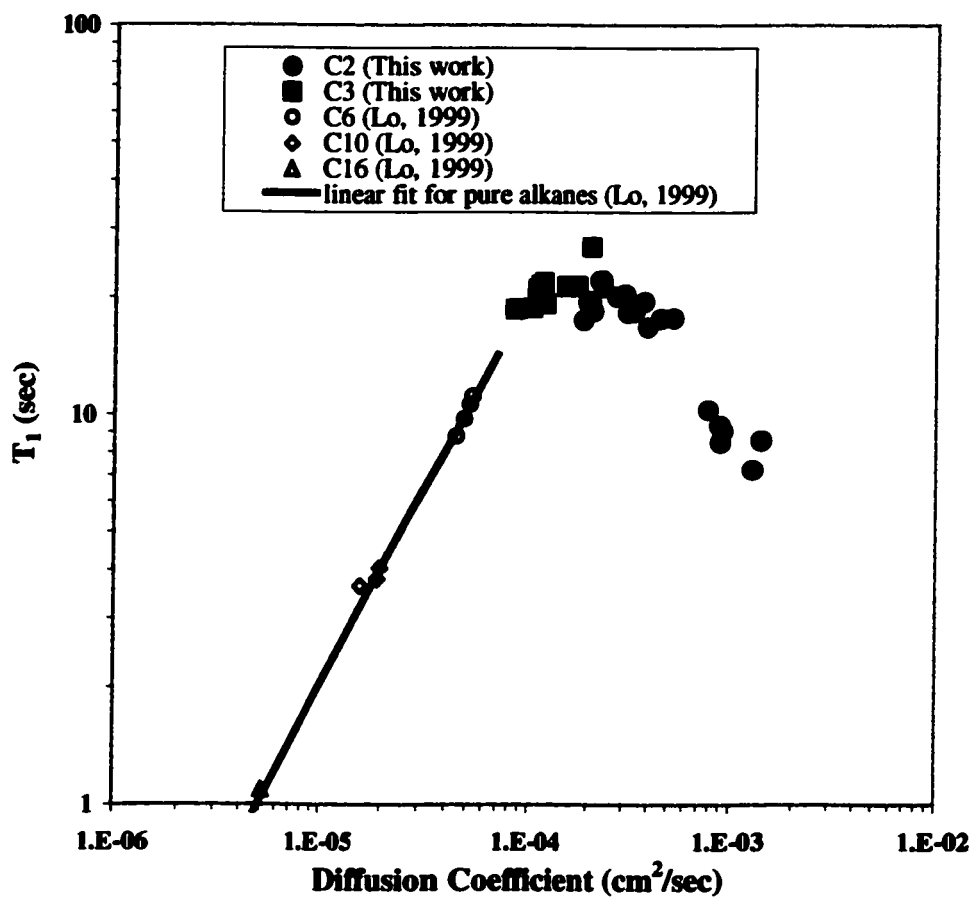
Figure 6.2.1 T_1 dependence on diffusion coefficient. Ethane and propane depart from the straight line of the pure higher alkanes.
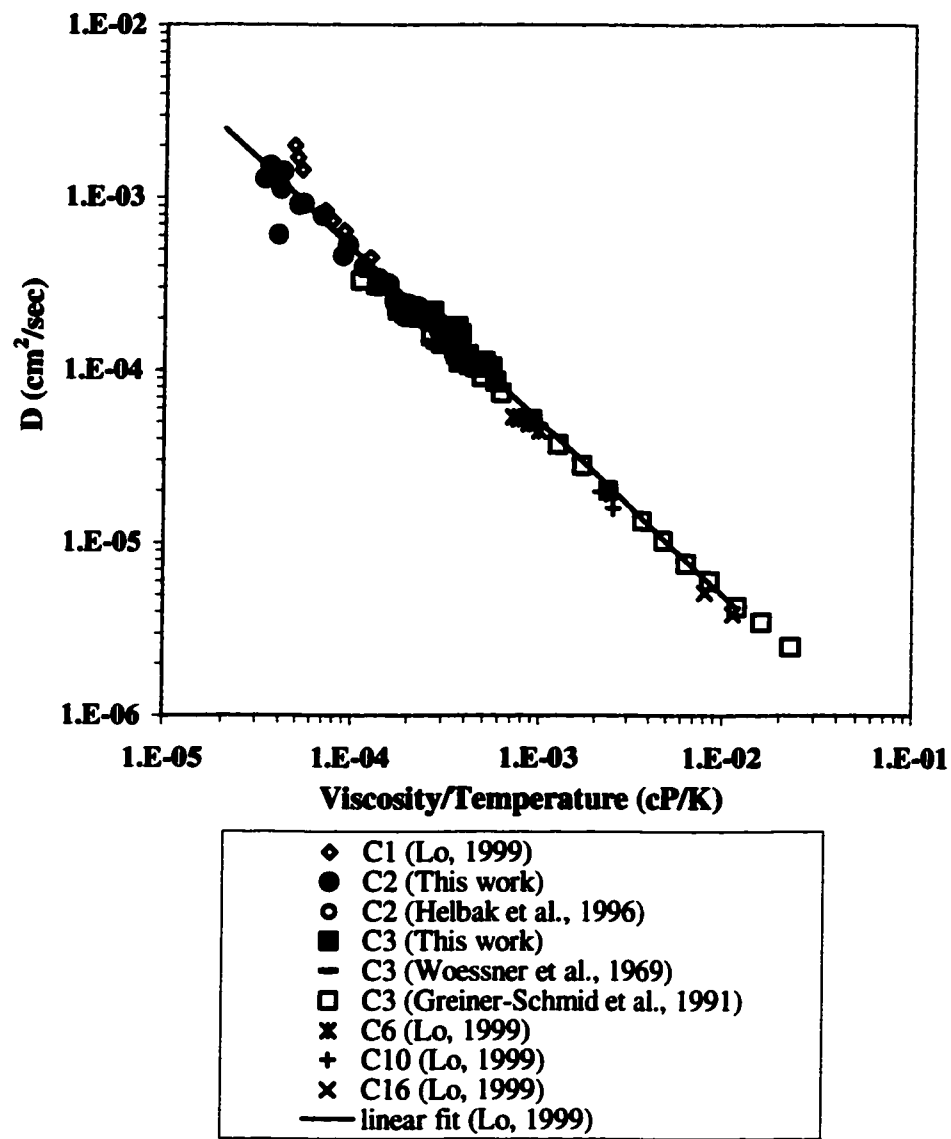
Figure 6.2.2 Diffusivity dependence on η/T for pure alkanes. The data from this work agree with the literature data. The inverse relationship between the self-diffusion coefficient and viscosity/temperature for methane, higher alkanes, and methane-higher alkane mixtures also applies to ethane and propane.

VII. Interpretation of Spin-Lattice Relaxation

7.1. Pure Components

7.1.1. Proton Spin Rotation Interaction in Methane Gas

Proton NMR relaxation times for methane have been measured by Gerritsma et al (Gerritsma et al., 1971; Lo, 1999). The contribution of the spin rotation interaction was extracted from proton T_1 data by assuming that gaseous methane relaxes only by the spin rotation interaction. Proton $T_{1, sr}$ data in methane were analyzed by both the kinetic model and the diffusion model.

The molecular constants of methane are presented in Table 7.1.1.

The numerical evaluation of Equation (3.2.22) and Equation (3.2.41) using the values in Table 7.1.1 for methane yields

$$\frac{1}{T_{1,sr}}(^1H) = 7.240 \times 10^8 T\tau_J \quad (CH_4, K.M., cgs),$$
(7.1.1)

$$\frac{1}{T_{1,sr}}(^1H) = 9.624 \times 10^8 T\tau_J \quad (CH_4, D.M., cgs).$$
(7.1.2)

In this thesis, K.M. represents the kinetic model, D.M. represents the diffusion model, and cgs represents cgs units. τ_J in the kinetic model can be evaluated by Equation (3.2.24). σ_J is available for methane in the literature and is listed in Table 7.2.1. So it is possible to predict the contribution of the spin rotation interaction in methane by theoretical equations.

Figure 7.1.1 shows $T_{1,sr}$ vs. $\rho/T^{1.5}$ plot for methane based on the kinetic model as shown by Equation (3.2.31). $T_{1,sr}$ is expressed in sec, ρ is expressed in mole/cm^3, and T is expressed in K. In order to be consistent with the discussion with ethane, we draw a straight line with the slope predicted by the models on the log-log plots to investigate the dependence of $T_{1,\ sr}$ on density and viscosity. The kinetic model can describe the spin rotation interaction in methane. As shown by Equation (3.2.45), the diffusion model predicts that T_1 by the spin rotation interaction is proportional to viscosity/temperature. A plot of $T_{1,sr}$ vs. viscosity/temperature based on the diffusion model is shown in Figure 7.1.2. It seems that the diffusion model fails to describe the spin rotation interaction in methane. The kinetic model is a better model for describing the spin rotation interaction in methane.

7.1.2. ^{1}H and ^{13}C Spin Rotation Interaction in Ethane Gas

Proton NMR T_1 for ethane has been measured in the temperature range from 293 K to 319 K. The contribution of the spin rotation interaction was extracted from proton T_1 data by assuming that ethane relaxes only by spin rotation interaction in the gaseous state. Whittenburg et al. (Whittenburg et al., 1992) measured the ^{13}C NMR T_1 for ethane in the temperature range from 172 to 323 K. They extracted the contribution of the spin rotation interaction from ^{13}C T_1 data based on NOE measurements. So with this data, it is possible to analyze ^{1}H and ^{13}C $T_{1,\ sr}$ data in ethane using both the kinetic model and the diffusion model.

The spin rotation constants for the protons in ethane have not been reported, however, they can be estimated from the average paramagnetic shielding, σ_p' of the

proton (Deverell, 1970; Flygare, 1964; Flygare and Goodisman, 1968; Rigny and Virlet, 1967). We may calculate the spin rotation constants from the well-known relationship between the shielding and the spin rotation constants (Deverell, 1970; Flygare, 1964),

$$\sigma_p' = \sigma_{total}' - \sigma_d' = \frac{2\pi}{3\hbar g}\frac{m_p}{m_e}\left(2C_\perp I_\perp + C_\parallel I_\parallel\right). \tag{7.1.3}$$

In this expression, g is the nuclear g factor, m_p and m_e are the mass of the proton and electron respectively, and σ_d' represents the atomic diamagnetic shielding, taken to be a constant 17.77 ppm (Flygare and Goodisman, 1968) for the proton. We then make use of the equations

$$\sigma_p' = \frac{1}{3}\left(2\sigma_\perp' + \sigma_\parallel'\right), \tag{7.1.4}$$

$$\Delta\sigma' = \sigma_\parallel' - \sigma_\perp'. \tag{7.1.5}$$

With $\sigma_p' = 12.2$ ppm and $\Delta\sigma' = 2.02$ ppm for ethane (Kaski et al., 1998), we obtain values for $\sigma_\parallel'$ and $\sigma_\perp'$. Now by equating Equation (7.1.3) and Equation (7.1.4), we obtain

$$\frac{1}{3}\left(2\sigma_\perp' + \sigma_\parallel'\right) = 6.23\times10^{36}\left(2C_\perp I_\perp + C_\parallel I_\parallel\right), \tag{7.1.6}$$

and therefore

$$\sigma_\perp' = 3\times6.23\times10^{36}C_\perp I_\perp, \tag{7.1.7}$$

and

$$\sigma_\parallel' = 3\times6.23\times10^{36}C_\parallel I_\parallel, \tag{7.1.8}$$

from which we obtain $C_\perp = 1.46\text{kHz}$ and $C_\parallel = 6.95\text{kHz}$.

The molecular constants of ethane are summarized in Table 7.1.2.

The numerical evaluation of theoretical equations using the values in Table 7.1.2 for ethane yields

$$\frac{1}{T_{1,sr}}(^1H) = 3.836 \times 10^8 T\tau_J \quad (C_2H_6, K.M., cgs) \tag{7.1.9}$$

$$\frac{1}{T_{1,sr}}(^1H) = T\left[9.255 \times 10^7 \tau_{J_\parallel} + 9.018 \times 10^7 (\tau_{J_\perp} + 1/D_\parallel) + 1.707 \times 10^8 \tau_{J_\perp}\right]$$
$$(C_2H_6, D.M., cgs) \tag{7.1.10}$$

$$\frac{1}{T_{1,sr}}(^{13}C) = 2.694 \times 10^9 T\tau_J \quad (C_2H_6, K.M., cgs) \tag{7.1.11}$$

$$\frac{1}{T_{1,sr}}(^{13}C) = T\left(5.853 \times 10^8 \tau_{J_\parallel} + 1.344 \times 10^8 \tau_{J_\perp}\right) \quad (C_2H_6, D.M., cgs)(7.1.12)$$

The theoretical equations of the diffusion model can predict the linear dependence of $T_{1,sr}$ on viscosity/temperature as shown by Equation (3.2.45). However, the analysis of NMR data indicates that $T_{1,sr}$ predicted by theoretical equations is almost always larger than the experimental result. The lack of knowledge of some parameters in the interpretation of τ_J by either the kinetic model or the diffusion model causes the difficulty in theoretical prediction of the contribution of the spin rotation interaction in ethane. Nevertheless, we can draw a straight line with the slopes predicted by both models on the log-log plots to investigate the dependence of $T_{1,sr}$ on density and viscosity. Figure 7.1.3 shows $T_{1,sr}$ vs. $\rho/T^{1.5}$ (K.M.) plots for ethane. The plots of $T_{1,sr}$ vs. viscosity/temperature (D.M.) are shown in Figure 7.1.4. Both the kinetic model and the diffusion model can describe ^1H $T_{1,sr}$ in ethane. It is apparent that ^{13}C $T_{1,sr}$ data in ethane follow the diffusion model better than they follow the kinetic model. Both ^1H and ^{13}C $T_{1,sr}$ data show that the diffusion model is an adequate model for the spin rotation interaction in ethane.

7.1.3. Proton Relaxation in Vapor and Liquid Ethane

For pure ethane, the total proton relaxation rate is accounted for by three interactions, i. e., the intra- and intermolecular dipole-dipole interactions and the spin rotation interaction. The total relaxation rate can be given by Equation (3.2.1).

7.1.3.1. Intermolecular Dipole-Dipole Interaction

In order to use Equation (3.2.3) to predict relaxation rates for ethane, we need to make two additional modifications.

Firstly, the effect of the radial distribution function is taken into account. The following equation for the intermolecular dipole-dipole interaction in ethane is obtained (Harmon, 1968; Harmon and Muller, 1969)

$$\frac{1}{T_{1,inter}} = R_{inter} = \frac{8\pi n v \gamma^4 \hbar^2 I(I+1)}{15 D \sigma}\left[1 + \frac{\langle r^2 \rangle}{\sigma^2}\left(\frac{5}{12} + 0.0672\Omega'\right) + 0.0521\Omega'\right],(7.1.13)$$

where $<r^2>$ is the root mean square distance of the random flight, and Ω' is as following

$$\Omega' = \frac{4}{3}\pi n \sigma^3 .\qquad(7.1.14)$$

For polyatomic molecules, such as ethane, a further effect must be considered. If the spins are not at the center of the molecule, the distance of closest approach of two spins will no longer be σ. In addition, the effect of rotation of the spin-bearing molecules on the purely translational relaxation should be considered. It turns out that these effects compete, the former tending to increase the relaxation rate, the latter decreasing it. Muller et al. (Muller, 1966) extended Hubbard's treatment to ethane and derived the following equation for the relaxation time by intermolecular dipole-dipole interaction

$$\frac{1}{T_{1,inter}} = R_{inter} = \frac{8\pi n v\gamma^4 \hbar^2 I(I+1)}{15D\sigma}\left[1+\frac{\langle r^2 \rangle}{\sigma^2}\left(\frac{5}{12}+0.0672\Omega\right)+0.0521\Omega\right]$$

$$\bullet\left[1+\alpha'\left(\frac{2d}{\sigma}\right)^2+\beta'\left(\frac{2d}{\sigma}\right)^4+...\right],\tag{7.1.15}$$

where d is the distance of protons from the center of the molecule and α' and β' are factors taken from the reference (Muller, 1966).

The result predicted by Equation (7.1.15) with two correction terms is in good agreement with Harmon's liquid ethane data (Harmon, 1968).

The numerical evaluation of Equation (7.1.15) gives

$$\frac{1}{T_{1,inter}} = 1.274 \times 10^5 \frac{\rho\eta}{T}\left[1+\left(\frac{5}{12}+0.0672\Omega\right)+0.0521\Omega\right]. \quad \text{(cgs)} \tag{7.1.16}$$

7.1.3.2. Intramolecular Dipole-Dipole Interaction

In contrast to the exponential autocorrelation function assumption, Moniz et al. (Moniz et al., 1963) used a Gaussian decay to evaluate the autocorrelation function and then the contribution of intramolecular dipole-dipole interaction to the relaxation rate can be written as

$$\frac{1}{T_{1,intra}} = R_{intra} = \frac{3\gamma^4\hbar^2}{4}\sum_{j=1}^{5}r_{ij}^{-6}\left(\frac{\pi d_{av}}{3kT}\right)^{1/2}. \tag{7.1.17}$$

Harmon (Harmon, 1968) has shown that Equation (7.1.17) can give good prediction for intramolecular dipole-dipole interaction in ethane at temperatures higher than 290K.

The numerical evaluation of Equation (7.1.17) gives

$$\frac{1}{T_{1,intra}} = \frac{0.125}{T^{1/2}} \qquad \text{(cgs)}. \qquad\qquad (7.1.18)$$

7.1.3.3. Spin Rotation Interaction

The validity of the diffusion model for the spin rotation interaction in ethane has been established. T_1 by the spin rotation interaction can be found in the form of

$$T_{1,sr} = C_1 \left(\frac{\eta}{T}\right)^{C_2}, \qquad\qquad (7.1.19)$$

where C_1 and C_2 can be found by fitting pure ethane T_1 data if we assume that ethane gas relaxes only by the spin rotation interaction. Figure 7.1.5 is the plot. Therefore, $T_{1,sr}$ of ethane is estimated by

$$T_{1,sr} = 4.23 \times 10^5 \left(\frac{\eta}{T}\right)^{0.74} \qquad \text{(cgs)}. \qquad\qquad (7.1.20)$$

The experimental data (Muller and Noble, 1963) of ethane proton relaxation times were compared with the relaxation times of ethane calculated from Equation (3.2.1), Equation (7.1.16), Equation (7.1.18) and Equation (7.1.20). The result was shown in Figure 7.1.6. The estimation compares closely with experimental results for proton relaxation in ethane.

The results of the analysis of the ethane T_1 data were presented in Figure 7.1.7. In the gaseous ethane, the contribution of the intermolecular dipole-dipole interaction is less than 0.5% and can be negligible. The relaxation rate is mainly accounted for by the spin rotation interaction in gaseous ethane. However, all three contributions become significant for liquid ethane with increasing viscosity. For liquid ethane at cryogenic

temperatures, the intermolecular dipole-dipole interaction becomes the dominant relaxation mechanism.

7.1.4 Comparison of Spin Rotation Interaction in Hydrogen, Methane, Ethane, and Propane Gases

It has been established that T_1/ρ follows the -1.5 power law relationship with T for many pure gases where spin rotation interaction is the dominant interaction (Armstrong and Courtney, 1969; Armstrong and Hanrahan, 1968; Armstrong and Tward, 1967; Courtney and Armstrong, 1970; Jameson et al., 1987a; Jameson et al., 1991; Jameson et al., 1987b; Rajan and Lalita, 1975; Tward and Armstrong, 1967). The spin rotation interaction in the gas phases of hydrogen, methane, ethane and propane was investigated. It is assumed that the spin rotation interaction is the dominant relaxation mechanism for the gas phases of hydrogen, methane, ethane and propane. Figure 7.1.8 compares the spin rotation interaction for these four gas systems (Bloom, 1957; Gerritsma et al., 1971; Lo, 1999) based on the T_1 versus $\rho/T^{1.5}$ plot. T_1 increases with increasing the molecular weight at the same temperature and molar density. Hydrogen gas has the relaxation time that is significantly shorter than those of the other three gases at the same temperature and molar density.

7.2. Mixtures

7.2.1. The General Mixing Rule for T_1

A mixing rule is developed for T_1 in the mixture with n components. The resonant nuclei may be ^1H or ^{13}C. For an n-component mixture, there may be n contributions to T_1. The logarithmic mean T_1 may be described as

$$T_{1,logmean} = T_{1,1}^{f_1} \cdots\cdots T_{1,i}^{f_i} \cdots\cdots T_{1,n}^{f_n},$$

(7.2.1)

where f_i is the fraction of the i-th component resonant nucleus in the mixture and $T_{1,i}$ is the individual relaxation time of the i-th component in the mixture. In general, the individual relaxation times of the i-th component can be given by Equation (3.2.1).

The intermolecular dipole-dipole relaxation rate can be given by Equation (3.2.3). In the n-component mixture, v can be calculated as

$$v = \sum_{j=1}^{n} v_j x_j,$$

(7.2.2)

where x_j is the mole fractions of the j-th component in the mixture and v_j is the number of resonant nuclei in the j-th molecule. The average molecular weight, MW of the mixture, can be calculated as

$$MW = \sum_{j=1}^{n} MW_j x_j,$$

(7.2.3)

where MW_j is the molecular weight of the j-th component.

The intramolecular dipole-dipole interaction relaxation time can be given by Equation (3.2.4). The medium effect may be included in the viscosity term.

The mixing rule for the spin rotation interaction by the kinetic model will be discussed in details in Section 7.2.2. For the diffusion model of spin rotation interaction, the medium effect may be included in the viscosity term.

7.2.2. The Mixing Rule of T_1 for Gas Mixtures

A mixing rule can be developed for T_1 in the gas mixtures with n components based on the kinetic model for the spin rotation interaction (Bloom et al., 1967; Gordon, 1966). It is assumed that the spin rotation interaction is dominant for all components in the mixture. For an n-component gas mixture, the logarithmic mean T_1 can be calculated by Equation (7.2.1).

The relaxation by the spin rotation interaction for the i-th component is caused by the collisions of the i-th molecule with various collision partners in the mixture. It has been empirically (Jameson and Jameson, 1990; Jameson et al., 1987a; Jameson et al., 1991; Jameson et al., 1987b; Rajan and Lalita, 1974; Rajan and Lalita, 1975) established that the contributions of various collision partners are additive

$$T_{1,i} = \sum_{j=1}^{n} \rho_j \left(\frac{T_1}{\rho} \right)_{i \cdot j} ,$$
(7.2.4)

where ρ_j is the partial molar density of the j-th component. In addition, Gordon has derived this additivity theoretically as a result of neglect of correlations between the effects of successive collisions and the assumption of binary collisions (Gordon, 1966).

For the gas mixtures, the relaxation time in the extreme narrowing limit may be derived from Equation (3.2.27)

$$\left(\frac{T_1}{\rho} \right)_{i-j} = A_i \frac{\sigma_{J(i-j)}}{\sqrt{T \mu_{(i-j)}}} ,$$
(7.2.5)

$$A_i = \frac{\hbar^2 N_A}{4\pi^2 I_{\perp i} C_{eff,i}^2} \sqrt{\frac{2}{\pi k}} .$$

(7.2.6)

The expression for the effective spin rotation constant, C_{eff}, depends on the detailed properties of the molecule. The spin rotation constant is a molecular constant which is characteristic of the nuclear spin in the molecule and provides a coupling between the nuclear spin angular momentum and the molecular rotational angular momentum. The reduced mass $\mu_{(i-j)}$ for unlike pairs is given by

$$\frac{1}{\mu_{(i-j)}} = \frac{1}{m_i} + \frac{1}{m_j} ,$$

(7.2.7)

where m_i and m_j are the mass of two colliding molecules respectively.

The cross section for angular momentum transfer by unlike pairs can be estimated by using a geometric mean,

$$\sigma_{J(i-j)} = \left[\sigma_{J(i-i)} \cdot \sigma_{J(j-j)} \right]^{1/2} .$$

(7.2.8)

In addition, we assume that the collision cross section for angular momentum transfer by like pairs is inversely proportional to temperature,

$$\sigma_J = \sigma_J (300 K) \frac{300}{T} .$$

(7.2.9)

Substituting Equations (7.2.8) and (7.2.9) into Equation (7.2.5), we obtain

$$\left(\frac{T_1}{\rho} \right)_{i-j} = \frac{G_{ij}}{T^{1.5}} ,$$

(7.2.10)

$$G_{ij} = 300 A_i \sqrt{\frac{m_i + m_j}{m_i m_j} \cdot \sigma_{J(i-i)}(300K) \cdot \sigma_{J(j-j)}(300K)} .$$

(7.2.11)

The coefficient G_{ij} describes the interaction between the probe molecule i and the molecule j. Natural gas is composed primarily of methane. In addition, ethane, propane,

CO_2 and N_2 are usually present. It is meaningful to calculate the coefficients G_{ij} for various collision partners in natural gas. For methane, Equation (7.1.1) can be used directly to evaluate the spin rotation interaction. The lack of knowledge of the molecular parameters causes the difficulty in theoretical prediction of the spin rotation interaction in ethane and propane. However, the experimental data can be used to estimate the coefficient A_i for ethane and propane. The cross sections for the collisions of various collision partners at 300 K were listed in Table 7.2.1. Based on the data in Table 7.2.1, the coefficients G_{ij} for the gas mixtures containing methane, ethane, propane, CO_2 and N_2 were calculated and summarized in Table 7.2.2. The calculations for the pure components correspond to the dashed lines in Figure 7.1.8.

7.2.3. Comparison of the Results from the Mixing Rule with Experiments for Proton Relaxation in CH_4 Gas Mixtures

The mixing rule is tested for two CH_4 gas mixtures, including CH_4-CO_2 and CH_4-N_2 gas mixtures. In these gas mixtures, only methane contributes to proton relaxation times of the mixtures. The other components contain no protons and are "invisible" in proton NMR relaxation. Previous work indicates that methane molecular motion is still in the gas kinetic limit even at liquid densities (Oosting and Trappeniers, 1971). It is therefore reasonable to use the kinetic model to predict proton relaxation in methane. It is assumed that the spin rotation interaction is the dominant mechanism for gaseous methane. The contribution by dipole-dipole interactions is neglected.

Using the values from Table 7.2.2, we calculated relaxation times of CH_4-CO_2 and CH_4-N_2 gas mixtures by the mixing rule. Figures 7.3.1-7.3.2 compared the calculated results with experimental results (Rajan and Lalita, 1975) for CH_4-CO_2 and

CH_4-N_2 gas mixtures respectively. The estimations from the mixing rule compare quite closely with experimental results for these two gas mixtures. Carbon dioxide and nitrogen do not contain protons but their presence in mixtures with methane will cause departures from pure methane data through their effects on the molecular dynamics. The change in the relaxation rate is due to the collision cross section of methane with other gas molecules being different from the methane-methane collision cross section.

Table 7.1.1 Molecular constants of methane

	Value	Reference
Moments of inertia (g.cm^2)	$I_A=I_B=I_C=5.33*10^{-40}$	(Bovey, 1953)
^{1}H spin rotation constants (kHz)	$C_{av}=10.4$; $\Delta C=18.5$	(Yi et al., 1971)
^{13}C spin rotation constants (kHz)	$C_{av}=15.94$; $\Delta C=0$	(Jameson et al., 1991)
Molecular diameter (Å)	3.83	(Hirschfelder et al., 1954)

Table 7.1.2 Molecular constants of ethane

	Value	Reference
Moments of inertia (g.cm^2)	$I_A=1.04*10^{-39}$, $I_B=I_C=4.23*10^{-39}$	(Hirota et al., 1981; Kuchitsu, 1968)
^{1}H spin rotation constants (kHz)	$C_{\parallel}=6.95$; $C_{\perp}=1.46$	This work
^{13}C spin rotation constants (kHz)	$C_{\parallel}=13$; $C_{\perp}=2.2$	(Whittenburg et al., 1992)
The angle of C-C-H	$111.5°$	(Hirota et al., 1981; Kuchitsu, 1968; Lafferty and Plyler, 1962)
The distance between protons (Å)	$r_{01}=r_{02}=1.77$; $r_{03}=r_{04}=2.55$; $r_{05}=3.10$	(Hirota et al., 1981; Kuchitsu, 1968; Lafferty and Plyler, 1962)
Molecular diameter (Å)	4.38	(Hirschfelder et al., 1954)

Table 7.2.1 Cross sections for angular momentum transfer for CH_4, C_2H_6, C_3H_8, CO_2, and N_2 molecules

Pair	σ_J (300K), Å^2	Reference
CH_4-CH_4	18.8	(Jameson et al., 1991)
C_2H_6-C_2H_6	60.0 [a]	This work
C_3H_8-C_3H_8	78.3 [a]	This work
CO_2-CO_2	59.9	(Jameson et al., 1987b)
N_2-N_2	14.9	(Jameson et al., 1987a)

[a] The collision cross sections are estimated from the geometric cross sections (πd_{ij}^2) by assuming that the collision efficiencies are 1 for ethane and propane. The values of the hard sphere diameter d_{ij} are taken from Maitland (Maitland et al., 1981) Table A3.2 based on corresponding states universal curve.

Table 7.2.2 Values of the coefficients G_{ij} (sec·$K^{1.5}$·cm^3·$mole^{-1}$) for proton relaxation in the gas mixture of CH_4, C_2H_6, C_3H_8, CO_2, and N_2

j ⟶	CH_4	C_2H_6	C_3H_8	CO_2	N_2
i ↓					
CH_4	$2.41×10^{6}$ [a] $2.52×10^{6}$ [b]	$3.77×10^6$	$4.06×10^6$	$3.55×10^{6}$ [c] $2.54×10^{6}$ [d]	$1.90×10^{6}$ [c] $1.85×10^{6}$ [d]
C_2H_6	$1.06×10^7$	$1.58×10^7$	$1.66×10^7$	$1.45×10^7$	$8.02×10^6$
C_3H_8	$3.09×10^7$	$4.47×10^7$	$4.60×10^7$	$2.84×10^7$	$2.28×10^7$
CO_2	0	0		0	0
N_2	0			0	0

[a] Calculated using Equation (7.1.1) and the values in Table 7.2.1

[b] Estimated from experimental data of methane (Lo, 1999)

[c] The collision cross sections by unlike pairs at 300 K were estimated using Equation (7.2.8) and the values in Table 7.2.1

[d] The collision cross sections by unlike pairs at 300 K were taken from Table A.1.
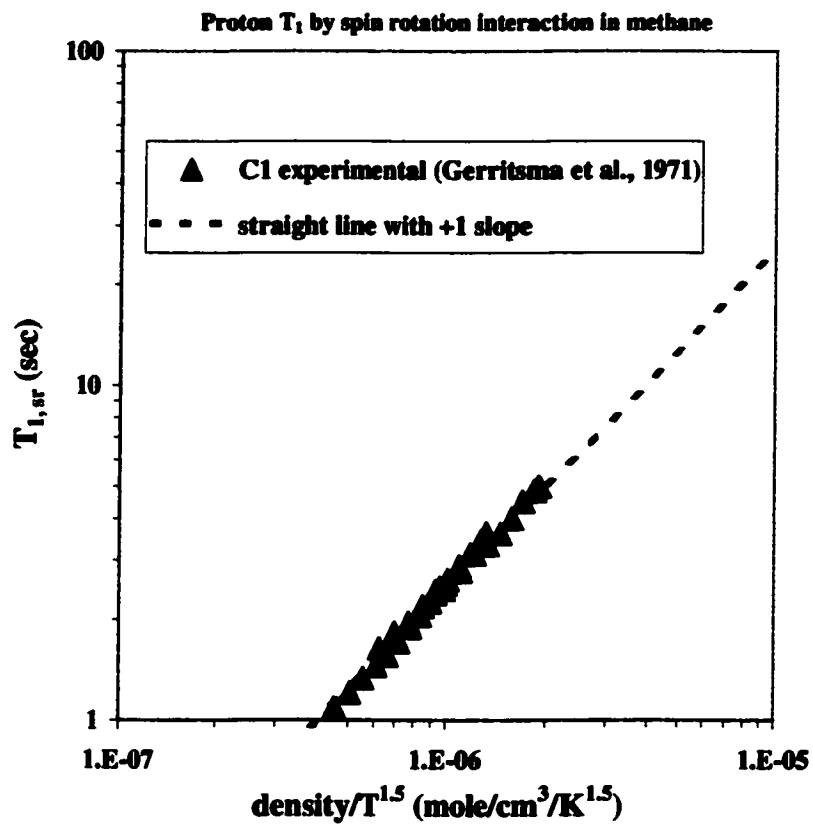
Figure 7.1.1 Proton $T_{1, sr}$ versus. $\rho/T^{1.5}$ plot in methane based on the kinetic model. The kinetic model can describe the spin rotation interaction in methane.
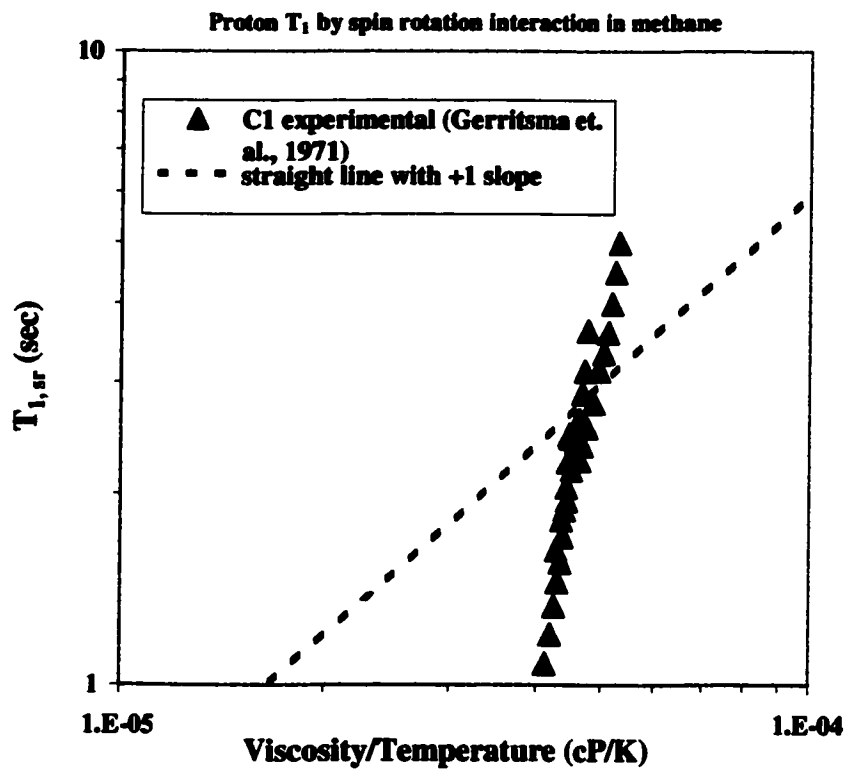
Figure 7.1.2 Proton $T_{1, sr}$ vs. η/T plot in methane based on the diffusion model. The diffusion model fails to describe spin rotation interaction in methane.

(a) ¹H data

(b) ¹³C data
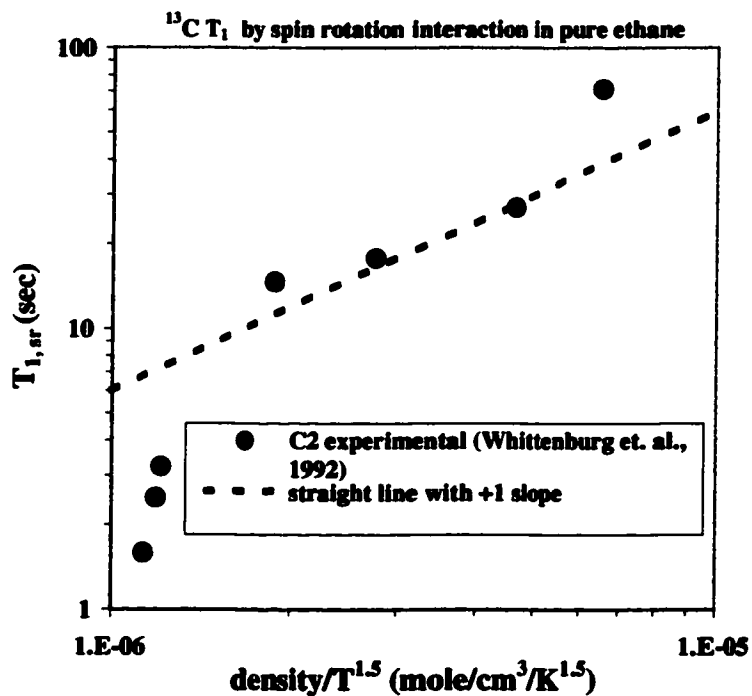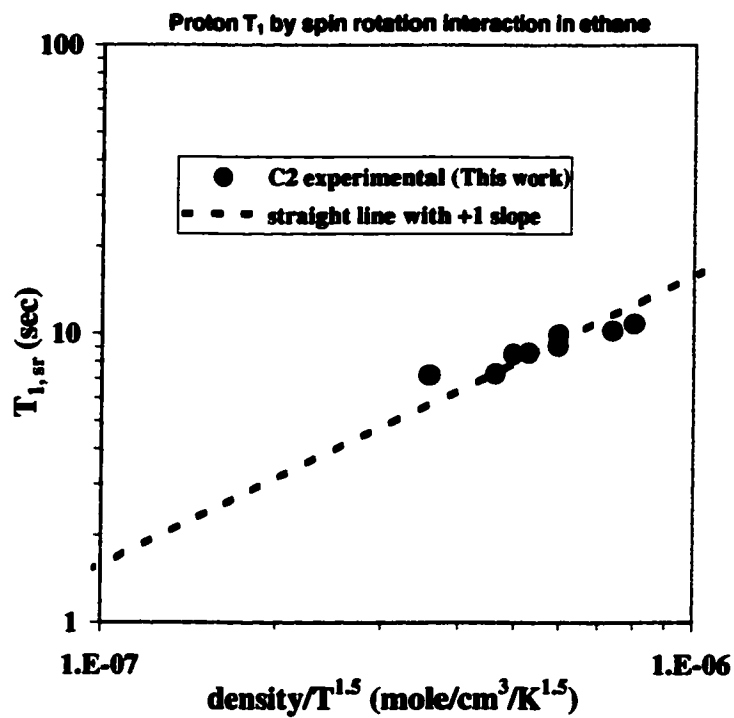
Figure 7.1.3 $T_{1,sr}$ vs. $\rho/T^{1.5}$ plots in ethane based on the kinetic model. The kinetic model can describe ¹H $T_{1,sr}$ in ethane

(a) ^1H data

(b) ^{13}C data
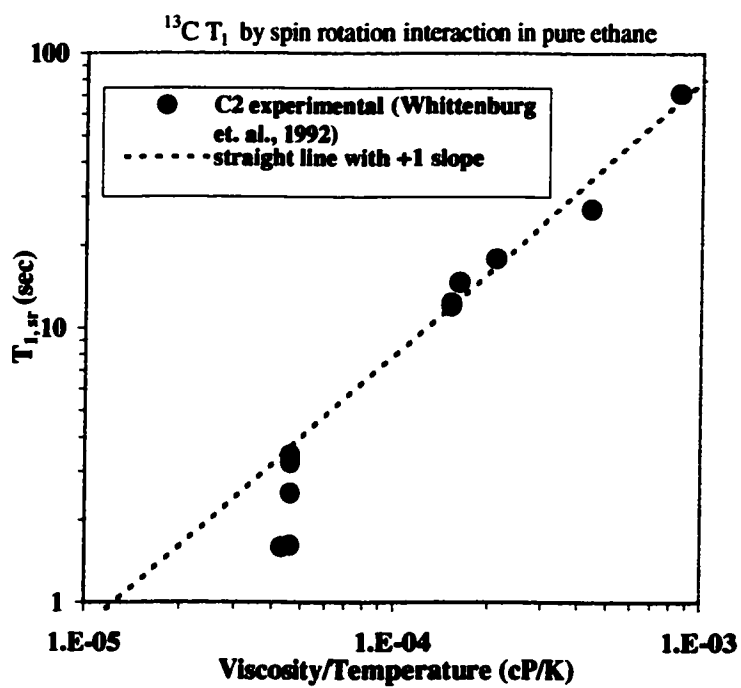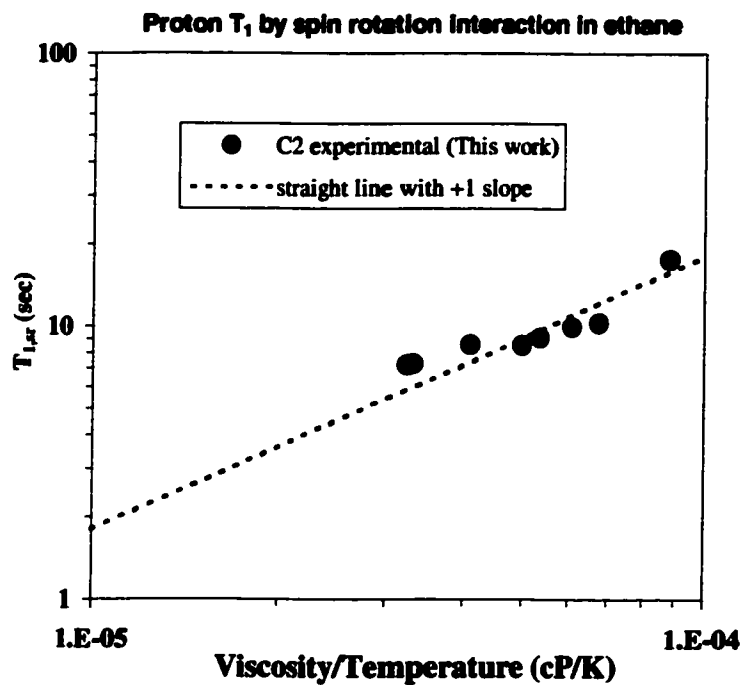
Figure 7.1.4 $T_{1, sr}$ vs. η/T plots in ethane based on the diffusion model. Both ^1H and ^{13}C $T_{1,sr}$ data show that the diffusion model is an adequate model for the spin rotation interaction ethane.
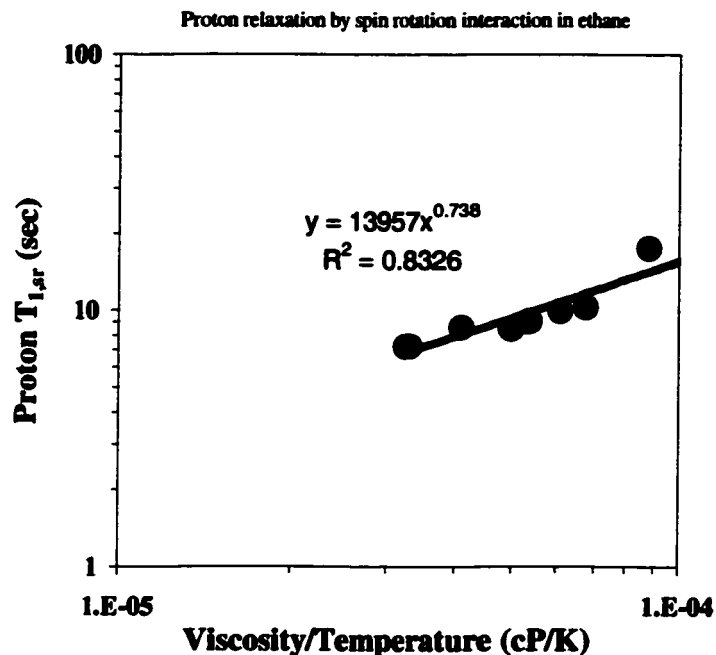
Figure 7.1.5 Correlation of spin rotation T_1, viscosity and temperature for ethane gas.
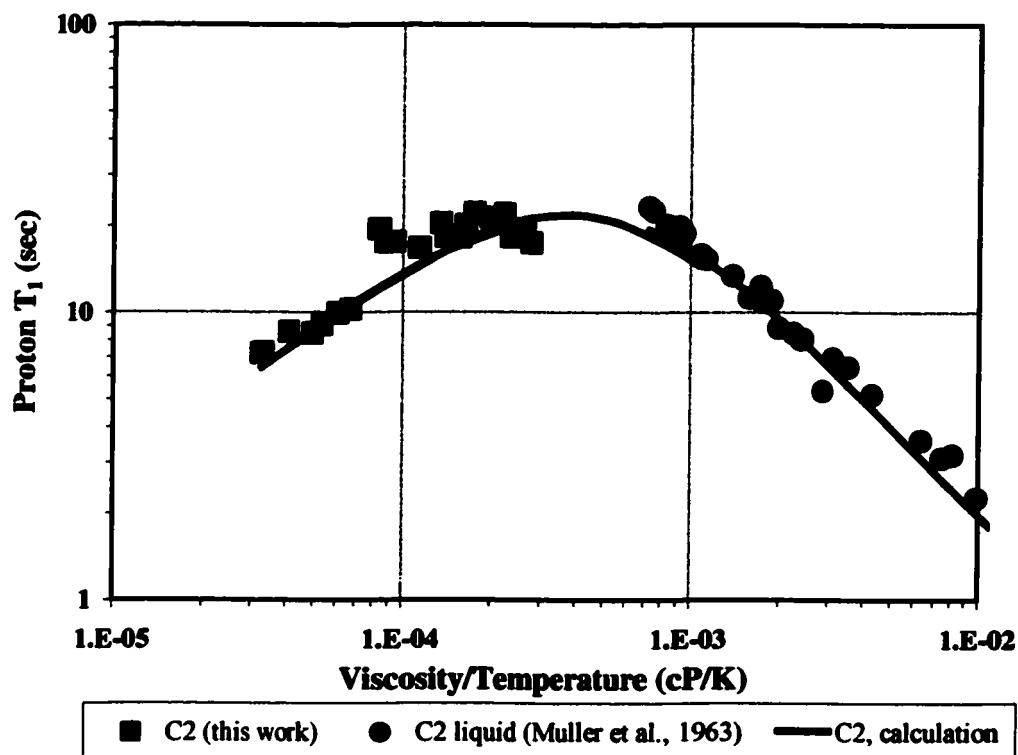
Figure 7.1.6 Comparison of experimental results and calculated results for pure ethane. The estimation compares closely with experimental results for proton relaxation in ethane.
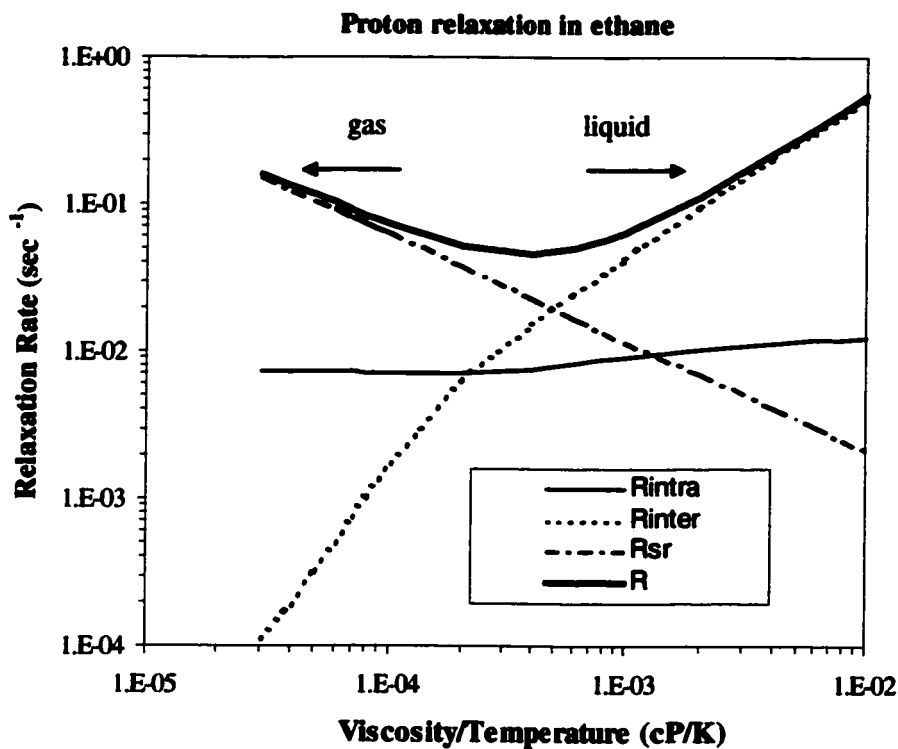
Figure 7.1.7 Contributions to the proton relaxation rate of ethane. The relaxation rate is mainly accounted for by the spin rotation interaction in gaseous ethane. However, all three contributions become significant for liquid ethane with increasing viscosity. For liquid ethane at cryogenic temperatures, intermolecular dipole-dipole interaction becomes the dominant relaxation mechanism.
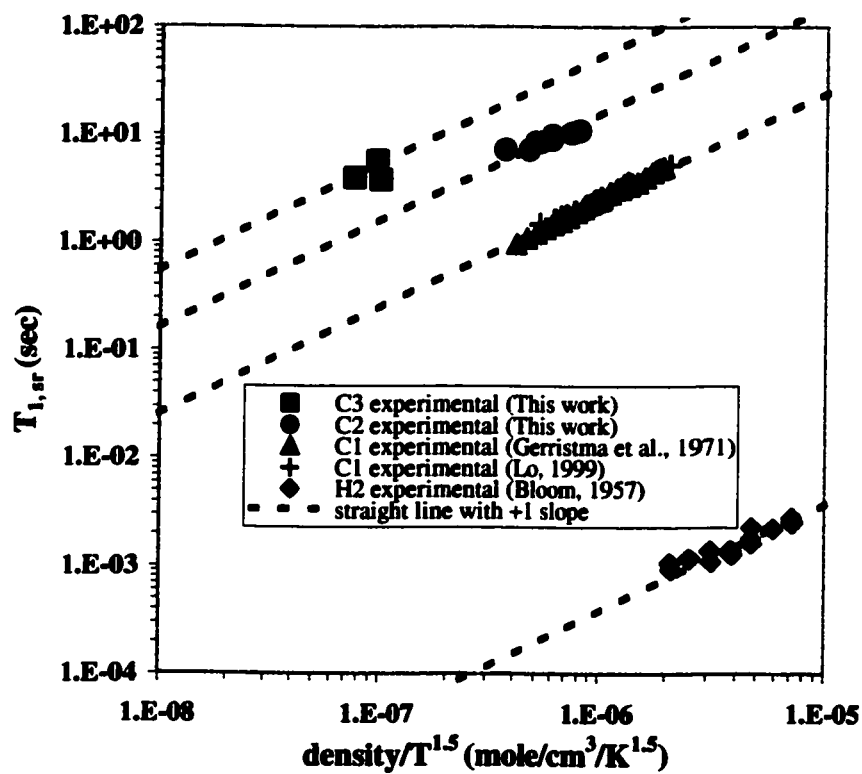
Figure 7.1.8 T_1 versus $\rho/T^{1.5}$ plot for hydrogen, methane, ethane, and propane gases. T_1 increases with increasing the molecular weight at the same temperature and molar density.
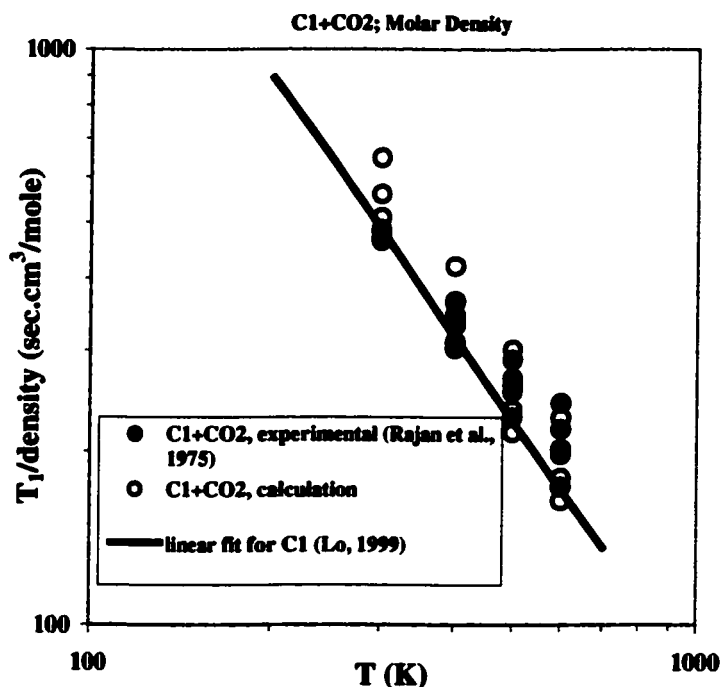
Figure 7.3.1 Comparison of experimental results and calculated results from the mixing rule for the CH$_4$-CO$_2$ gas mixture. The estimations from the mixing rule compare quite closely with experimental results.
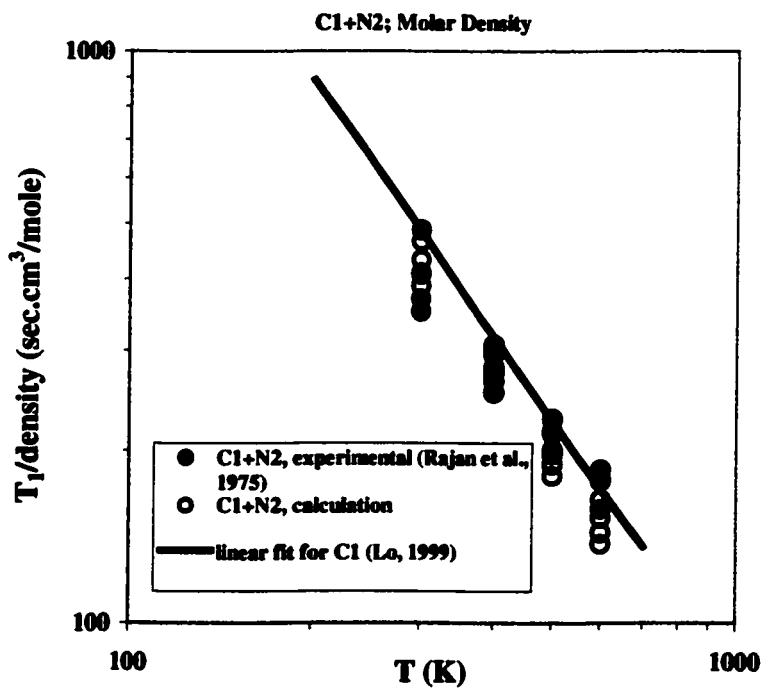
Figure 7.3.2 Comparison of experimental results and calculated results from the mixing rule for the CH$_4$-N$_2$ gas mixture. The estimations from the mixing rule compare quite closely with experimental results.

VIII. Relaxation Times of Crude Oils

Relaxation times of intermediate viscosity dead oils show a linear correlation with viscosity/temperature on a log-log plot. In contrast, heavy crude oils fail to follow this correlation. It is well known that the presence of heavy components in an oil complicates analysis and interpretation.

8.1. Viscosity and Larmor Frequency Dependence of Relaxation Times

The T_1 and T_2 distributions of a number of crude oils were measured with the 2 MHz, 7.5 MHz and 20 MHz NMR spectrometers. T_2 was measured with different values of the echo spacing (TE). The results are presented in Tables 8.1.1-8.1.3. They show that T_1/T_2 of heavy crude oils increases with increasing Larmor frequency.

Relaxation times of about ten crude oil samples and one oil-based mud (OBM) base oil from Baroid Drilling Fluids were measured by the 20 MHz Bruker NMR spectrometer with variable temperature controller unit over the temperature range 60-100 °C. The results are presented in Tables 8.1.4-8.1.5. They show that relaxation times of crude oils depend on temperature.

LaTorraca et al. (LaTorraca et al., 1999) pointed out that both the T_2 signal amplitude and the T_2 relaxation time constants of the heavy oils depend on the echo spacing (TE) used in the measurements. Figure 8.1.1 illustrates an example of the effect of the echo spacing on the T_2 distributions measured by the 20 MHz Bruker spectrometer. With increasing the echo spacing, T_2 time constants were shifted to longer times and the signal amplitude decreases. Heavy oils may have fast relaxing components that relax significantly before the first echo occurs and thus are not fully detected. The T_2

distribution at the longer echo spacing is truncated because of the loss of information. This will not only result in the misinterpretation of the relaxation time distributions but also result in an underestimate of the hydrogen index. T_2 data at short echo spacing are used in this thesis.

Figures 8.1.2-8.1.4 are representative relaxation time distributions of crude oils. The T_1 and T_2 distributions of the light oil (M11) overlay each other and the distributions are symmetrical. Moreover, the T_1 and T_2 distributions of the light oil are not sensitive to the Larmor frequency of the NMR spectrometer. The M13 crude oil has a T_2 distribution that is clearly shorter than the T_1 distribution. The M14 oil is so viscous that that it is almost solid at room temperature. The T_1 and T_2 distributions of this oil have separated. The separation between the T_1 and T_2 distributions becomes more obvious with increasing Larmor frequency.

Figures 8.1.5 and 8.1.6 investigate the relationship between T_1, T_2 and viscosity/temperature respectively. Also, some literature data are included on the plots (Jacob and Davis, 1999; LaTorraca et al., 1998; McCann et al., 1999; Straley et al., 1997; Vinegar et al., 1991). T_1 starts to level off at high viscosity. However, T_2 continues to shorten with increasing viscosity/temperature. T_2 is considerably less than T_1 at all Larmor frequencies for heavy oils. There is no gross frequency dependency for T_2. Generally, the difference between T_1 and T_2 of heavy crude oils increases with increasing Larmor frequency.

Dead crude oils relax mainly by intramolecular dipole-dipole interactions. The intramolecular dipole-dipole interaction mechanism is due to the interaction of nuclei in the same molecule. If the molecule is regarded as rigid, the relaxation results from the

rotational motion of the molecule (McConnell, 1987). For spherical molecules, the relaxation times by the intramolecular dipole-dipole interaction are expressed as (McConnell, 1987)

$$\frac{1}{T_1} = W_2 \tau_c \left[\frac{2/3}{1+(\omega_0 \tau_c)^2} + \frac{8/3}{1+(2\omega_0 \tau_c)^2} \right],$$

(8.1.1)

$$\frac{1}{T_2} = W_2 \tau_c \left[1 + \frac{5/3}{1+(\omega_0 \tau_c)^2} + \frac{2/3}{1+(2\omega_0 \tau_c)^2} \right],$$

(8.1.2)

$$W_2 = \frac{3(v-1)\gamma^4 \hbar^2 I(I+1)}{5r^6},$$

(8.1.3)

where ω_0 is the Larmor frequency, and τ_c is the rotational correlation time.

In the fast motion case (the extreme narrowing limit), Equations (8.1.1) and (8.1.2) will reduce to

$$\frac{1}{T_1} = \frac{1}{T_2} = \frac{10}{3} W_2 \tau_c, \quad \omega_0 \tau_c \ll 1.$$

(8.1.4)

The rotational correlation time can be related to measurable variables through the rotational diffusion coefficient D_r. For spherical molecules, the rotational correlation time is given by (McConnell, 1980)

$$\tau_c = \frac{1}{6D_r} = \frac{4\pi a^3 \eta}{3kT}.$$

(8.1.5)

The substitution of Equation (8.1.5) into Equation (8.1.4) yields

$$\frac{1}{T_1} = \frac{1}{T_2} = \frac{40 W_2 \pi a^3 \eta}{9kT}, \quad \omega_0 \tau_c \ll 1.$$

(8.1.6)

The significant result here is that liquids in the fast motion limit have T_1 and T_2 equal to each other and inversely proportional to viscosity/temperature. Dimensional analysis of Equations (8.1.1) and (8.1.2) shows that dimensionless relaxation time and

correlation time, respectively, are divided by and multiplied by the Larmor frequency. In order to investigate the dependence of relaxation times on viscosity/temperature and Larmor frequency, we defined the following normalized variables with respect to 2 MHz

$$T_{1,2N} = \frac{2}{\omega_0} T_{1,2},$$

(8.1.7)

$$\left(\frac{\eta}{T}\right)_N = \frac{\omega_0}{2}\left(\frac{\eta}{T}\right).$$

(8.1.8)

Using Equations (8.1.1), (8.1.2), (8.1.5), (8.1.7) and (8.1.8), we have

$$\frac{1}{T_{1N}} = \frac{W_2 S}{2}\left(\frac{\eta}{T}\right)_N \left\{\frac{2/3}{1+\left[S\left(\frac{\eta}{T}\right)_N\right]^2} + \frac{8/3}{1+\left[2S\left(\frac{\eta}{T}\right)_N\right]^2}\right\},$$

(8.1.9)

$$\frac{1}{T_{2N}} = \frac{W_2 S}{2}\left(\frac{\eta}{T}\right)_N \left\{1 + \frac{5/3}{1+\left[S\left(\frac{\eta}{T}\right)_N\right]^2} + \frac{2/3}{1+\left[2S\left(\frac{\eta}{T}\right)_N\right]^2}\right\},$$

(8.1.10)

$$\frac{T_1}{T_2} = \frac{1 + \dfrac{5/3}{1+\left[S\left(\frac{\eta}{T}\right)_N\right]^2} + \dfrac{2/3}{1+\left[2S\left(\frac{\eta}{T}\right)_N\right]^2}}{\dfrac{2/3}{1+\left[S\left(\frac{\eta}{T}\right)_N\right]^2} + \dfrac{8/3}{1+\left[2S\left(\frac{\eta}{T}\right)_N\right]^2}},$$

(8.1.11)

$$S = \frac{8\pi a^3}{3k}.$$

(8.1.12)

The relationships between normalized relaxation times T_1 and T_2 and normalized viscosity/temperature are shown in Figures 8.1.7 and 8.1.8 respectively. All of the T_1 data fall on the same curve for different Larmor frequencies. The T_1 curve reaches a

plateau with normalized viscosity/temperature greater than about 10 cP/K. T_1 does not follow the trend predicted by Equation (8.1.9). The black straight line is from the T_2 correlation by Morriss et al. (Morriss et al., 1997). T_2 of low viscosity crude oils is consistent with the correlation by Morriss et al. However, high viscosity crude oils depart this correlation, probably because of the echo spacing limitation discussed earlier. For low viscosity crude oils, T_1 is very close to T_2. With the increase of viscosity, the difference between T_1 and T_2 increases.

Combining the data of LaTorraca et al. (LaTorraca et al., 1998) and McCann et al. (McCann et al., 1999), we investigate the relationship between the ratio of T_1 and T_2 and normalized viscosity/temperature. In Figure 8.1.9, low viscosity oils have the ratio of T_1/T_2 close to 1 as predicted by Equation (8.1.11). However, the experimental data of heavy oils depart from the trend predicted by the theory. The molecular radii derived from these values of S are 11.8 Å and 5.48 Å respectively. This may be because crude oils are mixtures of many components and have a distribution of correlation times. The viscosity and frequency dependence of the ratio, T_1/T_2, may be due to the relationship between the rotational correlation time of molecular motions, τ_c, and the nuclear Larmor frequency, ω_0. In the limit of fast motions as in the case of low viscosity fluids, $\tau_c\omega_0 \ll 1$ and T_1 and T_2 are equal. When the molecular motions are slow as in high viscosity fluids or in macromolecules and/or the Larmor frequency is high, then the condition of $\tau_c\omega_0 \ll 1$ is not satisfied and T_1 will increase with increase in τ_c while T_2 will decrease as shown by Equations (8.1.1) and (8.1.2).

8.2. The Effects of Asphaltene Content and Free Radical Content on Relaxation Times

Asphaltenes are the heaviest components in crude oils. They are dark brown to black friable solids with no definite melting point, rich in heteratoms and containing metals such as vanadium and nickel. The "average" molecule of the asphaltene is represented as a very complex aromatic core surrounded and linked by aliphatic and heteroatom chains (Sheu and Mullins, 1995). In addition to viscosity and the Larmor frequency, asphaltene content may also contribute to the difference between T_1 and T_2 in heavy oils. Figure 8.2.1 illustrates the relationship between the ratio of T_1/T_2 and the asphaltene content at different Larmor frequencies. T_1/T_2 increases with the increase of asphaltene content.

In solutions of free radicals, the proton relaxation may be dominated by interactions between the electron spin of the free radicals and the spins of neighboring protons (Hausser and Krüger, 1965; Müller-Warmuth and Printz, 1966; Schwartz et al., 1979). Scalar coupling of electron and nuclear spins may contribute to the frequency dependence of T_1 in crude oils. In general, the electron resonance frequency, ω_e, is much larger than the nuclear resonance frequency, ω_0. When the product of ω_e and τ_c is large compared to unity, T_1 may become frequency dependent.

It is known that organic free radicals are present in crude oils (Montanari et al., 1998; Mujica et al., 2000). Electron spin resonance (ESR) spectroscopy is used to study organic free radicals and vanadium in crude oils. The ESR measurements in crude oils were made by Southwest Research Institute. Figure 8.2.2 is a typical ESR spectrum for a crude oil sample (M13). Organic free radicals usually show a single peak. The metal

species produce multiple peaks, with a broader range of absorption energy. For most of the other oil samples investigated, the vanadium signal is too small to be measurable. So currently, it is impossible to investigate the effect of vanadium quantitatively. The free radical content in the crude oil is represented by

$$\frac{h_{peak}}{m_{sample}},$$ (8.2.1)

where h_{peak} is the peak height and m_{sample} is the sample weight.

Figure 8.2.3 investigates the relationship between the free radical content and T_1/T_2 ratio. With increasing the free radical content, T_1/T_2 ratio increases. In general, viscosity, the Larmor frequency, asphaltene, and free radicals all contribute to the difference between T_1 and T_2 in crude oils.

8.3. The Effect of Temperature on Viscosity and Relaxation Times

The decreasing viscosity of crude oils at higher temperature can result in an increase in the "mobility" of the molecules. Figure 8.3.1 shows some representative plots of viscosity as a function of the reciprocal of the temperature for crude oils and the OBM base oil. Plots of viscosity as a function of the reciprocal of the temperature on a semilog scale show a strong degree of linearity. The semilog linearity indicates an exponential relationship between relaxation times and the reciprocal of the temperature. The results of the linear regression analysis are shown in Table 8.3.1.

Figure 8.3.2 illustrates relaxation time distributions of the OBM base oil at various temperatures. The OBM base oil with the viscosity of 2.4 cP at 40 °C has the narrow peak. With increasing the temperature, the peak moves to longer relaxation times. However, the peak shape does not change much. It is important to point out that

the measurements at 40 °C were done with the samples in the 13 mm diameter glass tubes by the 20 MHz NMR spectrometer with the fixed temperature. The measurements at 60 °C and 100 °C were done with the samples in the 10 mm diameter glass tubes by the 20 MHz NMR spectrometer with variable temperature controller unit. Figures 8.3.3-8.3.5 show representative relaxation time distributions for crude oils at different temperatures. With increasing temperature, the T_2 distributions become broader. For very heavy crude oils, the changes in the T_1 distributions are slight. This may be because the correlation times of these heavy crude oils are still not in the " fast motion" limit (Cowan, 1997). The Curie's law (Cowan, 1997) predicts that the magnetization is proportional to the applied field B_0 and inversely proportional to the temperature,

$$M_0 \propto \frac{B_0}{T}.$$

(8.3.1)

According to this formula, a decrease of the amplitude of the NMR signal during heating of the sample is expected. The measurements with the OBM base oil, M4, and CH10 samples demonstrate similar results. However, the relative magnitude for the M14 sample increases when the temperature goes from 60 °C to 100 °C. Mirotchnik et al. (Mirotchnik et al., 1999) also observed similar results for NMR measurements of heavy crude oils at different temperatures.

NMR relaxation times of dead crude oils are often correlated with viscosity by the literature (Morriss et al., 1997). However, the relaxation theory for the intramolecular dipole-dipole interaction predicts that the relaxation time is a function of viscosity/temperature (McConnell, 1987). Based on the data of heavy crude oils at various temperatures, relaxation times are correlated with viscosity as well as

viscosity/temperature. Figure 8.3.6 (a) illustrates the correlation of T_2 with viscosity on the log-log plot while Figure 8.3.6 (b) illustrates the correlation of T_2 with viscosity/temperature on the log-log plot. From the values of the regression coefficients, it is found that T_2 data are equally well correlated with both viscosity and viscosity/temperature for the crude oils investigated. The slope is about 0.7 for both correlations. Since viscosity changes significantly for heavy oils even when the change in the temperature is not big (from 40 °C to 100 °C), it is hard to distinguish the difference between the T_2 versus viscosity correlation and the T_2 versus viscosity/temperature correlation. From Figures 6.1.1 and 6.1.2, it is found that T_1 is better correlated with viscosity than correlated with viscosity/temperature for light hydrocarbons. However, this is not obvious in heavy oils. The slope of 0.7 differs from the slope of 0.9 in the T_2 correlation by Morriss et al. (Morriss et al., 1997). The correlations developed above are based on the data of high viscosity crude oils while the correlation by Morriss et al. is based on the data of low and medium viscosity crude oils. The T_2 measurements of high viscosity oils may be affected by the echo spacing of the NMR instrument.

Jacob et al. (Jacob and Davis, 1999) also measured the T_2 relaxation times of some intermediate viscosity crude oils at different temperatures. The T_2 data by Jacob et al. (Jacob and Davis, 1999) are equally well correlated with both viscosity and viscosity/temperature as shown in Figures 8.3.7 (a) and 8.3.7 (b). T_2 follows the power law relationship with both viscosity and viscosity/temperature for Jacob et al.'s crude oil data.

The correlations of relaxation times are shown in Table 8.3.2. The T_2 correlations for heavy oils by this work have different slopes compared to those for intermediate viscosity oils by Jacob et al. (Jacob and Davis, 1999).

Figure 8.3.8 investigates the dependence of relaxation times on viscosity/temperature for crude oils (Jacob and Davis, 1999), OBM base oils (Kumar et al., 2000), OBM filtrates (Kumar et al., 2000), and pure higher alkanes. Jacob et al.'s light oil data follow the correlation by Morriss et al. (Morriss et al., 1997). However, their crude oil data depart from the correlation by Morriss et al. with increasing viscosity/temperature. Although they deoxygenated the crude oil samples, their data points are below the straight line of deoxygenated pure higher alkanes. This might be due to the effect of diffusion in the T_2 measurements. The crude oil data by this work are consistent with the correlation by Morriss et al. if viscosity/temperature is lower than 1 cP/K. The departure of high viscosity oils from the correlation is caused by the limitation of the echo spacing in T_2 measurements. Kumar et al. (Kumar et al., 2000) measured the relaxation times for the deoxygenated OBM base oils and filtrates at various temperatures. The relaxation time data of the OBM samples by Kumar et al. (Kumar et al., 2000) follow different trend compared with pure higher alkanes and the T_2 correlation for crude oils by Morriss et al. (Morriss et al., 1997). These OBM samples have a much steeper dependence of T_1 and T_2 on viscosity/temperature. T_2 data of the OBM base oil were also measured at 40 °C, 60 °C and 100 °C by this work. The OBM base oil data by this work fall between the straight line of pure higher alkanes and the correlation by Morriss et al. Although the OBM base oil used in this work was not deoxygenated, it has longer T_2 than crude oils at the same viscosity/temperature. This difference might result

from the additives in the OBM base oil. Both Jacob and Kumar came from the same group in Texas Technology University. Their data by NMR measurements show departure from the usual correlation and the data from other laboratories.

8.4. Hydrogen Index

The hydrogen index (HI) of a fluid is defined as the proton density of the fluid at any given temperature and pressure divided by the proton density of pure water at standard temperature and pressure. The HI of a fluid sample can be measured in the laboratory by measuring the response of the sample of known volume at the conditions of interest,

$$HI = \frac{(M_{0,fluid} / V_{fluid})_{\text{at conditions of interest}}}{(M_{0,H_2O} / V_{H_2O})_{\text{at standard conditions}}}. \tag{8.4.1}$$

The amplitude of the magnetization before attenuation by relaxation processes, M_0, can be determined by the cumulative distribution of relaxation times after inverting the measured signal decay. In this work, a solution of 0.05% C_uSO_4 in water is used as the calibration sample to estimate HI. Since the measured signal intensity is also a function of the temperature, the HI of the samples was determined from the ratio of cumulative signal intensity of the oil sample and the C_uSO_4 solution, both measured at the same temperature. The hydrogen index should be a quantity independent of measurement methods. LaTorraca et al. (LaTorraca et al., 1999) pointed out that apparent rather than true hydrogen index is measured for heavy oils due to limitations of measurement methods, such as the finite echo spacing time in T_2 measurements.

The hydrogen index was calculated for some crude oils based on NMR measurements. The results are listed in Table 8.4.1. Figure 8.4.1 illustrates the relationship between apparent *HI* and temperature for some crude oil samples. In general, apparent *HI* of heavy crude oils will increase with increasing temperature. This has also been demonstrated by Mirotchnik et al. (Mirotchnik et al., 1999). Insufficient sampling of the short T_2 of heavy crude oils might account for the decrease in *HI* at low temperatures (below 40 °C). Increasing the temperature shifts the T_2 distribution to longer relaxation times, and more of the signal can be measured for a given echo spacing.

LaTorraca et al. (LaTorraca et al., 1999) investigated the effect of the echo spacing on apparent *HI* for some medium and heavy crude oils. They claim that the apparent *HI* depends strongly on the echo spacing and this dependence is caused by the fast T_2 relaxation rate of heavy oils being too rapid to be adequately sampled by the NMR instruments. Figures 8.4.2 and 8.4.3 show the plots of apparent *HI* measured by 2 MHz and 20 MHz NMR spectrometers as a function of API gravity at various echo spacings. With increasing the echo spacing, apparent *HI* decreases. More of the signal can be collected with decreasing the echo spacing. The measurements by this work corroborate LaTorraca et al.'s conclusions (LaTorraca et al., 1999).

Figure 8.4.4 illustrates the *HI* correlation by Kleinberg et al. (Kleinberg and Vinegar, 1996) along with the *HI* data for some crude oils. The correlation by Kleinberg et al. (Kleinberg and Vinegar, 1996) is based on the data of low and medium density oils. It has the *HI* equal to unity for oils lighter than 25° API and decreasing for heavy oils. This correlation works well for intermediate viscosity oils. However, heavy crude oils show some departure from the correlation.

Table 8.1.1 Relaxation times of crude oils (T=30 °C, 2 MHz)

Sample	Viscosity (cP)	T_1 (ms)	T_2 (ms) (TE=0.24 ms)	T_2 (ms) (TE=1.00 ms)	T_1/T_2 (TE=0.24 ms)
BC3	55.6	61.05	46.50	52.58	1.31
BC2	171.2	15.90	7.65	9.10	2.08
BP	193.6	18.66	8.59	10.84	2.17
BC1	442.6	10.55	4.44	5.47	2.38
CH1	44491	4.99	0.49	1.14	10.18
CH2	999.8	8.71	2.03	3.03	4.29
CH3	35267	5.27	0.41	0.99	12.85
CH4	50000	4.98	0.43	0.88	11.58
CH5	41258	4.93	0.43	0.99	11.47
CH6	44630	4.83	0.48	0.95	10.06
CH7	106.3	29.71	15.41	20.96	1.93
CH8	847.9	47.36	20.99	24.56	2.26
CH9	2110	6.64	1.62	2.33	4.10
CH10	71035	5.28	0.39	0.85	13.54

Table 8.1.2 Relaxation times of crude oils (T=40 °C, 7.5 MHz)

Sample	Viscosity (cP)	T_1 (ms)	T_2 (ms) (short TE)	T_2 (ms) (TE=1.00 ms)	T_1/T_2 (short TE)
M11		547.3	493.5 [a]	496.5	1.11
CO	5.93	229.7	121.7 [a]	167.8	1.89
M2	6.46	186.3	144.7 [a]	168.6	1.29
NB	7.40	249.3	196.5 [a]	198.8	1.27
SMID	8.92	185.6	78.54 [a]	89.45	2.36
SMP69	11.3	144.2	107.6 [a]	106.8	1.34
SMY	16.1	78.29	37.81 [a]	39.49	2.07
M10	16.3	93.45	32.84 [a]	34.98	2.85
SWCQ	17.7	133.8	100.2 [a]		1.34
DB	19.7	66.97	29.95 [a]	43.32	2.24
M1	21.0	99.33	80.86 [a]	92.72	1.23
BC3	30.3	120.2	86.30 [a]	94.09	1.39
SMT	34.5	57.04	28.39 [a]	24.08	2.01
BC2	94.5	31.06	17.67 [a]	24.59	1.76
BP	110.6	43.36	21.33 [a]	24.19	2.03
SMP	145.4	25.38	11.06 [a]	5.12	2.29
BC1	219.5	30.13	13.03 [b]	16.92	2.31
M13	222.2	26.04	6.73 [b]	5.75	3.87
M4	644.8	18.27	5.57 [b]	6.10	3.28
M14	96000	15.13	0.70 [b]	1.24	21.61
CH1	13482	16.57	0.73 [b]		22.70
CH2	451.7	21.47	6.15 [b]	9.54	3.49
CH7	65.7	61.23	34.70 [b]	45.89	1.76

[a]: TE=0.24 msec.

[b]: TE=0.20 msec.

Table 8.1.3 Relaxation times of crude oils and the OBM base oil (T=40 °C, 20 MHz)

Sample	Viscosity (cP)	T_1 (ms)	T_2 (ms) (short TE)	T_2 (ms) (TE=1.00 ms)	T_1/T_2 (short TE)
M11		576.1	508.5 [a]	491.2	1.13
CO	5.93	460.2	187.4 [a]	190.3	2.46
M2	6.46	254.2	215.4 [a]	208.3	1.18
NB	7.40	278.4	316.5 [a]	312.7	0.88
SMID	8.92	285.0	95.00 [a]	105.0	3.00
SMP69	11.3	216.6	179.8 [a]	181.4	1.20
SMY	16.1	156.6	87.76 [a]	93.24	1.78
M10	16.3	155.9	67.43 [a]	79.04	2.31
SWCQ	17.7	161.8	117.7 [a]	119.4	1.37
DB	19.7	133.87	33.50 [a]	27.55	4.00
M1	21.0	142.8	111.4 [a]	115.6	1.28
BC3	30.3	161.76	117.2 [a]	117.0	1.38
SMT	34.5	124.14	33.01 [a]	38.60	3.76
BC2	94.5	63.39	18.37 [b]	19.23	3.45
BP	110.6	73.04	22.42 [b]	25.15	3.26
SMP	145.4	59.19	9.86 [b]	12.80	6.00
BC1	219.5	52.40	13.75 [b]	16.60	3.81
M13	222.2	50.79	4.59 [b]	6.43	11.07
M4	644.8	37.16	4.13 [b]	5.81	9.00
M14	96000	41.01	0.54 [b]	0.90	75.94
CH1	13482	39.45	0.72 [b]	1.52	54.79
CH2	451.7	45.52	6.93 [b]	9.53	6.57
CH3	10321	46.12	0.75 [b]	1.55	61.49
CH4	13000	37.46	0.65 [b]	1.48	57.63
CH5	11452	41.11	0.68 [b]		60.46
CH6	11941	41.12	0.68 [b]	1.49	60.47
CH7	65.7	82.15	30.18 [b]	36.34	2.72
CH8	88.1	147.88	53.76 [b]	58.90	2.75
CH9	906.7	41.68	4.25 [b]	6.00	9.81
CH10	22068	42.73	0.54 [b]	1.22	79.13
OBM base oil (SF olefin base)	2.40	874.0	836.4 [a]	833.0	1.04

[a]: TE=0.24 msec.

[b]: TE=0.08 msec.

Table 8.1.4 Relaxation times of crude oils and the OBM base oil (T=60 °C, 20 MHz)

Sample	Viscosity (cp)	T_1 (ms)	T_2 (ms) (TE=0.20 ms)	T_2 (ms) (TE=1.00 ms)	T_1/T_2 (TE=0.20 ms)
CH1	1671	37.30	2.31	4.55	16.14
CH2	118.3	69.35	20.75	24.58	3.34
CH3	1596	44.41	3.07	5.77	14.46
CH4	1740	37.09	3.06	4.63	12.12
CH5	1695	39.77	2.49	3.57	16.00
CH6	1653	39.74	2.49	3.70	15.93
CH9	259.2	58.96	12.56	3.70	4.69
CH10	2727	41.41	2.44	4.13	16.95
M14	9648	35.76	1.14	1.99	31.32
M13	73.9	67.55	10.05	15.42	6.72
SMT	18.1		58.95	68.57	
M4	151.2	48.22	13.07	14.24	3.69
OBM base oil (SF olefin base)	1.86		976.04	1145.50 [a]	4.69

[a]: TE=0.12 msec.

Table 8.1.5 Relaxation times of crude oils and the OBM base oil (T=100 °C, 20 MHz)

Sample	Viscosity (cp)	T_1 (ms)	T_2 (ms) (TE=0.20 ms)	T_2 (ms) (TE=1.00 ms)	T_1/T_2 (TE=0.20 ms)
CH1	203	60.05	13.40	16.38	4.48
CH3	113.1	75.93	23.98	27.26	3.17
CH4	168.8	52.13	16.34	18.99	3.19
CH5	152.6	65.94	17.16	19.92	3.84
CH6	141.2	61.59	18.41	21.43	3.34
CH9	45	137.91	66.10	74.53	2.09
CH10	302.2	56.38	13.36	18.39	4.22
M14	709.7	45.44	4.39	7.51	10.35
M13	19		31.61	28.56	
M4	25.2	120.92	60.12	64.96	2.01
OBM base oil (SF olefin base)	1.27		1803.38 [a]	1785.24	2.09

[a]: TE=0.40 msec.

Table 8.3.1 Viscosity of crude oils and the OBM base oil. The observed temperature dependence is described by $\eta = \eta(300K)\exp\left[\dfrac{\Delta E_a}{R}\left(\dfrac{1}{T}-\dfrac{1}{300}\right)\right]$. ($R$ is the gas constant)

Sample	API gravity	Expression	Regression coefficient R^2
CH1	10.3	$\eta = 4.64\times10^4 \exp\left[8.65\times10^3\left(\dfrac{1}{T}-\dfrac{1}{300}\right)\right]$	0.9809
CH2	14.4	$\eta = 1.26\times10^3 \exp\left[7.16\times10^3\left(\dfrac{1}{T}-\dfrac{1}{300}\right)\right]$	0.9996
CH3	9.7	$\eta = 4.07\times10^4 \exp\left[9.17\times10^3\left(\dfrac{1}{T}-\dfrac{1}{300}\right)\right]$	0.9953
CH4	9.2	$\eta = 5.22\times10^4 \exp\left[9.08\times10^3\left(\dfrac{1}{T}-\dfrac{1}{300}\right)\right]$	0.9850
CH5	10.2	$\eta = 4.43\times10^4 \exp\left[8.93\times10^3\left(\dfrac{1}{T}-\dfrac{1}{300}\right)\right]$	0.9895
CH6	10.9	$\eta = 4.77\times10^4 \exp\left[9.17\times10^3\left(\dfrac{1}{T}-\dfrac{1}{300}\right)\right]$	0.9891
CH9	14.1	$\eta = 2.29\times10^3 \exp\left[9.17\times10^3\left(\dfrac{1}{T}-\dfrac{1}{300}\right)\right]$	0.9942
CH10	9.4	$\eta = 7.65\times10^4 \exp\left[8.78\times10^3\left(\dfrac{1}{T}-\dfrac{1}{300}\right)\right]$	0.9843
M14		$\eta = 4.37\times10^5 \exp\left[1.02\times10^4\left(\dfrac{1}{T}-\dfrac{1}{300}\right)\right]$	0.9853
M4		$\eta = 1.69\times10^3 \exp\left[6.61\times10^3\left(\dfrac{1}{T}-\dfrac{1}{300}\right)\right]$	0.9912
M13		$\eta = 4.54\times10^2 \exp\left[4.98\times10^3\left(\dfrac{1}{T}-\dfrac{1}{300}\right)\right]$	0.9922
OBM base oil		$\eta = 2.81\exp\left[1.22\times10^3\left(\dfrac{1}{T}-\dfrac{1}{300}\right)\right]$	0.9995

Table 8.3.2 Correlations of relaxation times in crude oils

	Correlation	Regression coefficient R^2
T_2 data from this work	$T_2 = 591.3\eta^{-0.71}$	0.98
	$T_2 = 9.43\left(\dfrac{\eta}{T}\right)^{-0.69}$	0.98
T_2 data from Jacob et al.	$T_2 = 3330\eta^{-1.34}$	0.97
	$T_2 = 1.81\left(\dfrac{\eta}{T}\right)^{-1.26}$	0.97

Table 8.4.1 *HI* of crude oils and the OBM base oil at different temperatures

Sample	T=30 °C, 2 MHz		
		HI (T_2, TE=0.24 ms)	*HI* (T_2, TE=1.00 ms)
CH1		0.56	0.23
CH2		0.89	0.73
CH3		0.50	0.15
CH4		0.46	0.18
CH5		0.52	0.18
CH6		0.54	0.24
CH7		0.96	0.91
CH8		0.91	0.88
CH9		0.85	0.69
CH10		0.40	0.11
	T=40 °C, 20 MHz		
	HI (T_2, TE=0.08 ms)	*HI* (T_2, TE=0.20 ms)	*HI* (T_2, TE=1.00 ms)
CH1	0.69	0.55	0.41
CH2	0.73	0.64	0.58
CH3	0.71	0.58	0.40
CH4	0.66	0.54	0.35
CH5	0.50	0.41	0.00
CH6	0.71	0.58	0.39
CH7	0.75	0.66	0.63
CH8	0.68	0.58	0.58
CH9	0.73	0.64	0.57
CH10	0.78	0.60	0.38
OBM base oil		0.90	0.89
	T=60 °C, 20 MHz		
		HI (T_2, TE=0.20 ms)	*HI* (T_2, TE=1.00 ms)
CH1		0.67	0.48

CH2		0.65	0.63
CH3		0.65	0.49
CH4		0.86	0.76
CH6		0.75	0.64
CH9		0.77	0.73
CH10		0.92	0.68
M14		0.76	0.66
OBM base oil		0.94	0.94
	T=100 °C, 20 MHz		
		HI (T_2, TE=0.20 ms)	HI (T_2, TE=1.00 ms)
CH1		0.91	0.86
CH2			
CH3		0.78	0.84
CH4		0.94	0.91
CH5			
CH6		0.98	0.94
CH9			
CH10			
M14		0.99	0.96
M13		0.93	0.82
M4		1.05	0.83
OBM base oil		1.03	0.99
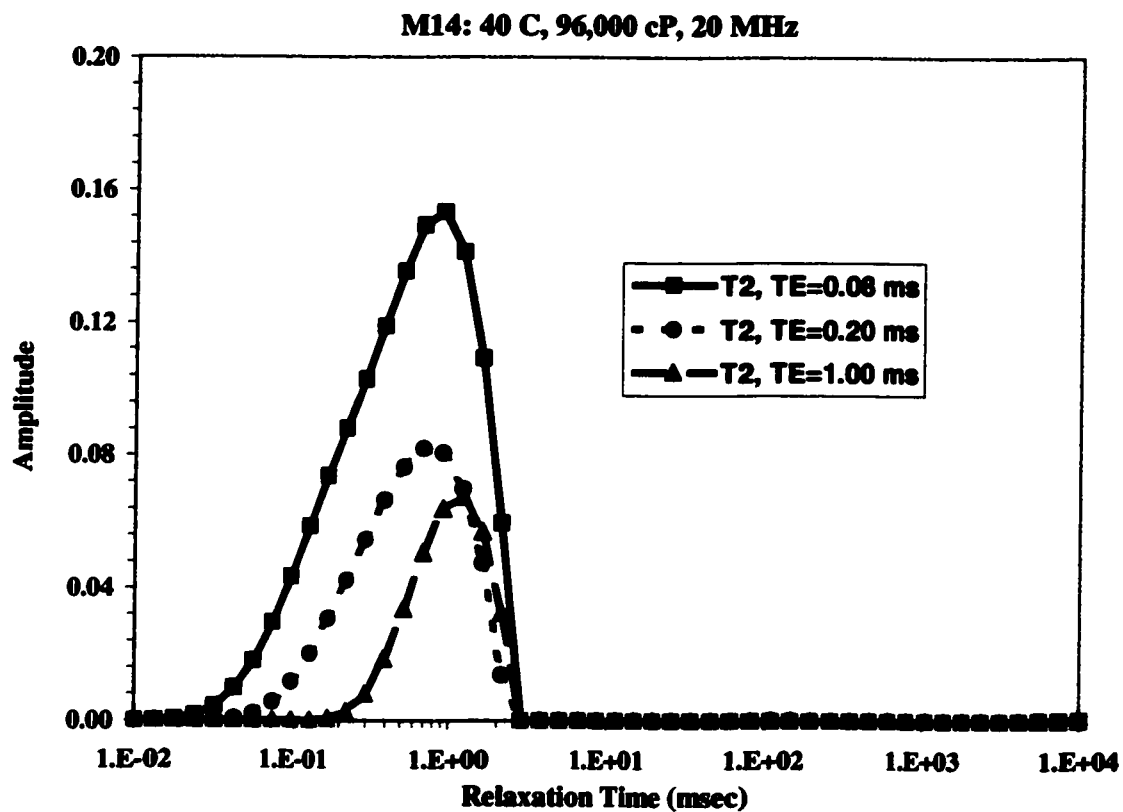
Figure 8.1.1 T_2 distributions varying echo spacing (TE) for a very heavy oil (M14). The apparent T_2 distributions were measured by the 20 MHz Bruker spectrometer. With increasing the echo spacing, apparent T_2 time constants were shifted to longer times and the signal amplitude decreases.
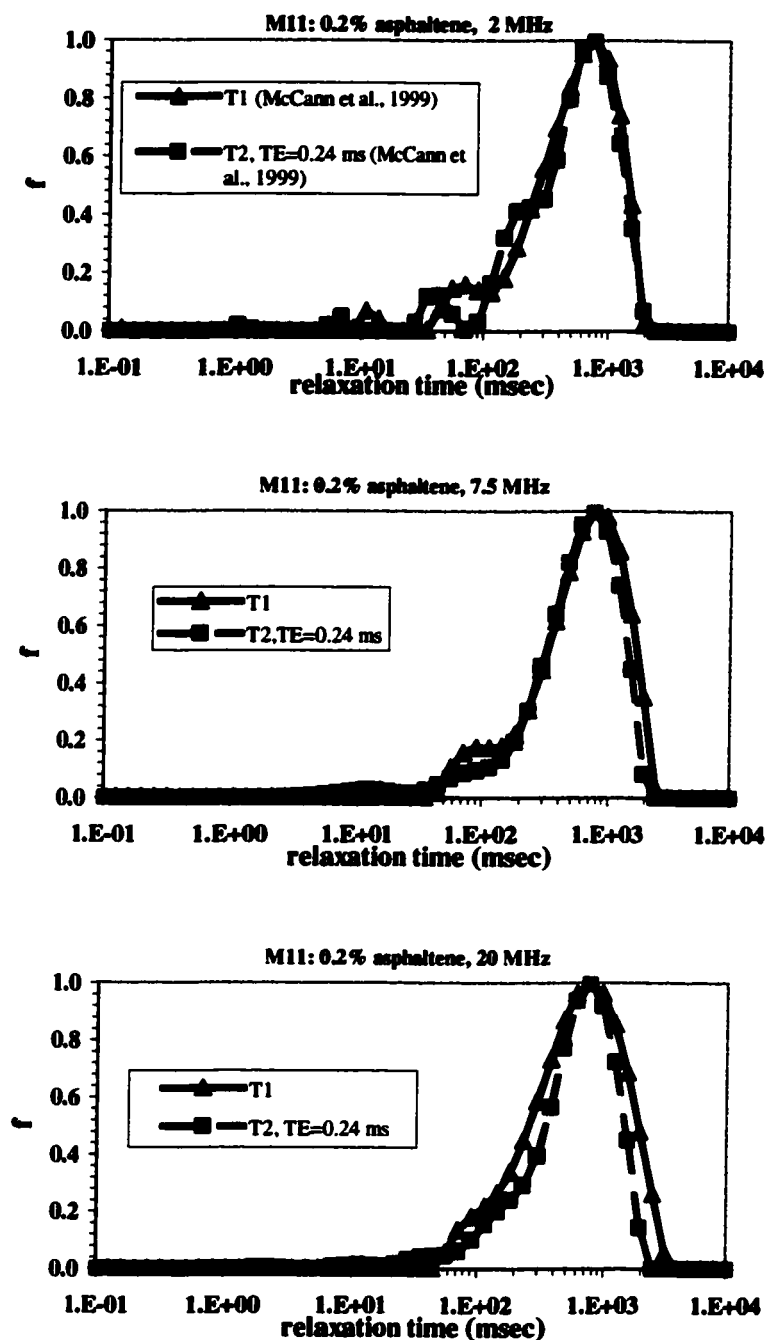
Figure 8.1.2 Relaxation time distributions of a light oil (M11). The temperature is 30 °C for the 2 MHz NMR spectrometer. The temperature is 40 °C for 7.5 MHz and 20 MHz NMR spectrometers. The viscosity of the M11 oil is 3.7 cP at 30 °C. The T_1 and T_2 distributions of the M11 oil overlay each other. In addition, the T_1 and T_2 distributions of the light oil are not sensitive to the Larmor frequency.
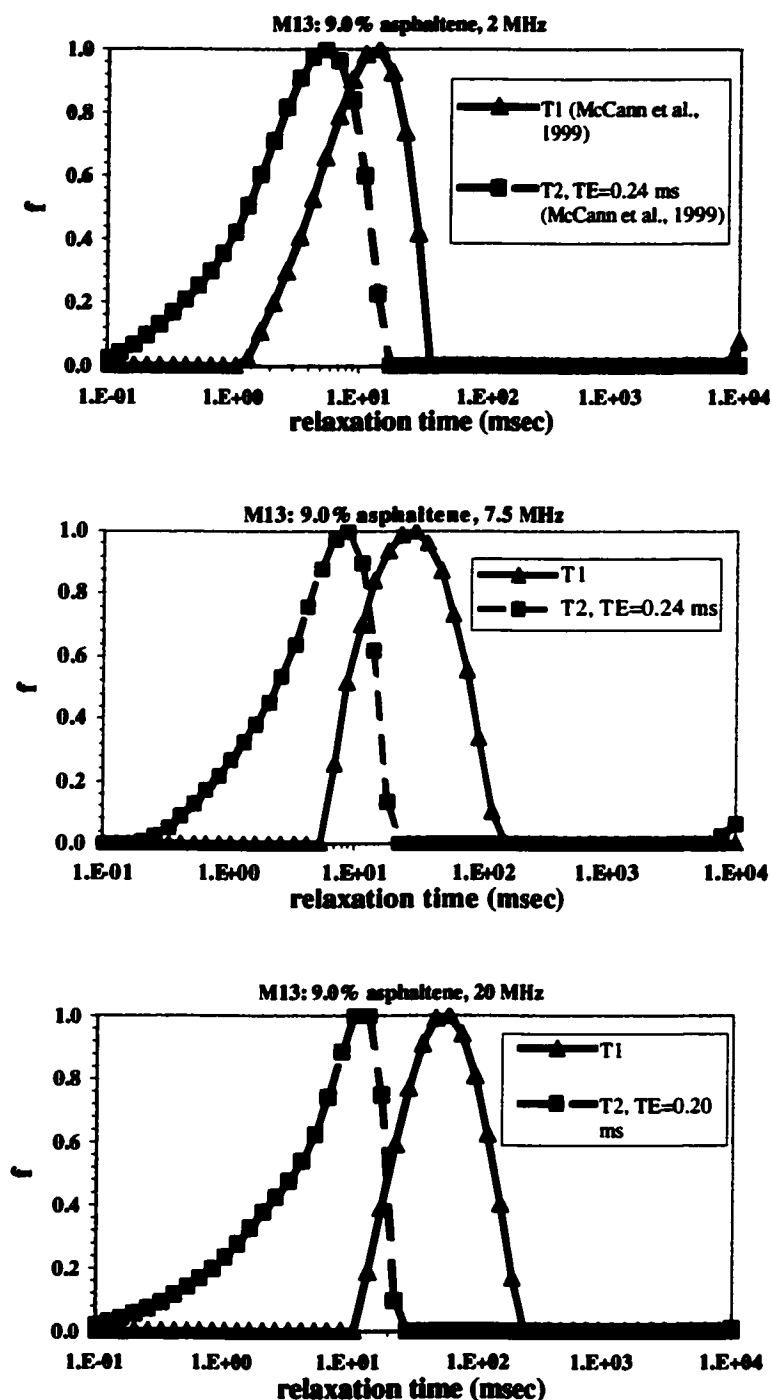
Figure 8.1.3 Relaxation time distributions of a viscous oil (M13). The temperature is 30 °C for the 2 MHz NMR spectrometer. The temperature is 40 °C for 7.5 MHz and 20 MHz NMR spectrometers. The viscosity of the M13 oil is 421 cP at 30 °C and is 222 cP at 40 °C. The M13 crude oil has a T_2 distribution that is clearly shorter than the T_1 distribution.
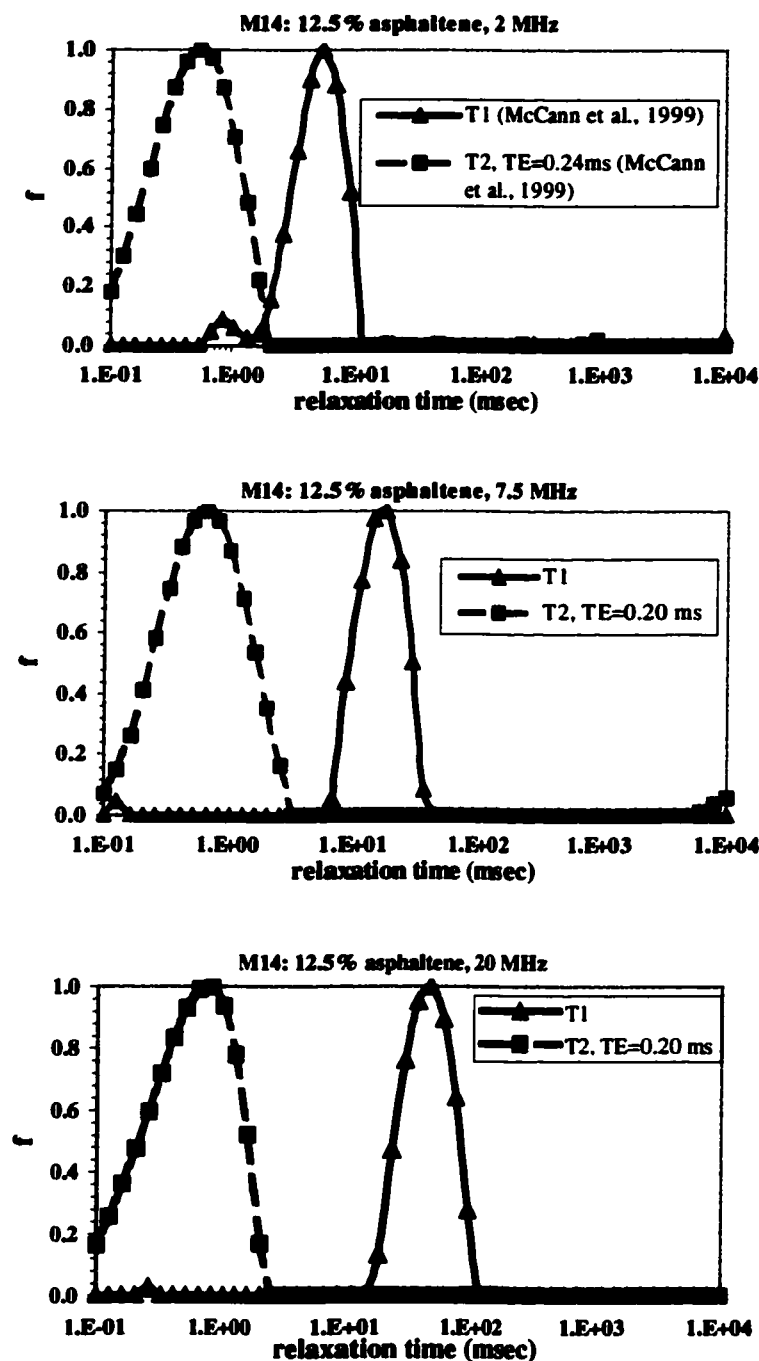
Figure 8.1.4 Relaxation time distributions of a very heavy oil (M14). The temperature is 30 °C for the 2 MHz NMR spectrometer. The temperature is 40 °C for 7.5 MHz and 20 MHz NMR spectrometers. The viscosity of the M14 oil is 415,000 cP at 30 °C and is 96,000 cP at 40 °C. The T_1 and T_2 distributions of this oil have separated. The separation between the T_1 and T_2 distributions becomes more obvious with increasing the Larmor frequency.
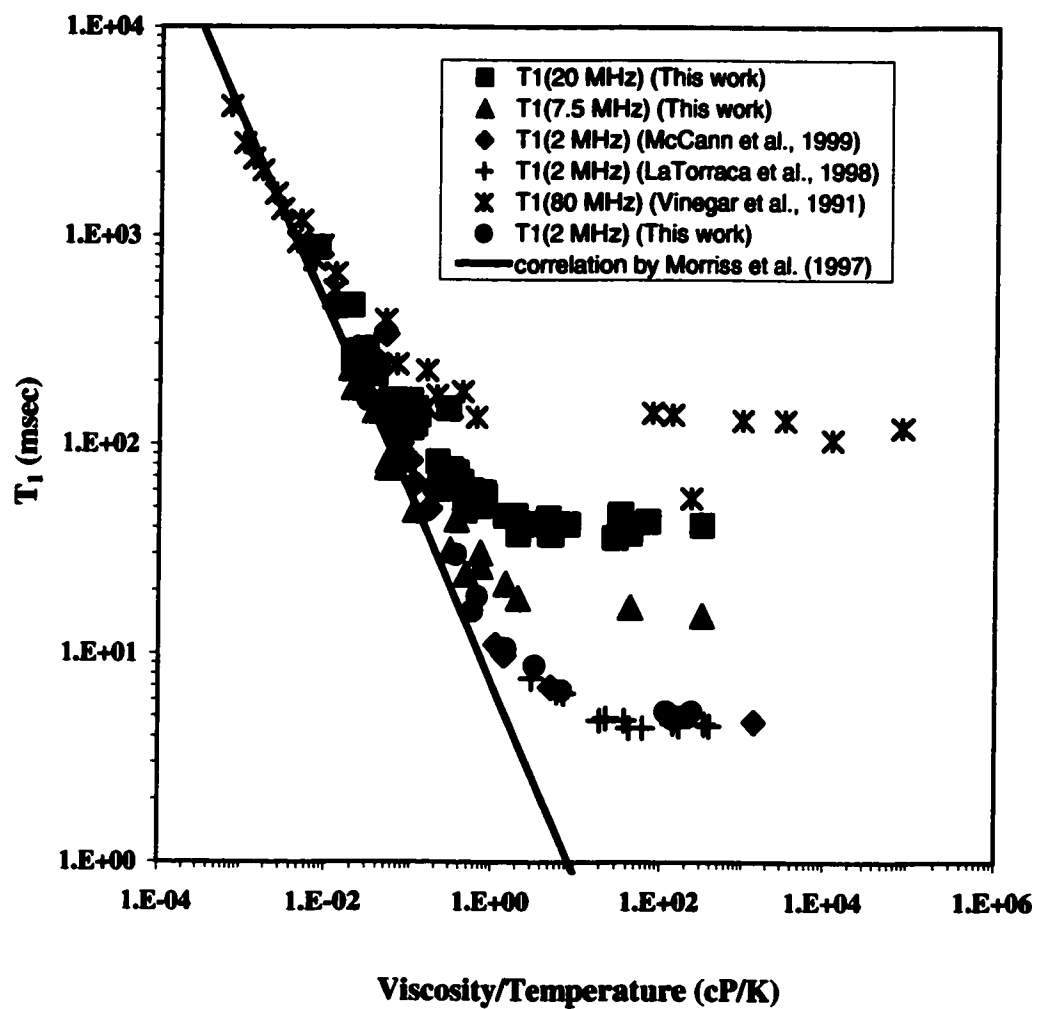
Figure 8.1.5 T_1 versus viscosity/temperature plot for crude oils. T_1 starts to level off at high viscosity.
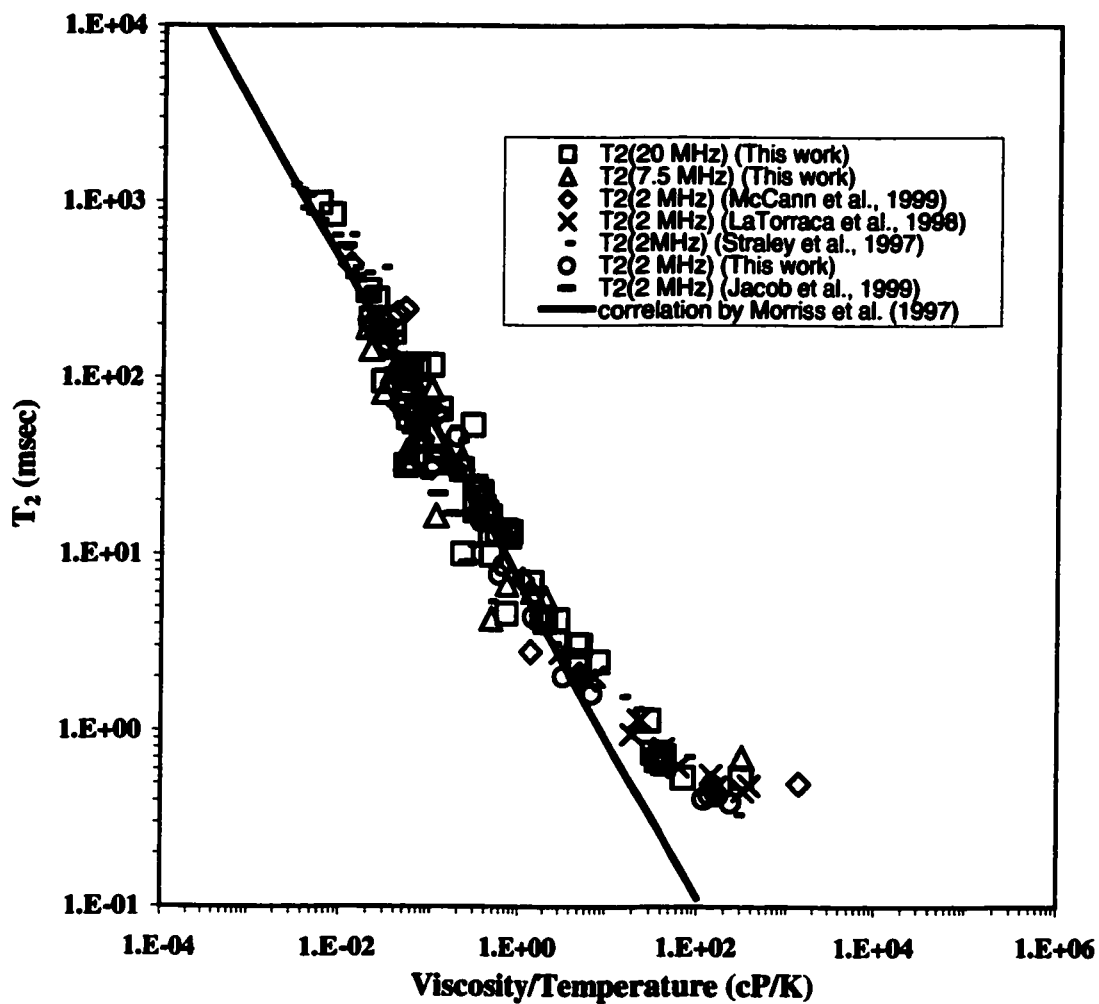
Figure 8.1.6 T_2 versus viscosity/temperature plot for crude oils. T_2 continues to shorten with increasing viscosity.
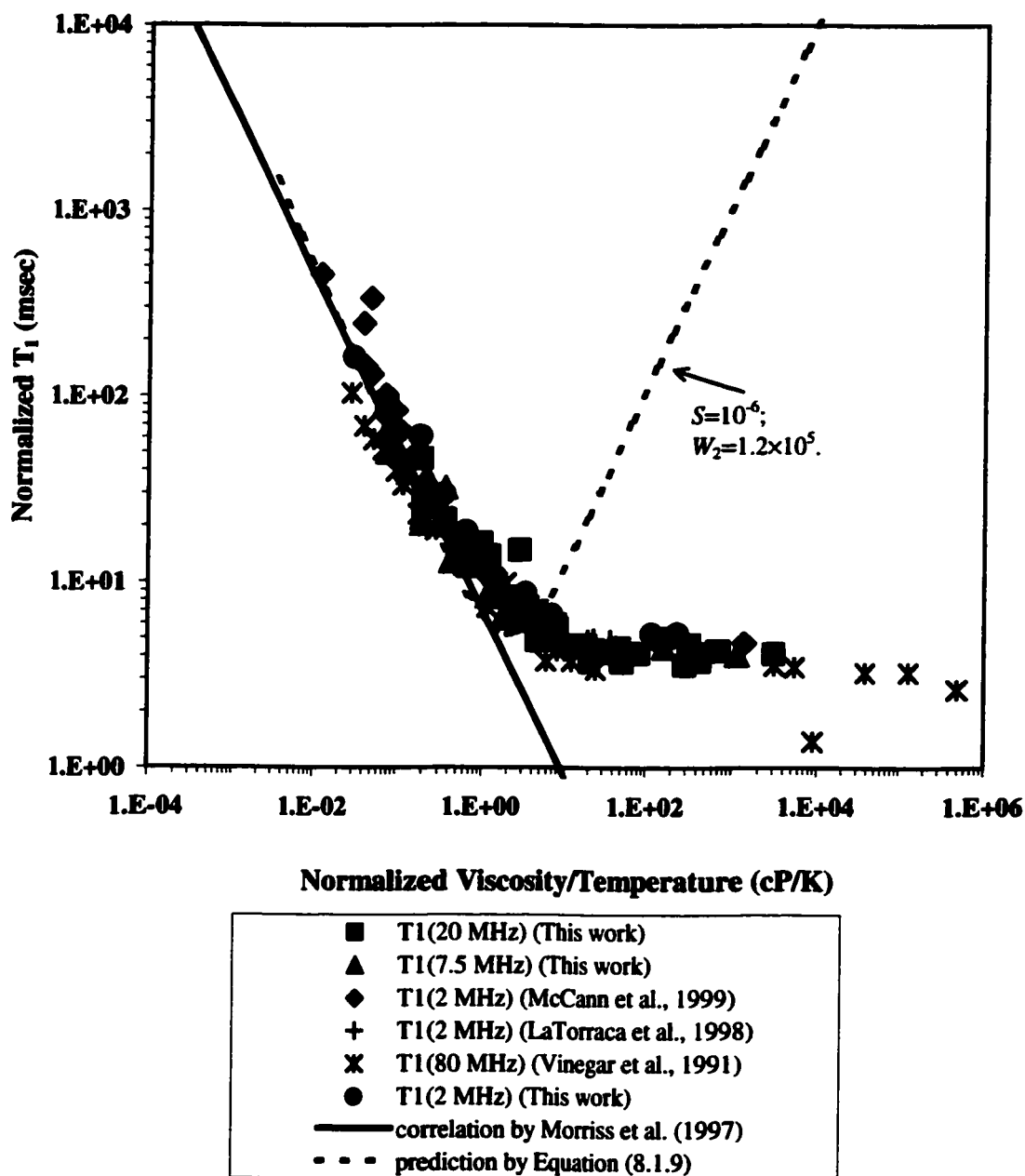
Figure 8.1.7 Dependence of the normalized T_1 relaxation time on normalized viscosity/temperature. All of the T_1 data fall on the same curve for different Larmor frequencies. The T_1 curve reaches a plateau with normalized viscosity/temperature greater than about 10 cP/K. T_1 does not follow the trend predicted by Equation (8.1.9).
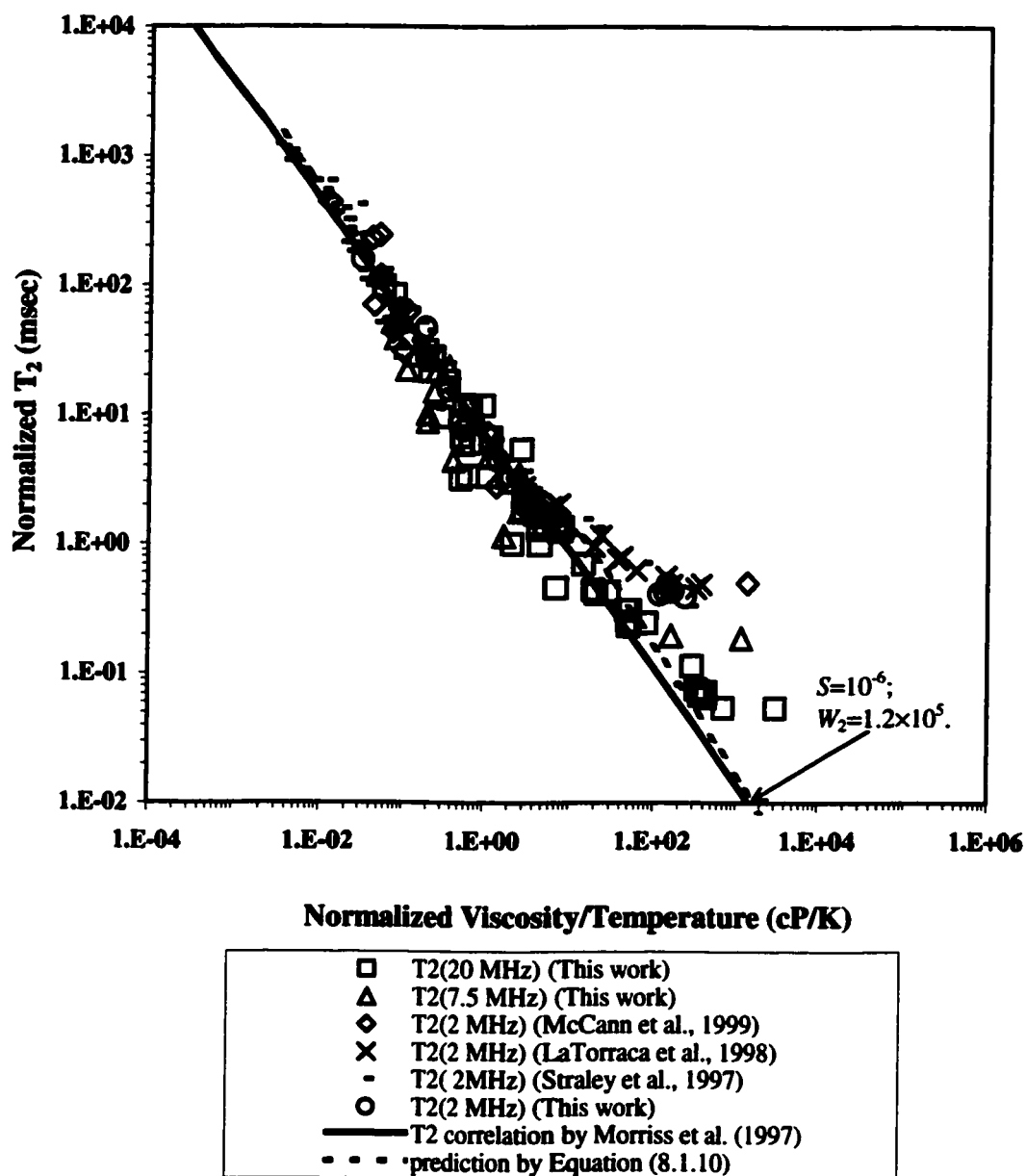
Figure 8.1.8 Dependence of the normalized T_2 relaxation time on normalized viscosity/temperature. T_2 of low viscosity crude oils is consistent with the correlation by Morriss et al. However, high viscosity crude oils depart this correlation, probably because of the echo spacing limitation.
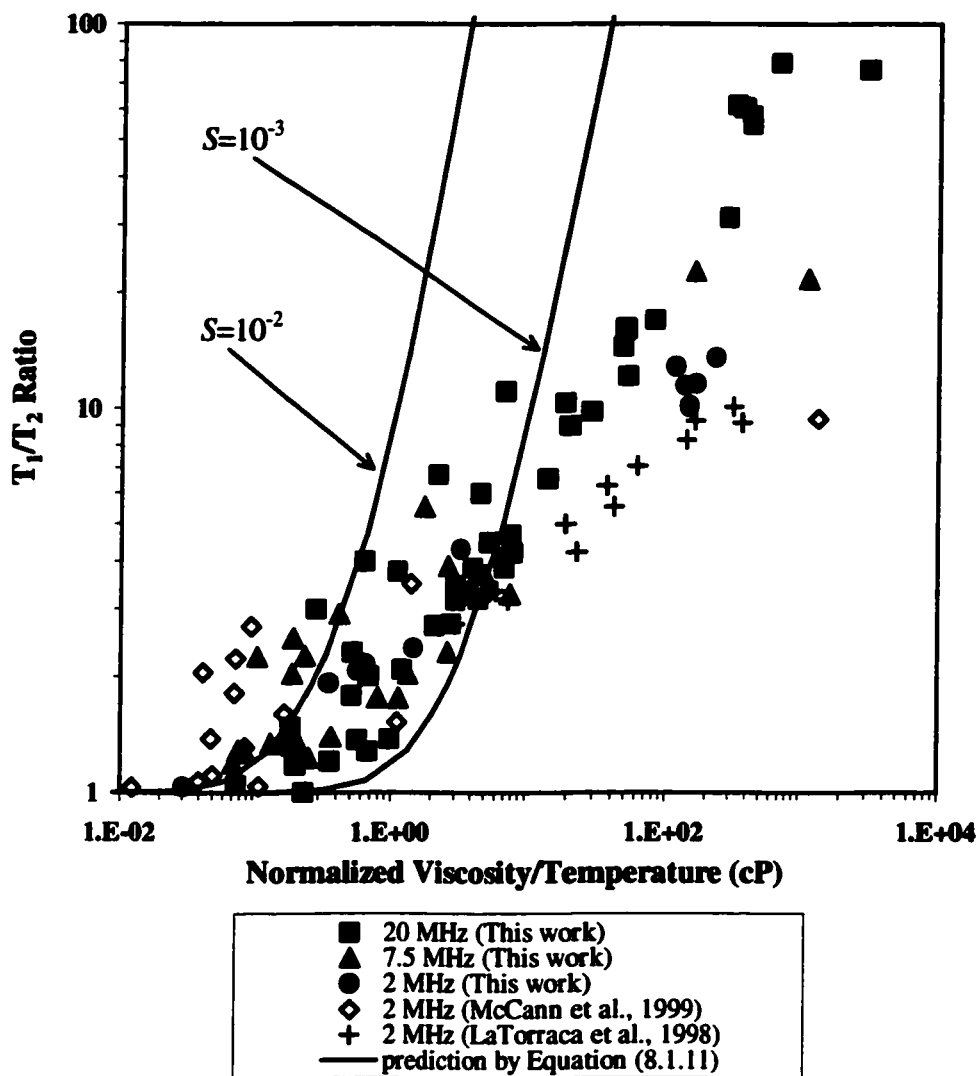
Figure 8.1.9 T_1/T_2 dependence on normalized viscosity/temperature in crude oils. Low viscosity oils have the ratio of T_1/T_2 close to 1 as predicted by Equation (8.1.11). The experimental data of heavy oils depart from the trend predicted by the theory.
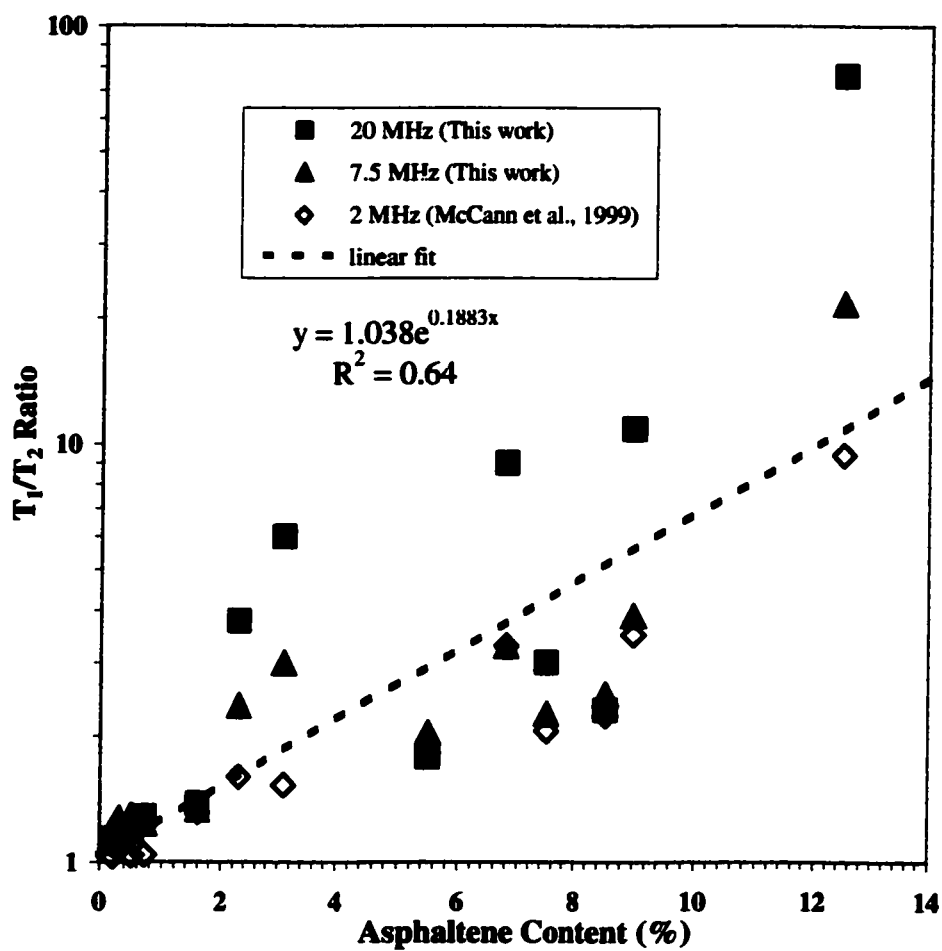
Figure 8.2.1 T_1/T_2 versus asphaltene content plot in crude oils. T_1/T_2 increases with the increase of asphaltene content.
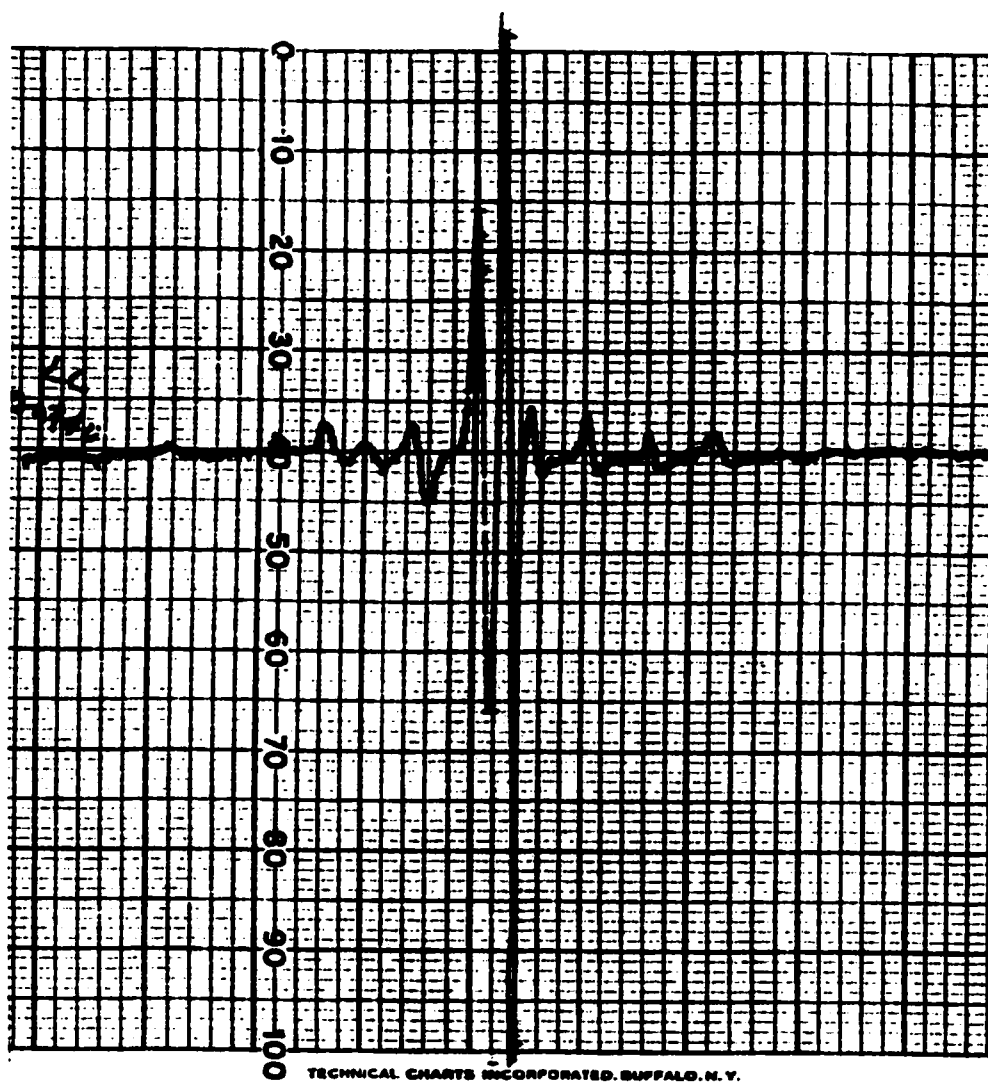
Figure 8.2.2 The ESR spectrum of the M13 crude oil. The big peak in the middle is the free radical signal. The small peaks are vanadium signals.
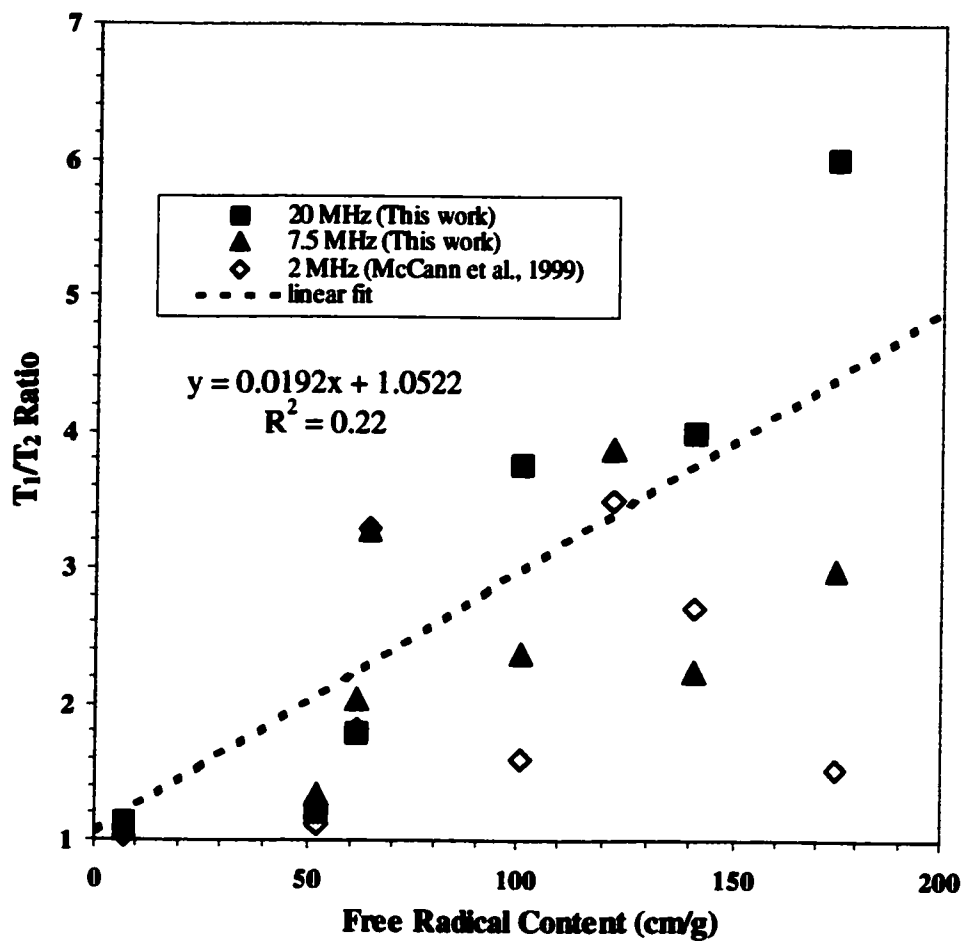
Figure 8.2.3 Free radical content versus T_1/T_2 ratio plot for crude oils. With increasing the free radical content, T_1/T_2 ratio increases.
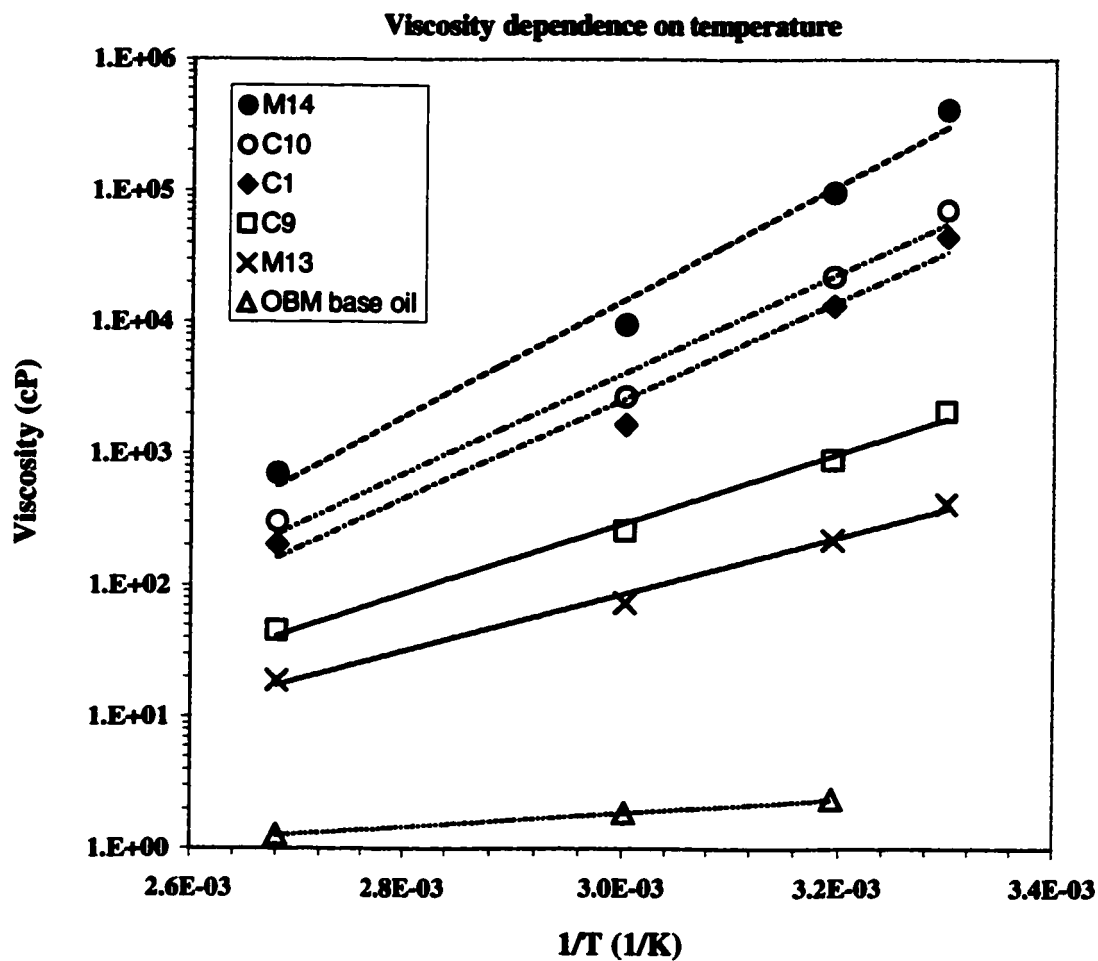
Figure 8.3.1 Viscosity dependence on temperature for crude oils and the OBM base oil. There is an exponential relationship between relaxation times and the reciprocal of the temperature.
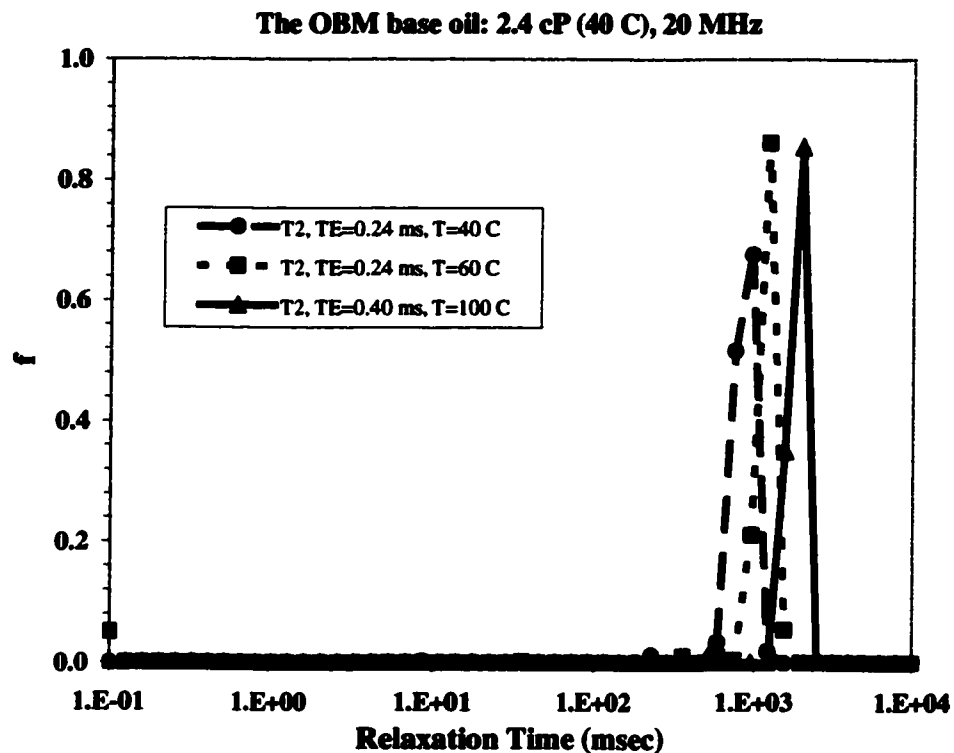
Figure 8.3.2 Relaxation time distributions of the OBM base oil at different temperatures. The measurements at 40 °C were done with the samples in the 13 mm diameter glass tubes by the 20 MHz NMR spectrometer with the fixed temperature. The measurements at 60 °C and 100 °C were done with the samples in the 10 mm diameter glass tubes by the 20 MHz NMR spectrometer with variable temperature controller unit. With increasing the temperature, the peak moves to longer relaxation times.
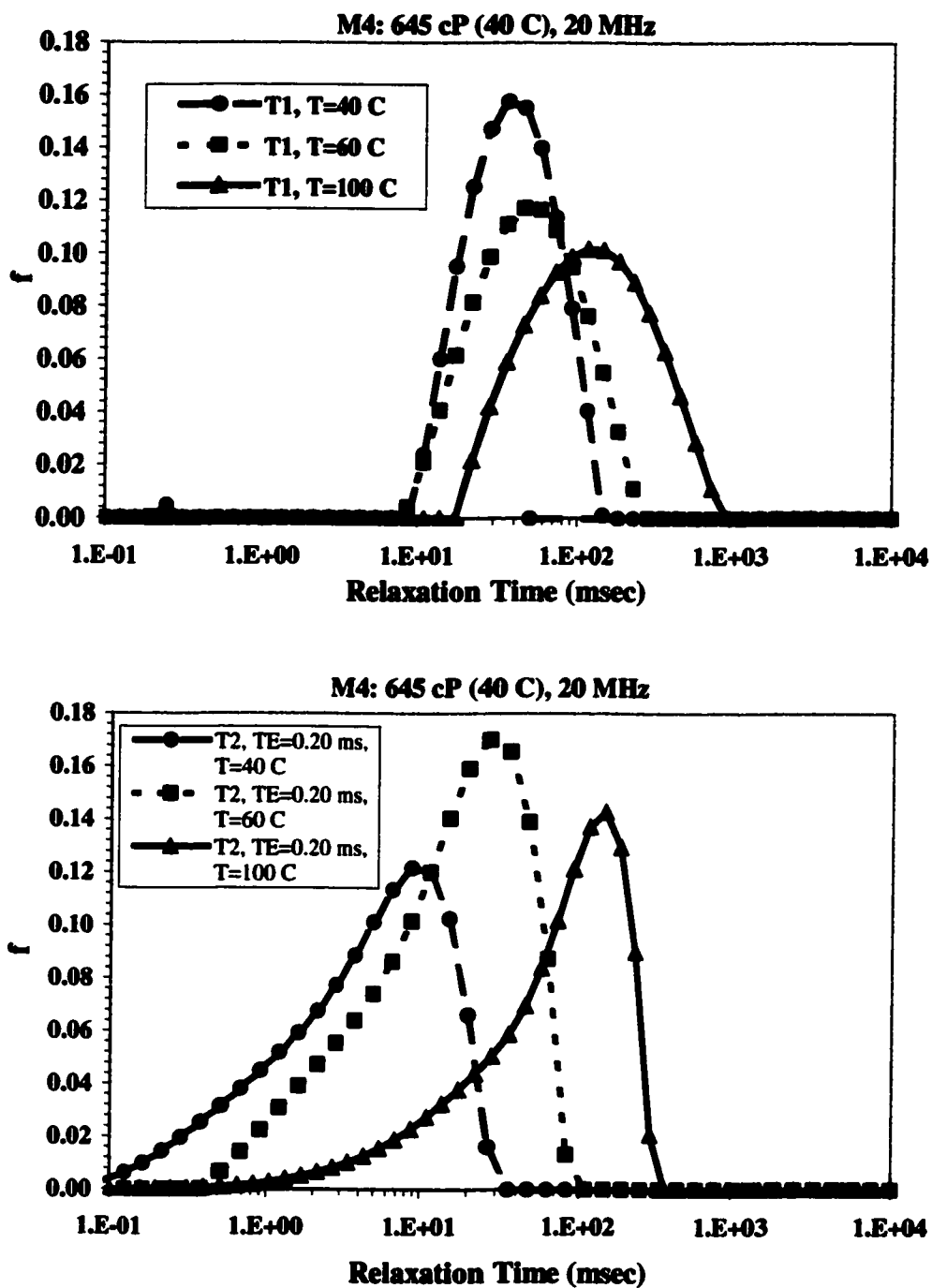
Figure 8.3.3 Relaxation time distributions of a viscous oil (M4) at different temperatures. With increasing temperature, the T_2 distribution becomes broader.
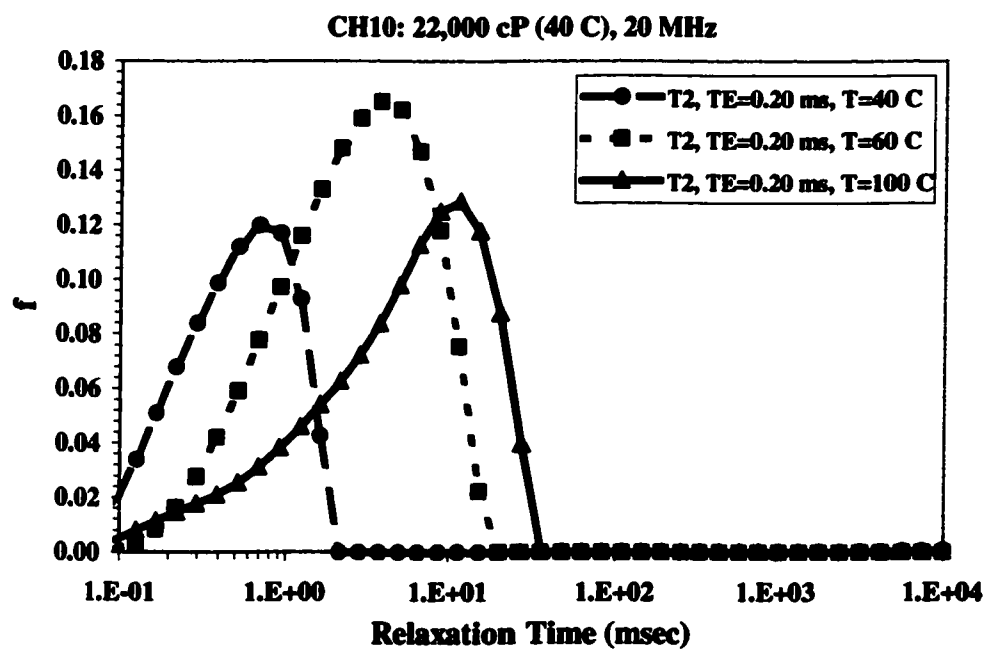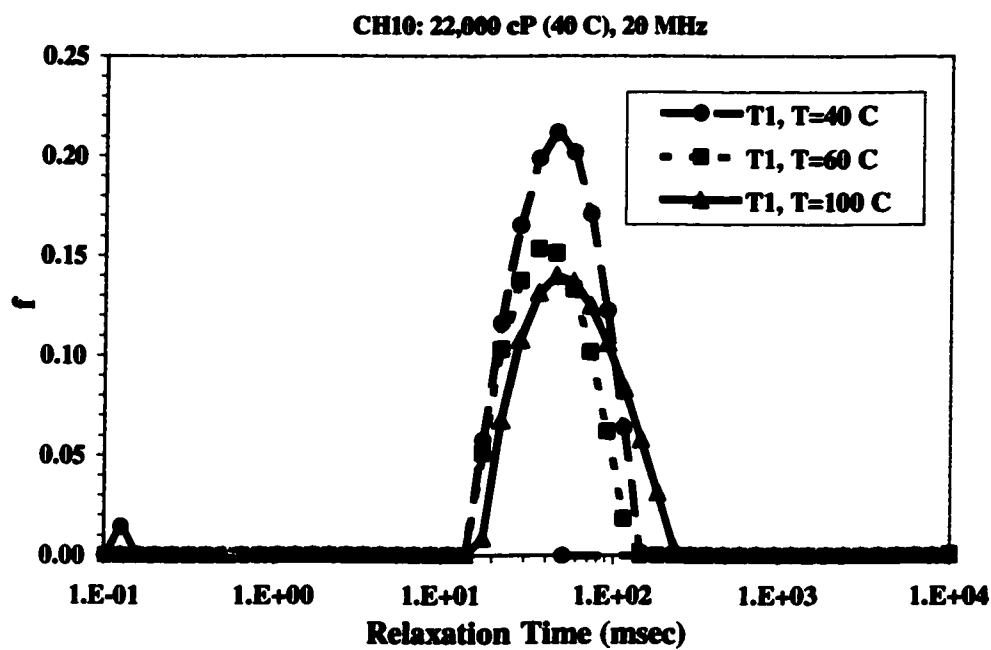
Figure 8.3.4 Relaxation time distributions of a heavy oil (CH10) at different temperatures. With increasing temperature, the T_2 distribution becomes broader.
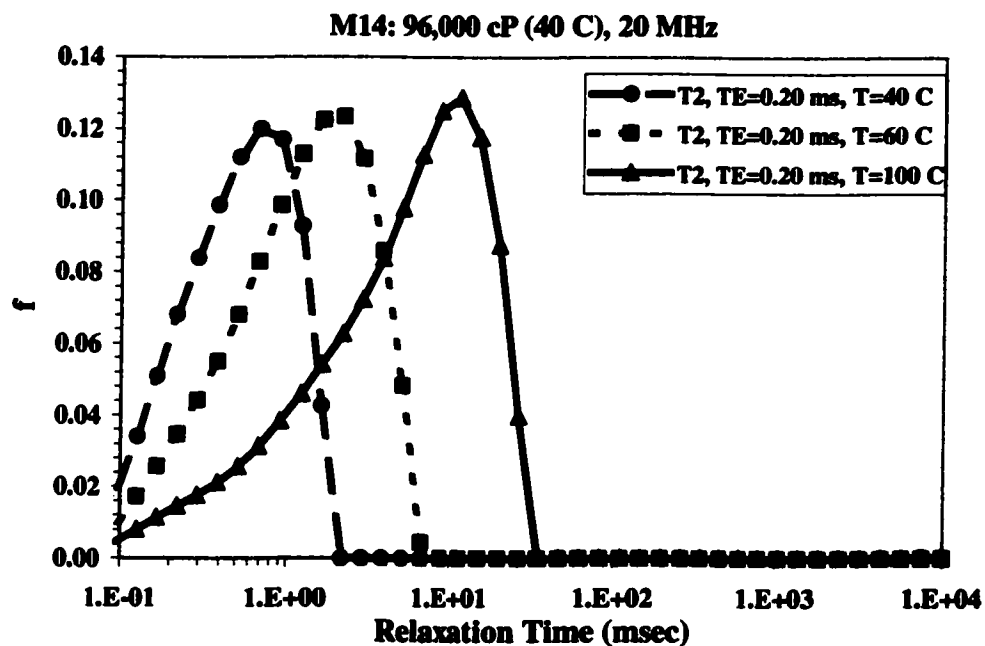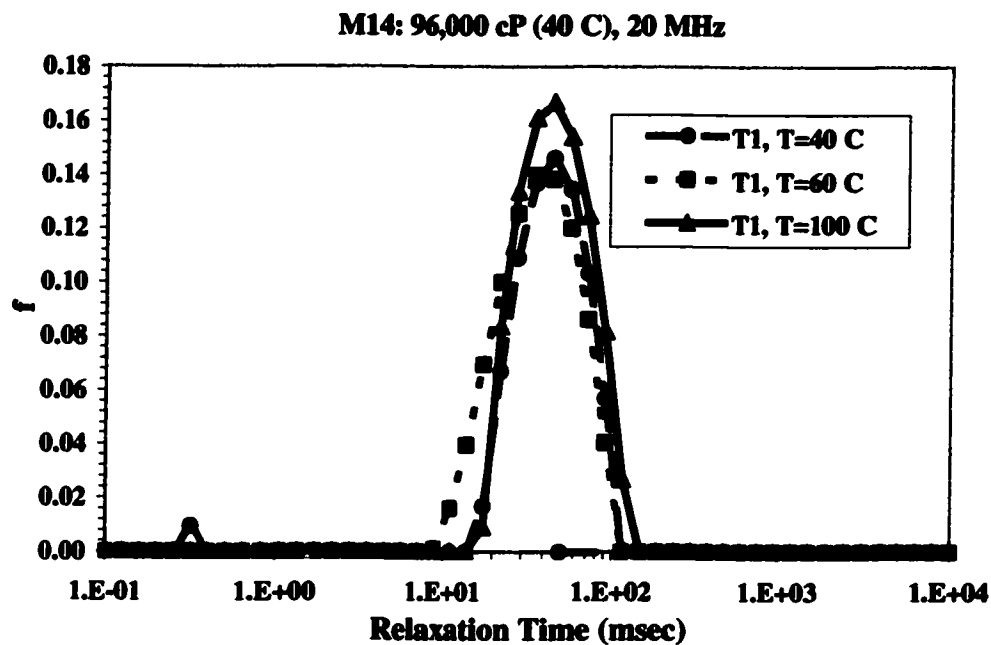
Figure 8.3.5 Relaxation time distributions of a very heavy oil (M14) at different temperatures. With increasing temperature, the T_2 distribution becomes broader. For very heavy crude oils, the changes in the T_1 distributions are slight.
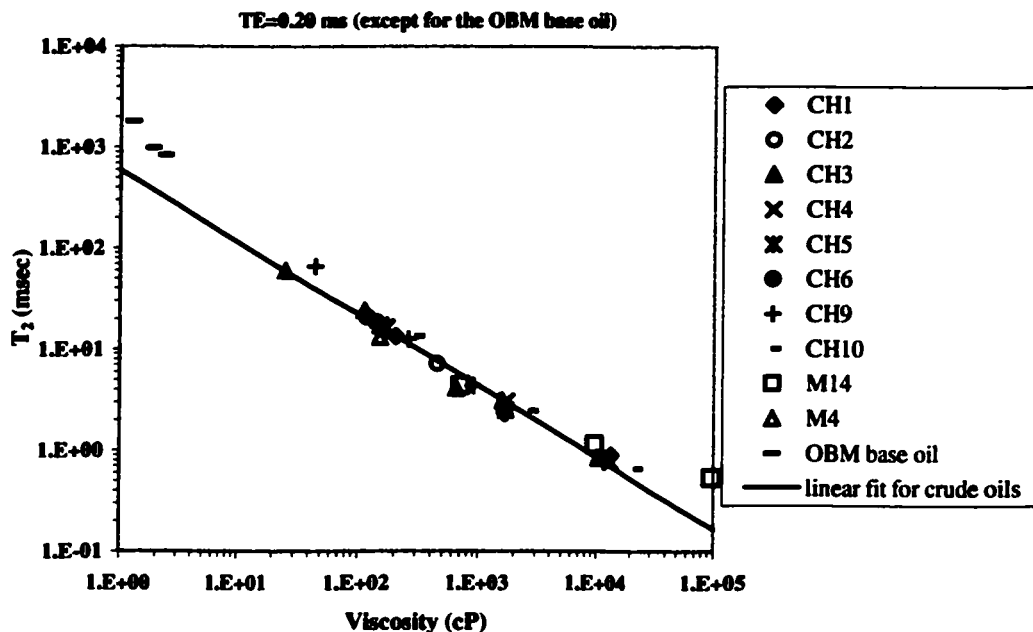
Figure 8.3.6 (a) The correlation of T_2 with viscosity for crude oils measured by this work. For the OBM base oil, TE is 0.24 msec at 40 °C and 60 °C and is 0.40 msec at 100 °C. The correlation is $T_2 = 591.3\eta^{-0.71}$ (R^2=0.98).
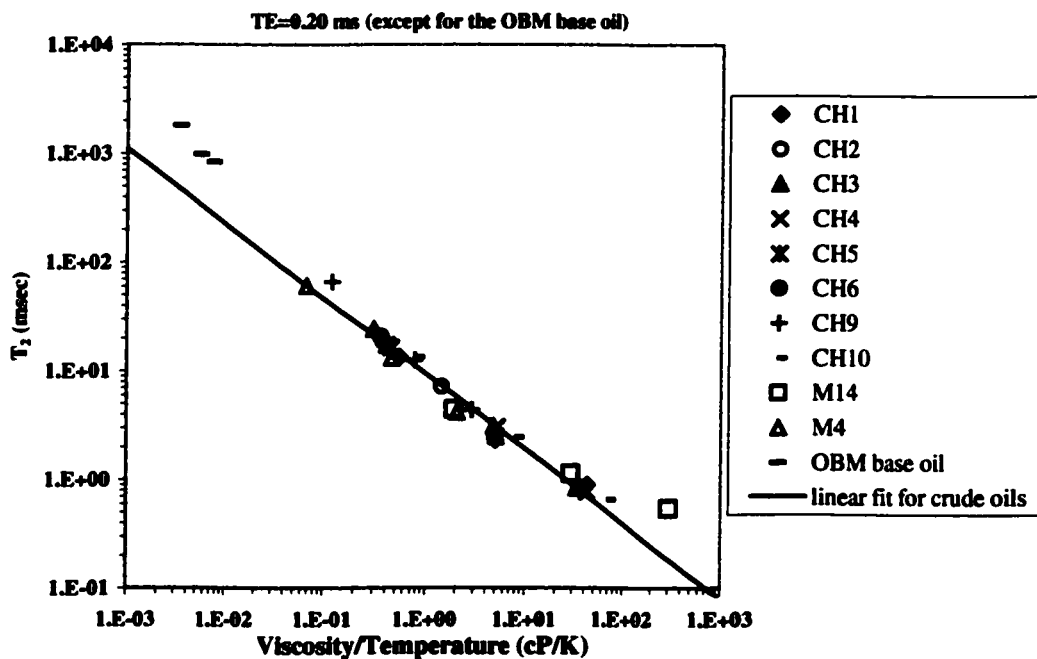

Figure 8.3.6 (b) The correlation of T_2 with viscosity/temperature for crude oils measured by this work. For the OBM base oil, TE is 0.24 msec at 40 °C and 60 °C and is 0.40 msec at 100 °C. The correlation is $T_2 = 9.43\left(\dfrac{\eta}{T}\right)^{-0.69}$ (R^2=0.98). T_2 data are equally well correlated with both viscosity and viscosity/temperature.
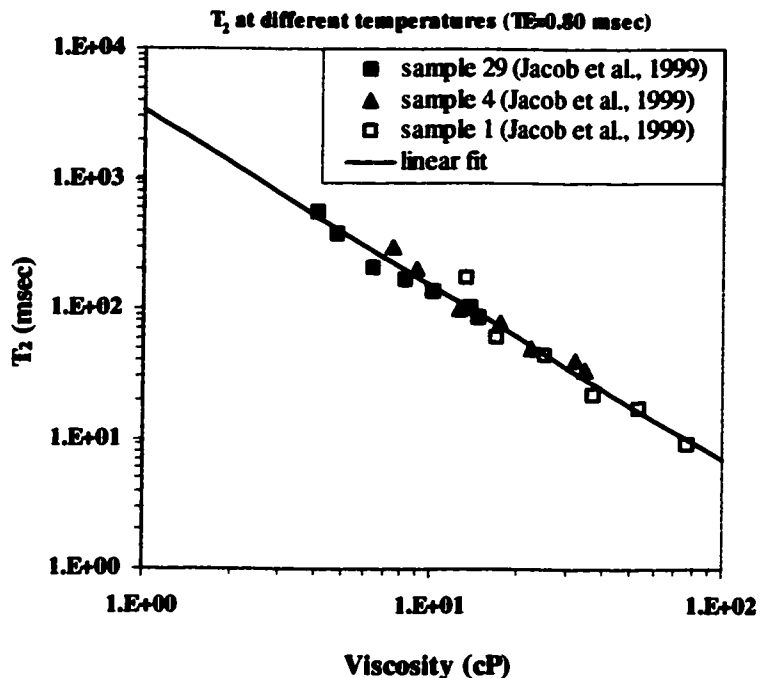
T₂ at different temperatures (TE=0.80 msec)

Figure 8.3.7 (a) The correlation of T_2 with viscosity for crude oils measured by Jacob et al. (Jacob and Davis, 1999). The correlation is $T_2 = 3330\eta^{-1.34}$ (R^2=0.97).

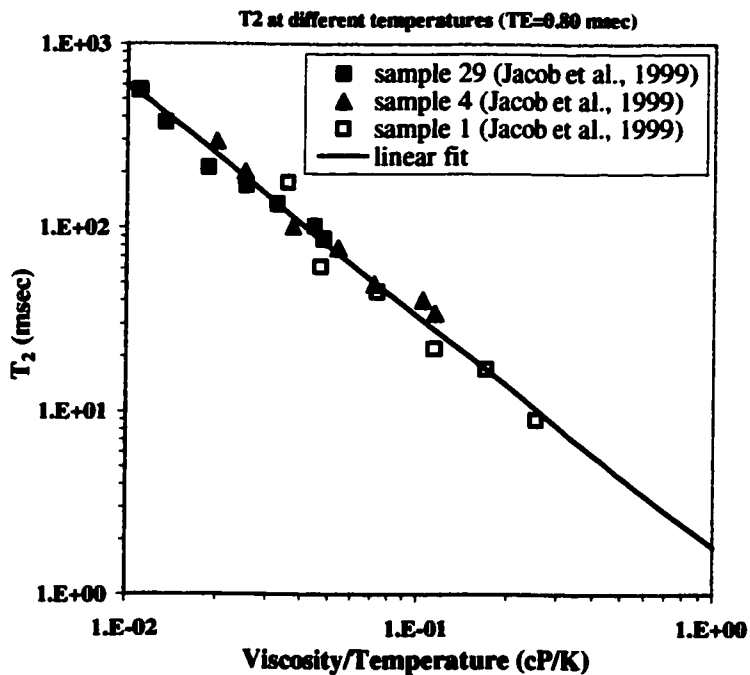**T2 at different temperatures (TE=0.80 msec)**

Figure 8.3.7 (b) The correlation of T_2 with viscosity/temperature for crude oils measured by Jacob et al. (Jacob and Davis, 1999). The correlation is $T_2 = 1.81\left(\dfrac{\eta}{T}\right)^{-1.26}$ (R^2=0.98). T_2 data are equally well correlated with both viscosity and viscosity/temperature.
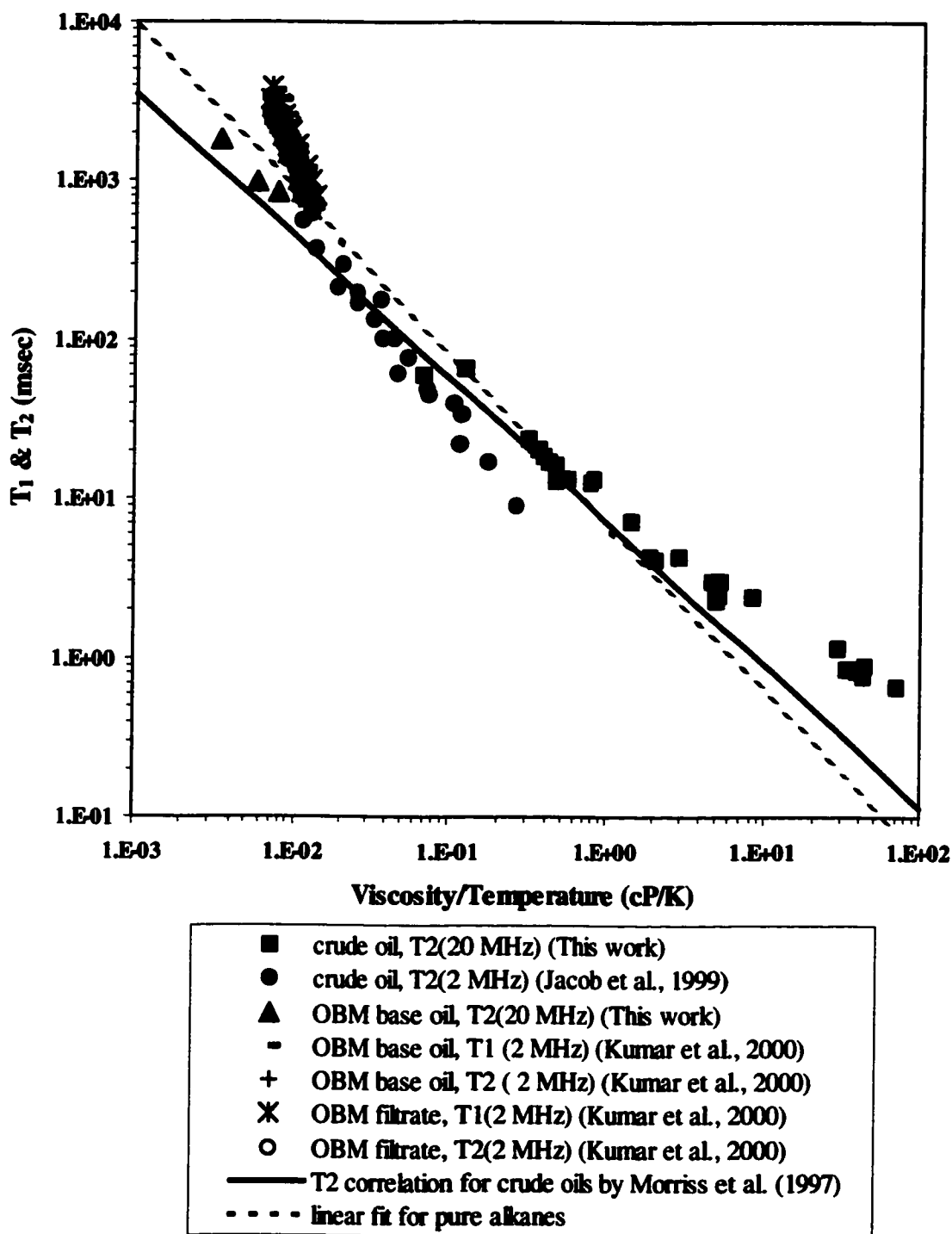
Figure 8.3.8 Relaxation times as a function of viscosity/temperature for crude oils, OBM samples, and pure higher alkanes. Jacob et al.'s light oil data follow the correlation by Morriss et al. (Morriss et al., 1997). However, their crude oil data depart from the correlation by Morriss et al. with increasing viscosity/temperature. The crude oil data by this work are consistent with the correlation by Morriss et al. if viscosity/temperature is lower than 1 cP/K.
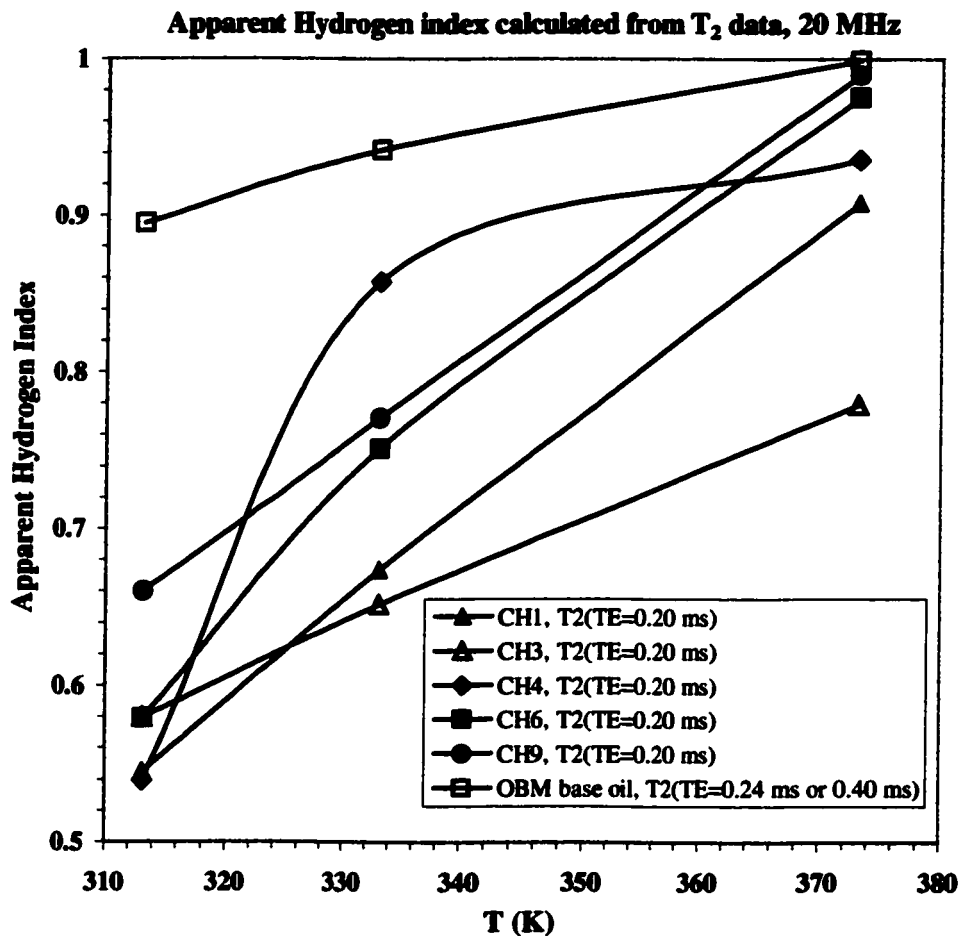
Figure 8.4.1 Apparent hydrogen index from T_2 data versus temperature plot for crude oils and the OBM base oil. For the OBM sample, TE is 0.24 msec for the measurements at 40 °C and 60 °C and is 0.40 msec for the measurements at 100 °C. Apparent HI of heavy crude oils will increase with increasing temperature.
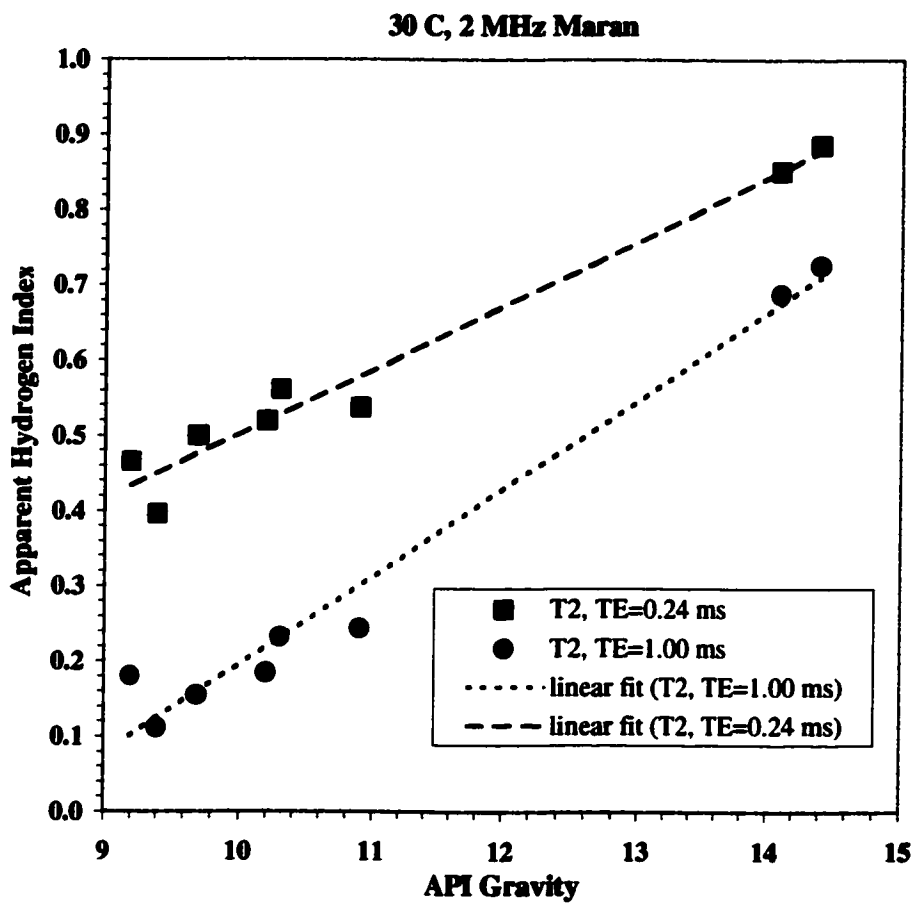
Figure 8.4.2 Apparent hydrogen index versus API gravity plots for crude oils measured by the 2 MHz NMR spectrometer. With increasing echo spacing, apparent *HI* decreases.
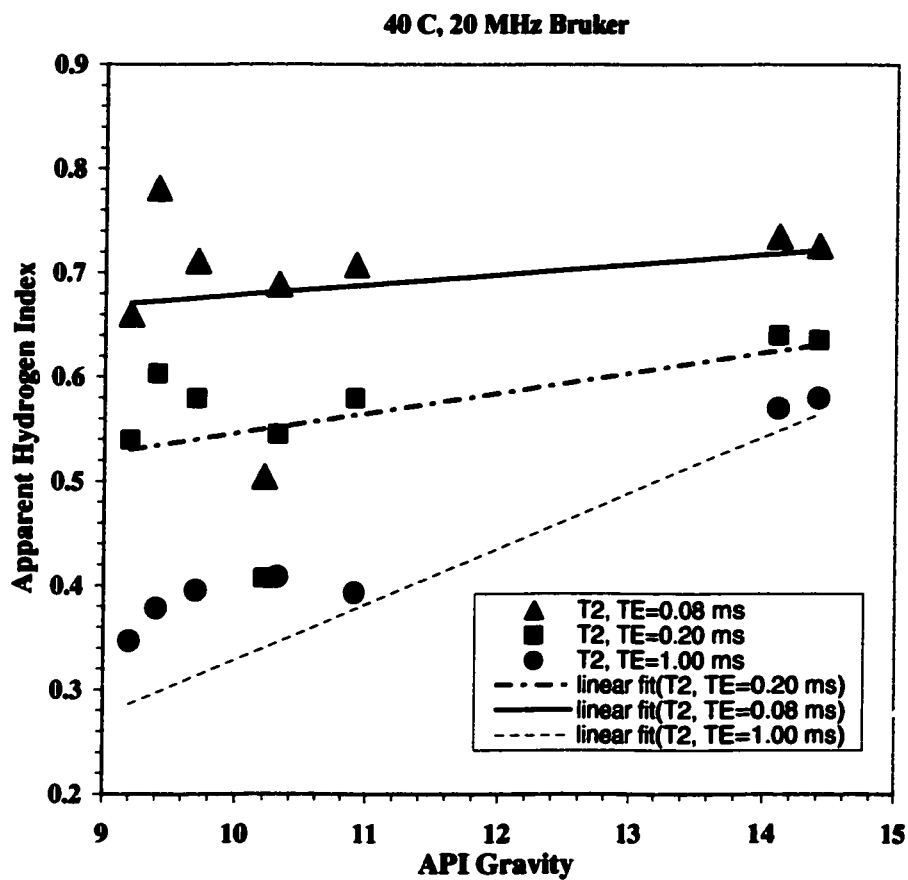
Figure 8.4.3 Apparent hydrogen index versus API gravity plots for crude oils measured by the 20 MHz NMR spectrometer. With increasing echo spacing, apparent *HI* decreases.
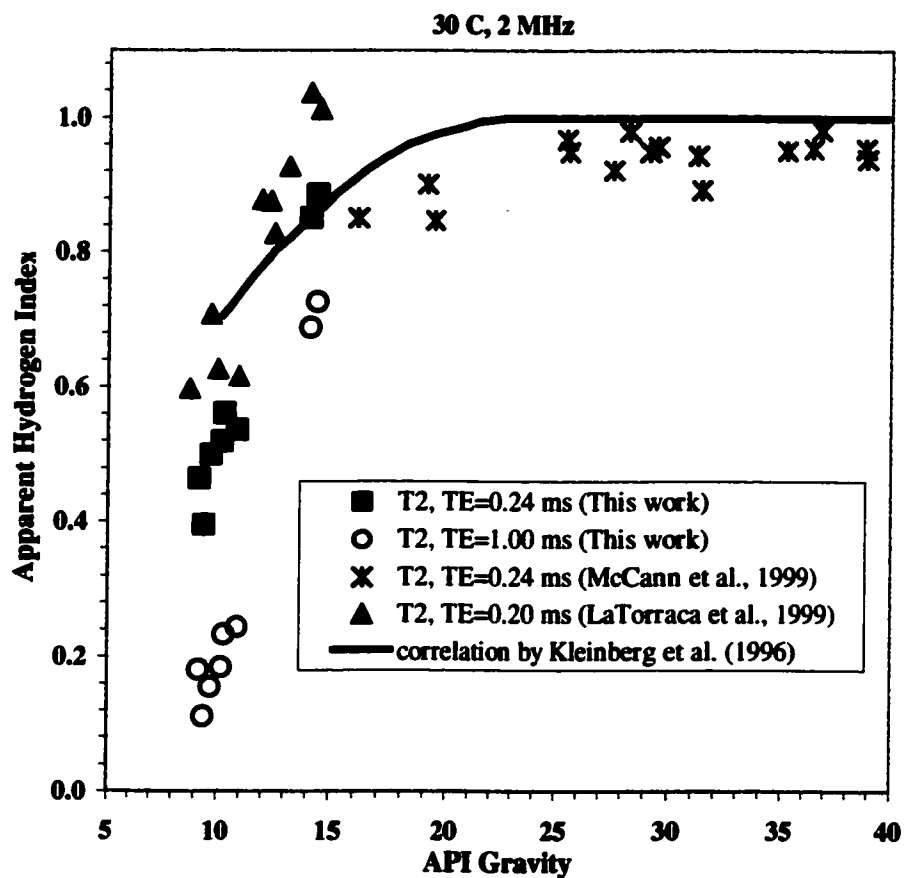
Figure 8.4.4 Comparison of the correlation by Kleinberg et al. with NMR measurements in crude oils. The correlation by Kleinberg et al. (Kleinberg and Vinegar, 1996) is based on the data of low and medium density oils. It has the *HI* equal to unity for oils lighter than 25° API and decreasing for heavy oils. This correlation works well for intermediate viscosity oils. However, heavy crude oils show some departure from the correlation.

IX. Conclusions and Future Work

9.1. Conclusions

Relaxation times and self-diffusion coefficients of pure ethane and propane at elevated pressures and temperatures were measured. The NMR relaxation data are the first for these fluids at elevated pressures and temperatures. The self-diffusion coefficient measurements for ethane and propane are consistent with the literature data. The linear correlations between relaxation time and viscosity/temperature and diffusivity for pure higher alkanes do not apply to pure ethane and propane. Pure ethane and propane depart from the linear correlation of pure higher alkanes due to the spin rotation relaxation mechanism. The inverse relationship between the diffusion coefficient and viscosity/temperature for pure methane, pure higher alkanes, and methane-higher alkane mixtures holds for pure ethane and propane. This result is consistent with the Stokes-Einstein equation.

The estimation based on Equations (3.2.1), (7.1.16), (7.1.18) and (7.1.20) compares closely with experimental results for proton relaxation in ethane. The spin rotation interaction is shown to be the main contribution in gaseous ethane. At liquid densities, intra- and intermolecular dipole-dipole interactions and the spin rotation interaction all have significant contributions.

A mixing rule was developed for multi-component gas mixtures. It was assumed that the gas components relax by the spin rotation interaction in the mixture. The T_1 estimations from the mixing rule and experimental measurements agree with one another for CH_4-CO_2 and CH_4-N_2 gas mixtures.

T_1, and T_2 relaxation times of about 30 crude oils were measured with 2 MHz, 7.5 MHz, and 20 MHz NMR spectrometers. In addition, relaxation times of about ten crude oil samples and one oil-based mud (OBM) base oil were measured by the 20 MHz Bruker NMR spectrometer with variable temperature controller unit over the temperature range 60-100 °C. Light oils have identical T_1 and T_2 relaxation time distributions. However, heavy or asphaltene crude oils have different T_1 and T_2 with the ratio of T_1/T_2 increasing with increasing viscosity, asphaltene content, and Larmor frequency, and free radical content. For heavy oils, apparent T_2 time constants increase and the signal amplitude decreases with increasing echo spacing. Apparent HI of heavy crude oils increases with increasing temperature. With increasing echo spacing, HI of heavy oils decreases.

9.2. Future Work

It is recommended that the 90 MHz NMR system be used to study methane-ethane gas mixtures. Then the mixing rule for gas mixtures can be tested on this mixture. Measurements of ethane-hydrocarbon mixtures are also of interest since some oil reservoirs contain significant amount of ethane. The first type of mixture recommended is the ethane-n-hexadecane mixture since the vapor-liquid equilibrium data of this system is available.

It is useful to integrate the density and viscosity measurement apparatus to the high pressure NMR system. In this way the density and viscosity data can be collected for the systems in addition to NMR data.

It is meaningful to study the effects of temperature and paramagnetic ions on frequency dependency of relaxation times in crude oils systematically. It is also recommended that relaxation times for the mixture of two components with high molecular weight be examined as a function of viscosity and Larmor frequency. This might help find why T_1 of crude oils reached a plateau with increasing viscosity. In addition, relaxation times of OBM base oils and filtrates can be measured at various temperatures and are compared with the data by Kumar et al., which depart from the usual correlation of dead crude oils and pure higher alkanes.

References

Abragam, A., 1961, *The Principles of Nuclear Magnetism*: Oxford University Press, London.

Akkurt, R., Vinegar, H. J., Tutunjian, P. N., and Guillory, A. J., 1996, NMR Logging of Natural Gas Reservoirs: *The Log Analyst*, v. 37, p. 33-42.

Alms, G. R., Bauer, D. R., Brauman, J. I., and Pecora, R., 1973a, Depolarized Rayleigh Scattering and Orientational Relaxation of Molecules in Solution. I. Benzene, Toluene, and para-Xylene: *The Journal of Chemical Physics*, v. 58, p. 5570-5578.

Alms, G. R., Bauer, D. R., Brauman, J. I., and Pecora, R., 1973b, Depolarized Rayleigh Scattering and Orientational Relaxation of Molecules in Solution. II. Chloroform and Nitrobenzene: *The Journal of Chemical Physics*, v. 59, p. 5310-5320.

Alms, G. R., Bauer, D. R., Brauman, J. I., and Pecora, R., 1973c, Depolarized Rayleigh Scattering and Orientational Relaxation of Molecules in Solution. III. Carboxylic Acids: *The Journal of Chemical Physics*, v. 59, p. 5321-5328.

Armstrong, R. L., and Courtney, J. A., 1969, Spin-Lattice Relaxation in Dilute Gases. IV. Proton Relaxation in PH_3: *The Journal of Chemical Physics*, v. 51, p. 457-461.

Armstrong, R. L., and Courtney, J. A., 1972a, A Nuclear Spin Relaxation Study of the Spin-Rotation Interaction in Spherical Top Molecules: *Canadian Journal of Physics*, v. 50, p. 1252-1261.

Armstrong, R. L., and Courtney, J. A., 1972b, A Nuclear Spin Relaxation Study of the Spin-Rotation Interaction in Symmetric Top Molecules: *Canadian Journal of Physics*, v. 50, p. 1262-1272.

Armstrong, R. L., and Hanrahan, T. A. J., 1968, Spin-Lattice Relaxation in Dilute Gases. III. ^{1}H Relaxation in NH_3 and ^{19}F Relaxation in BF_3: *The Journal of Chemical Physics*, v. 49, p. 4777-4780.

Armstrong, R. L., and Tward, E., 1967, Spin-Lattice Relaxation in Dilute Gases. II. ^{19}F Relaxation in CF_4 and SiF_4: *The Journal of Chemical Physics*, v. 48, p. 332-334.

Bartoli, F. J., and Litovitz, T. A., 1972, Raman Scattering: Orientational Motions in Liquids: *The Journal of Chemical Physics*, v. 56, p. 413-425.

Bauer, D. R., Brauman, J. I., and Pecora, R., 1975, Depolarized Rayleigh Scattering and Orientational Relaxation of Molecules in Solution. IV. Mixtures of Hexafluorobenzene with Benzene and with Mesitylene: *The Journal of Chemical Physics*, v. 63, p. 53-59.

Blicharski, J. S., 1963, Spin Rotational Magnetic Relaxation for Nonlinear Molecules: *Acta Physica Polonica*, v. XXIV, p. 817-821.

Bloom, M., 1957, Nuclear Spin Relaxation in Hydrogen I. The Gas: *Physica*, v. 23, p. 237-247.

Bloom, M., Bridges, F., and Hardy, W. N., 1967, Nuclear Spin Relaxation in Gaseous Methane and Its Deuterated Modifications: *Canadian Journal of Physics*, v. 45, p. 3533-3554.

Bovey, L. F. H., 1953, Rotation-Vibration Spectra of Diatomic and Simple Polyatmoic Molecules with Long Absorbing Paths. X. The Spectrum of Tri-Deuteromethane in the Photographic Infrared: *The Journal of Chemical Physics*, v. 21, p. 830-836.

Carnahan, N. F., and Starling, K. E., 1969, Equation of State for Nonattracting Rigid Spheres: *The Journal of Chemical Physics*, v. 51, p. 635-636.

Carr, H., and Purcell, E. M., 1954, Effects of Diffusion on Free Precession in NMR Experiments: *Physical Review*, v. 94, p. 630-638.

Chuah, T. L., 1996, *Estimation of Relaxation Time Distribution for NMR CPMG Measurements*: M.S. thesis, Rice University, Houston.

Courtney, J. A., and Armstrong, R. L., 1970, Spin-Lattice Relaxation in Dilute Gases. V. ^{19}F Relaxation in Fluorine Gas: *The Journal of Chemical Physics*, v. 52, p. 2158-2159.

Cowan, B., 1997, *Nuclear Magnetic Resonance and Relaxation*: Cambridge University Press, New York.

Debye, P., 1929, *Polar Molecules*: The Chemical Catalog Company, Inc., New York.

Deverell, C., 1970, Nuclear Magnetic Relaxation by Spin-Rotation Interaction. Determination of Spin-Rotation Interaction Constants from Nuclear Magnetic Shielding Constants: *Molecular Physics*, v. 18, p. 319-325.

Dong, R. Y., and Bloom, M., 1970, Determination of Spin Rotation Interaction Constants in Fluorinated Methane Molecules by Means Of Nuclear Spin Relaxation Measurements: *Canadian Journal of Physics*, v. 48, p. 793-804.

Dymond, J. H., 1985, Hard-sphere Theories of Transport Properties: *Chemical Society Reviews*, v. 14, p. 317-356.

Eakin, B. E., Starling, K. E., Dolan, J. P., and Ellington, R. T., 1962, Liquid, Gas and Dense Fluid Viscosity of Ethane: *Journal of Chemical and Engineering Data*, v. 7, p. 33-36.

Einstein, A., 1956, *Investigations on the Theory of the Brownian Movement*: Dover Publications, INC., New York.

Etesse, P., 1992, *High Pressure NMR Study of CO_2 and Supercritical CO_2-n-Hexadecane Mixtures*: Ph.D. dissertation, Rice University, Houston.

Evans, G. T., and Kivelson, D., 1986, The Orientational-Correlation Time Intercept in Liquids: *The Journal of Chemical Physics*, v. 84, p. 385-390.

Farrar, T. C., and Becker, E. D., 1971, *Pulse and Fourier Transform NMR Introduction to Theory and Methods*: Academic Press, New York.

Flygare, W. H., 1964, Spin-Rotation Interaction and Magnetic Shielding in Molecules: *The Journal of Chemical Physics*, v. 41, p. 793-800.

Flygare, W. H., and Goodisman, J., 1968, Calculation of Diamagnetic Shielding in Molecules: *The Journal of Chemical Physics*, v. 49, p. 3122-3124.

Freedman, R., Lo, S. W., Flaum, M., Hirasaki, G. J., Matteson, A., and Sezginer, A., 2001, A New NMR Method of Fluid Characterization in Reservoir Rocks: Experimental Confirmation and Simulation Results: *SPE Journal*, December, p. 452-464.

Fukushima, E., and Roeder, A. B. W., 1993, *Experimental Pulse NMR A Nuts and Bolts Approach*: Addison-Wesley Publishing Company, INC., Massachusetts.

Gerritsma, C. J., Oosting, P. H., and Trappeniers, N. J., 1971, Proton-Spin-Lattice Relaxation and Self-Diffusion in Methanes II. Experimental Results for Proton-Spin-Lattice Relaxation Times: *Physica*, v. 51, p. 381-394.

Gordon, R. G., 1966, Kinetic Theory of Nuclear Spin Relaxation in Gases: *The Journal of Chemical Physics*, v. 44, p. 228-234.

Gordon, R. G., 1968, Nuclear Spin Relaxation and Collision Frequency in Dense Gases: *The Journal of Chemical Physics*, v. 48, p. 2655-2657.

Greiner-Schmid, A., Wappmann, S., Has, M., and Lüdemann , H.-D., 1991, Self-Diffusion in the Compressed Fluid Lower Alkanes: Methane, Ethane, and Propane: *The Journal of Chemical Physics*, v. 94, p. 5643-5649.

Harmon, J. F., 1968, *Molecular Motion in Liquid Ethane, An NMR Study*: Ph.D. dissertation, University of Wyoming, Laramie.

Harmon, J. F., and Muller, B. H., 1969, Nuclear Spin Relaxation by Translational Diffusion in Liquid Ethane: *Physical Review*, v. 182, p. 400-410.

Hausser, K. H., and Krüger, G. J., 1965, Frequenzabhängigkeit der Protonenrelaxation in Lösungen organischer Radikale: *Z. Naturforschg*, v. 20a, p. 91-94.

Helbæk, M., Hafskjold, B., Dysthe, D. K., and Sørland, G. H., 1996, Self-Diffusion Coefficients of Methane or Ethane Mixtures with Hydrocarbons at High Pressure by NMR: *Journal of Chemical and Engineering Data*, v. 41, p. 598-603.

Hirota, E., Endo, Y., and Saito, S., 1981, Microwave Spectra of Deuterated Ethanes: Internal Rotation Potential Function and r_z Structure: *Journal of Molecular Spectroscopy*, v. 89, p. 285-295.

Hirschfelder, J. O., Curtiss, C. F., and Bird, R. B., 1954, *Molecular Theory of Gases and Liquids*: John Wiley & Sons, INC., New York.

Hore, P. J., 1995, *Nuclear Magnetic Resonance*: Oxford University Press, New York.

Hu, C., and Zwanzig, R., 1974, Rotational Friction Coefficients for Spheroids with the Slipping Boundary Condition: *The Journal of Chemical Physics*, v. 60, p. 4354-4357.

Huang, C. C., 1997, *Estimation of Rock Properties by NMR Relaxation Methods*: M.S. thesis, Rice University, Houston.

Hubbard, P. S., 1963, Theory of Nuclear Magnetic Relaxation by Spin-Rotational Interactions in Liquids: *Physical Review*, v. 131, p. 1155-1165.

Jacob, J., and Davis, L. A., 1999, The NMR T_2 Response of Crude Oils at Elevated Temperatures, SPE 56797, *in* the 1999 SPE ATCE: Society of Petroleum Engineers.

Jameson, C. J., and Jameson, A. K., 1990, Angular Momentum Relaxation in Binary Collisions. Comparison of Cross Sections: *The Journal of Chemical Physics*, v. 93, p. 3237-3244.

Jameson, C. J., Jameson, A. K., and Smith, N. C., 1987a, [15]N Spin-Relaxation Studies of N_2 in Buffer Gases. Cross Sections for Molecular Reorientation and Rotational Energy Transfer: *The Journal of Chemical Physics*, v. 86, p. 6833-6838.

Jameson, C. J., Jameson, A. K., Smith, N. C., Hwang, J. K., and Zia, T., 1991, ^{13}C and [1]H Spin Relaxation in CH_4 in the Gas Phase: *The Journal of Physical Chemistry*, v. 95, p. 1092-1098.

Jameson, C. J., Jameson, A. K., Smith, N. C., and Jackowski, K., 1987b, Cross Sections for Transfer of Rotational Angular Momentum in CO_2 from [13]C Spin Relaxation Studies in the Gas Phase: *The Journal of Chemical Physics*, v. 86, p. 2717-2722.

Johnson, C. J., JR, and Waugh, J. S., 1961, Nuclear Relaxation in Gases: Mixtures of Methane and Oxygen: *The Journal of Chemical Physics*, v. 35, p. 2020-2024.

Kashaev, S. K. G., Le, B., and Zinyatov, M. Z., 1964, Proton Spin-Lattice Relaxation, Viscosity, and Vibration of Molecules in the Series of n-Paraffins: *Doklady Akademii Nauk SSSR*, v. 157, p. 1438-1440.

Kaski, J., Lantto, P., Vaara, J., and Jokisaari, J., 1998, Experimental and Theoretical *ab Initio* Study of the ^{13}C-^{13}C Spin-Spin Coupling and ^1H and ^{13}C Shielding Tensors in Ethane, Ethene, and Ethyne: *Journal of the American Chemical Society*, v. 120, p. 3993-4005.

Kleinberg, R. L., and Vinegar, H. J., 1996, Nuclear Properties of Reservoir Fluids: *The Log Analyst*, v. 37, p. 20-32.

Kuchitsu, K., 1968, Comparison of Molecular Structures Determined by Electron Diffraction and Spectroscopy. Ethane and Diborane: *The Journal of Chemical Physics*, v. 49, p. 4456-4462.

Kumar, N., Jacob, J., and Davis, L. A., 2000, NMR T_1 and T_2 Relaxation in Oil-Based Mud Filtrates at Reservoir Temperatures, SPE 62852, *in* the 2000 SPE/AAPG Western Regional Meeting: Society of Petroleum Engineers.

Lafferty, W. J., and Plyler, E., 1962, Molecular Parameters of Ethane: *Journal of Chemical Physics*, v. 37, p. 2688-2692.

LaTorraca, G. A., Dunn, K. J., Webber, P. R., and Carlson, R. M., 1998, Low-Field NMR Determinations of the Properties of Heavy Oils and Water-in-Oil Emulsions: *Magnetic Resonance Imaging*, v. 16, p. 659-662.

LaTorraca, G. A., Stonard, S. W., Webber, P. R., Carlson, R. M., and Dunn, K. J., 1999, Heavy Oil Viscosity Determination Using NMR Logs, *in* 40th Annual Logging Symposium: Society of Professional Well Log Analysts.

Lo, S. W., 1999, *Correlations of NMR Relaxation Time with Viscosity/Temperature, Diffusion Coefficient and Gas/Oil Ratio of Methane-Hydrocarbon Mixtures*: Ph.D. dissertation, Rice University, Houston.

Lo, S. W., Hirasaki, G. J., House, W. V., and Kobayashi, R., 2000, Mixing Rules and Correlations of NMR Relaxation Time with Viscosity, Diffusivity, and Gas/Oil Ratio of Methane/Hydrocarbon Mixtures, SPE 63217, *in* the 2000 SPE ATCE: Society of Petroleum Engineers.

Maitland, G. C., Rigby, M., Smith, E. B., and Wakeham, W. A., 1981, *Intermolecular Forces Their Origin and Determination*: Clarendon Press, Oxford.

McCann, K. E., Vinegar, A., and Hirasaki, G. J., 1999, NMR Analysis of Crude Oil and Pure Hydrocarbon Fluids, (private communication).

McClung, R. E. D., 1972, Rotational Diffusion of Symmetric Top Molecules in Liquids: *Journal of Chemical Physics*, v. 57, p. 5478-5491.

McClung, R. E. D., and Kivelson, D., 1968, ESR Linewidths in Solution. V. Studies of Spin-Rotational Effects Not Described by Rotational Diffusion Theory: *The Journal of Chemical Physics*, v. 49, p. 3380-3391.

McConnell, J., 1980, *Rotational Brownian Motion and Dielectric Theory*: Academic Press, New York.

McConnell, J., 1987, *The Theory of Nuclear Magnetic Relaxation in Liquids*: Cambridge University Press, New York.

Mirotchnik, K. D., Allsopp, K., and Kantzas, A., 1999, Low Field NMR-Tool for Bitumen Sands Characterization: A New Approach, *in* the 1999 SPE ATCE: Society of Petroleum Engineers.

Moniz, W. B., Steele, W. A., and Dixon, J. A., 1963, Nuclear Spin Relaxation in Liquids. Spheroidal Molecules: *The Journal of Chemical Physics*, v. 38, p. 2418-2426.

Montanari, L., Clericuzio, M., Del Piero, G., and Scotti, R., 1998, Asphaltene Radicals and Their Interaction with Molecular Oxygen: an EPR Probe of Their Molecular Characteristics and Tendency to Aggregate: *Applied Magnetic Resonance*, v. 14, p. 81-100.

Morriss, C. E., Freedman, R., Straley, C., Johnston, M., Vinegar, H. J., and Tutunjian, P. N., 1997, Hydrocarbon Saturation and Viscosity Estimation from NMR Logging in the Belridge Diatomite: *The Log Analyst*, v. 38, p. 44-59.

Mujica, V., Nieto, P., Puerta, L., and Acevedo, S., 2000, Caging of Molecules by Asphaltenes. A Model for Free Radical Preservation in Crude Oils: *Energy &Fuels*, v. 14, p. 632-639.

Muller, B. H., 1966, Comment on The Articles: "Nuclear Magnetic Relaxation by Intermolecular Dipole-Dipole Interactions", and "Nuclear Spin Relaxation in Liquid and Solid Methane: Isotope Effects": *Canadian Journal of Physics*, v. 44, p. 2511-2513.

Muller, B. H., and Noble, J. D., 1963, Proton Spin-Lattice Relaxation in Pure Liquid Ethane and Some of Its Deuterated Modifications: *The Journal of Chemical Physics*, v. 38, p. 777-779.

Müller-Warmuth, W., and Printz, V., 1966, Kernrelaxation und Molekülbewegungen in Lösungen freier Radikale: *Z. Naturforschg*, v. 21a, p. 1849-1856.

NIST, 1999, *NIST Thermophysical Properties of Hydrocarbon Mixtures Database (SUPERTRAPP)*, National Institute of Standards and Technology.

Oosting, P. H., and Trappeniers, N. J., 1971, Proton-Spin-Lattice Relaxation and Self-Diffusion in Methanes III. Interpretation of Proton Spin Lattice Relaxation Experiments: *Physica*, v. 51, p. 395-417.

Rajan, S., and Lalita, K., 1974, Nuclear Spin-Lattice Relaxation in CH_4-Inert Gas Mixtures: *Journal of Magnetic Resonance*, v. 1974, p. 115-129.

Rajan, S., and Lalita, K., 1975, Intermolecular Potentials from NMR Data: I. CH_4-N_2 and CH_4-CO_2: *Canadian Journal of Physics*, v. 53, p. 1624-1630.

Rigny, P., and Virlet, J., 1967, Molecular Motion and ^{19}F Relaxation in the Liquid Hexafluorides of Molybdenum, Tungsten, and Uranium: *The Journal of Chemical Physics*, v. 47, p. 4645-4652.

Schwartz, R. N., Jones, L. L., and Bowman, M. K., 1979, Electron Spin-Echo Studies of Nitroxide Free Radicals in Liquids: *The Journal of Physical Chemistry*, v. 83, p. 3429-3434.

Sheu, E. Y., and Mullins, O. C., 1995, Asphaltenes: Fundamentals and Aplications: Plenum Press, New York.

Starling, K. E., Eakin, B. E., and Ellington, R. T., 1960, Liquid, Gas and Dense-Fluid Viscosity of Propane: *A.I.Ch.E. Journal*, v. 6, p. 438-442.

Straley, C., Rossini, D., Vinegar, A., Tutunjian, P. N., and Morriss, C. E., 1997, Core Analysis by Low-Field NMR: *The Log Analyst*, v. 38, p. 84-94.

Tanner, J. E., and Stejskal, E. O., 1968, Restricted Self-Diffusion of Protons in Colloidal Systems by the Pulsed-Gradient Spin-Echo Method: *The Journal of Chemical Physics*, v. 49, p. 1768-1777.

Tward, E., and Armstrong, R. L., 1967, Spin-Lattice Relaxation in Dilute Gases. I. Proton Relaxation in HCl, HBr, and HI: *The Journal of Chemical Physics*, v. 47, p. 4068-4071.

Vinegar, H. J., Tutunjian, P. N., Edelstein, W. A., and Roemer, P. B., 1991, Whole Core Analysis by ^{13}C NMR: *SPE Formation Evaluation*, June, p. 183-189.

Wang, C. H., 1973, Anisotropic-Rotational Diffusion Model Calculation of T_1 Due to Spin-Rotation Interaction in Liquids: *Journal of Magnetic Resonance*, v. 9, p. 75-83.

Whittenburg, S. L., Evilia, R. F., and Robert, J. R., 1992, Studies of Rotational Relaxation Times at Low Viscosity: Ethane: *Journal of Molecular Liquids*, v. 51, p. 115-122.

Woessner, D. E., Snowden, B. S., JR., George, R. A., and Melrose, J. C., 1969, Dense Gas Diffusion Coefficients for the Methane-Propane System: *I & EC Fundamentals*, v. 8, p. 779-786.

Yi, P. N., Ozier, I., and Ramsey, N. F., 1971, Low-Field Hyperfine Spectrum of CH_4: *The Journal of Chemical Physics*, v. 55, p. 5215-5227.

Zega, J. A., 1987, *Spin-Lattice Relaxation in Pure and Mixed Alkanes and Their Correlation with Thermodynamic and Macroscopic Transport Properties*: M.S. thesis, Rice University, Houston.

Zega, J. A., 1990, *Spin-Lattice Relaxation in Normal Alkanes at Elevated Pressures*: Ph.D. dissertation, Rice University, Houston.

Appendix

For CH_4 with CH_4, CO_2, N_2, He, Ne, and Ar, the collision cross sections can also be obtained from the literature. In general, the collision cross section for angular momentum transfer can be reasonably expressed as a power law (Jameson et al., 1991; Rajan and Lalita, 1975a, b),

$$\sigma_j = \sigma_j(300K)\left(\frac{T}{300}\right)^p .$$

(A.1)

The cross sections for the collisions of CH_4 with CH_4, CO_2, N_2, He, Ne and Ar were listed in Table A.1. In particular, cross sections for angular momentum transfer for CH_4-He and CH_4-Ne pairs are estimated by fitting the data from NMR measurements (Rajan and Lalita, 1974) in the form of Equation (A.1). Figures A.1 and A.2 are the plots. The temperature dependence of the collision cross sections is close to T^1 for CH_4 with CH_4, CO_2, N_2, and Ar. However, the temperature dependence of the collision cross sections is significantly different from T^1 for CH_4 with He and Ne. In particular, the CH_4-He collision pair has the positive value for p. Based on the data in Table A.1, the assumption made about the collision cross sections in Equation (7.2.9) is found to be reasonable for the gas mixtures of CH_4, C_2H_6, C_3H_8, CO_2, and N_2.

Using Equations (7.1.1) and (7.2.4) as well as the data from Table A.1, proton relaxation times of five CH_4 gas mixtures were estimated. Figures A.3-A.7 compared the estimated results with experimental results (Rajan and Lalita, 1974; Rajan and Lalita, 1975a) for CH_4-CO_2, CH_4-N_2, CH_4-He, CH_4-Ne and CH_4-Ar gas mixtures respectively. The estimated results compare quite closely with experimental results. For the CH_4-CO_2 gas mixture, the prediction using the collision cross section data from Table A.1 falls on

the straight line of pure methane at various temperatures. This is because the coefficient

G_{ij} for the CH$_4$-CO$_2$ system calculated from the collision cross section data in Table A.1

is very close to the coefficient G_{ij} for pure methane from the experimental data.

Table A.1 Cross sections for angular momentum transfer for CH$_4$ molecules with various collision partners

Pair	$\sigma_J(T)$ (Å^2)	Reference
CH$_4$-CH$_4$	$18.4(T/300)^{-0.90}$	(Jameson et al., 1991)
CH$_4$-CO$_2$	$24.1(T/300)^{-0.98}$	(Jameson et al., 1991)
CH$_4$-N$_2$	$16.3(T/300)^{-0.87}$	(Jameson et al., 1991)
CH$_4$-He	$4.48(T/300)^{+0.23}$	This work
CH$_4$-Ne	$10.1(T/300)^{-0.55}$	This work
CH$_4$-Ar	$14.4(T/300)^{-0.79}$	(Jameson et al., 1991)
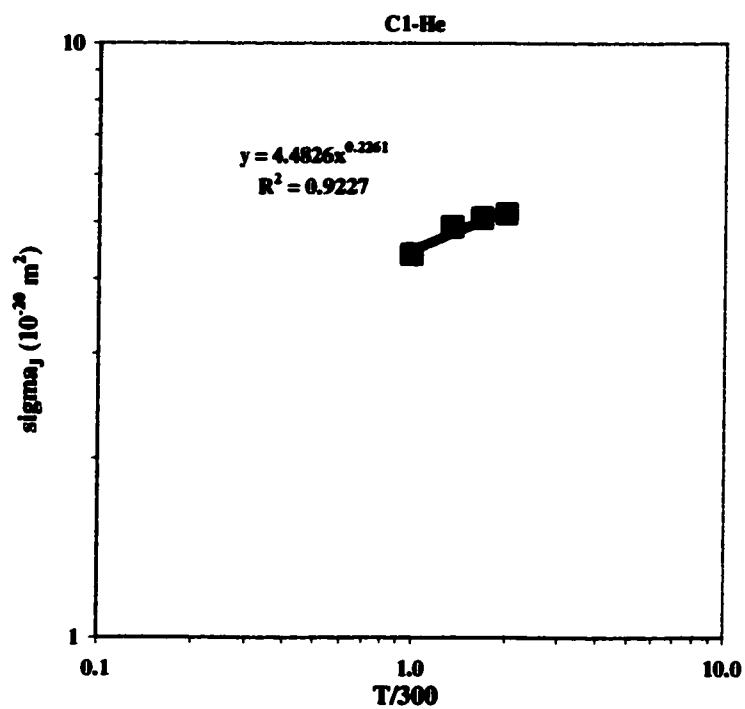
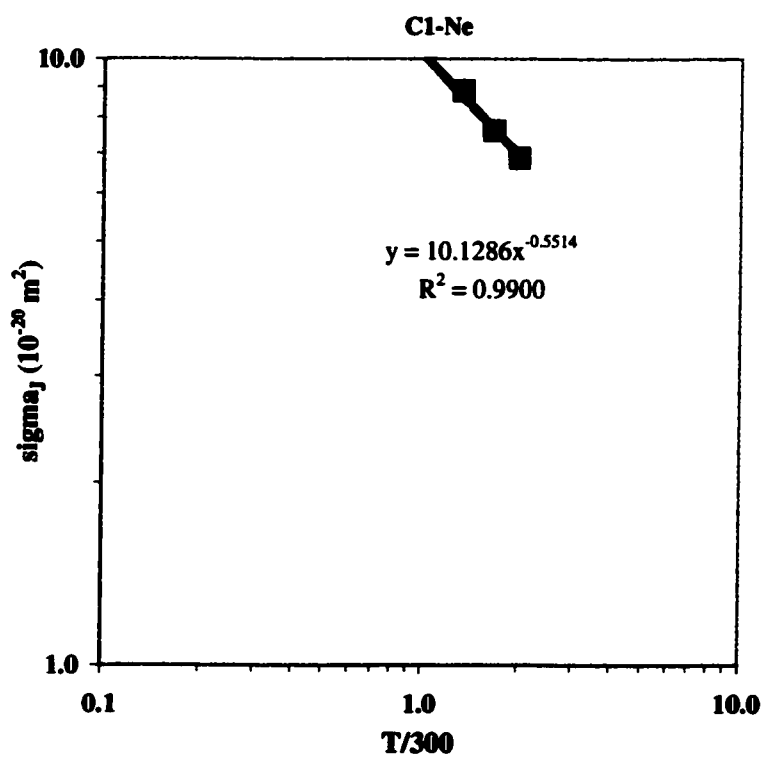Figure A.1 Correlation of cross section for angular momentum transfer by collisions for CH_4-He

Figure A.2 Correlation of cross section for angular momentum transfer by collisions for CH_4-Ne
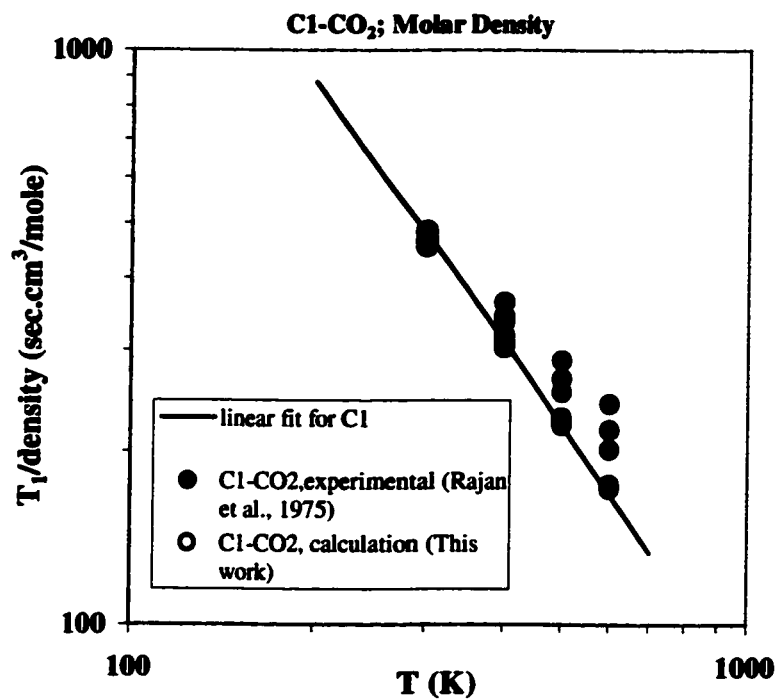
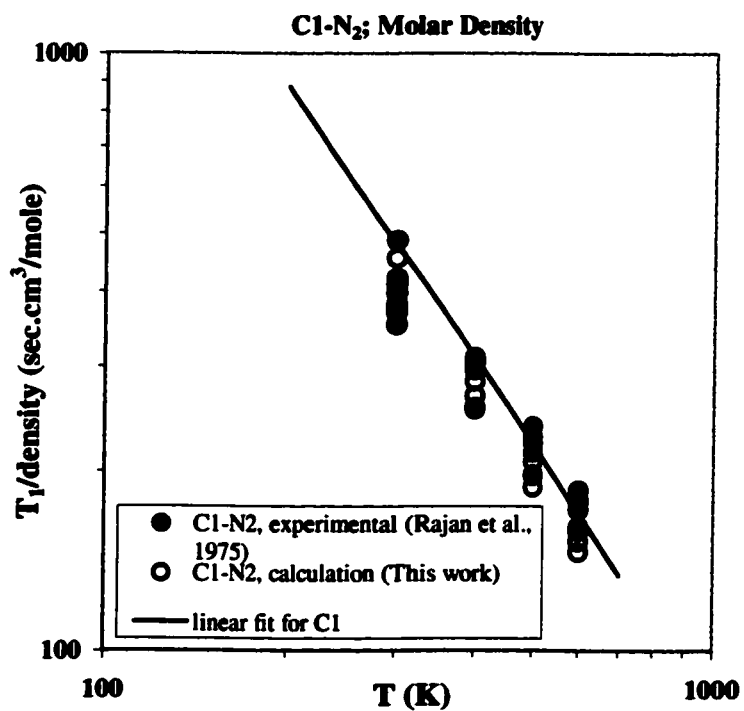Figure A.3 Comparison of experimental results and calculated results for CH4-CO2

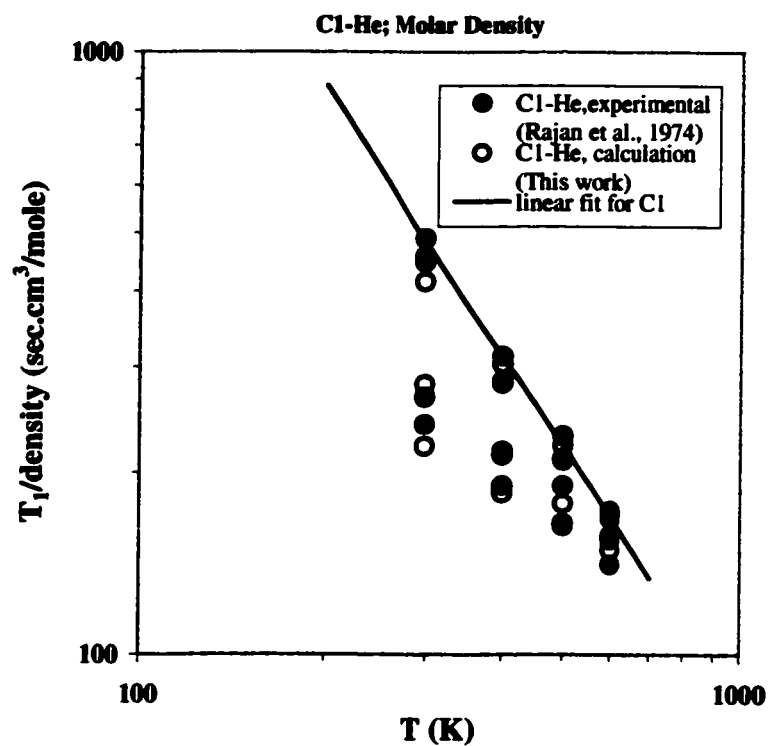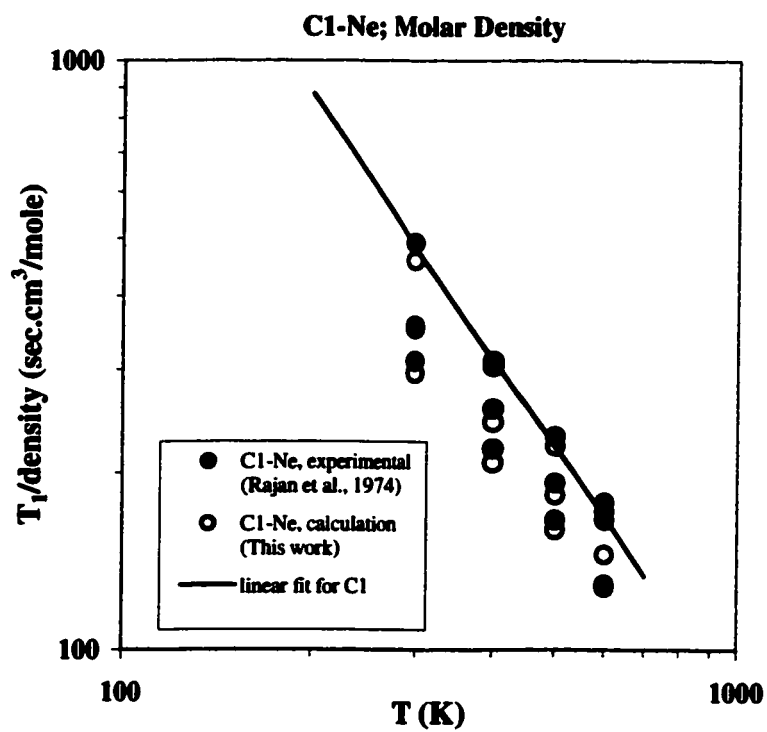Figure A.4 Comparison of experimental results and calculated results for CH4-N2

Figure A.5 Comparison of experimental results and calculated results for CH_4-He

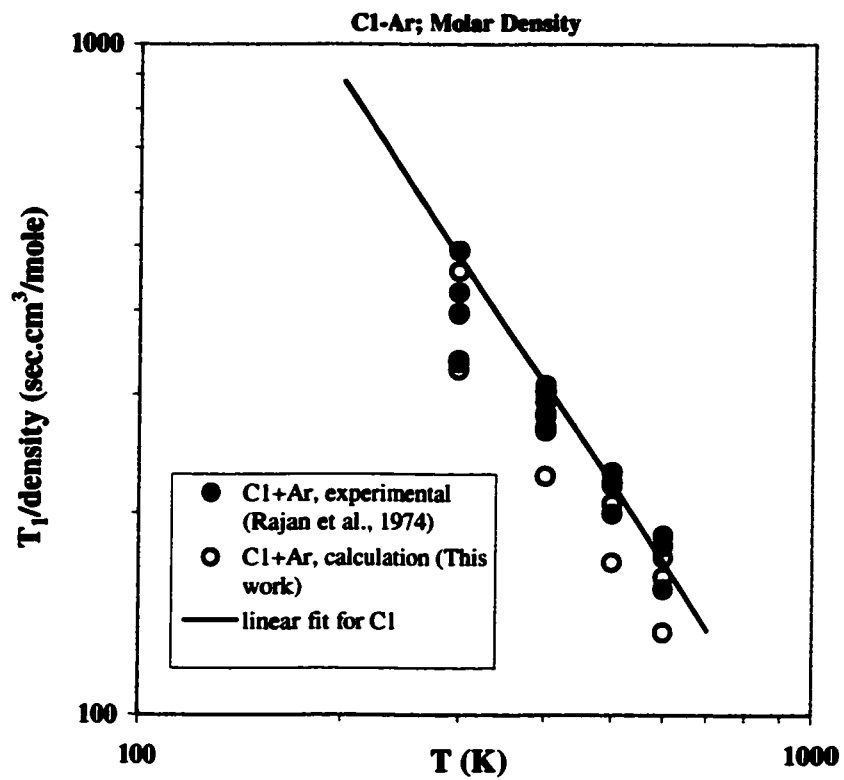Figure A.6 Comparison of experimental results and calculated results for CH_4-Ne

Figure A.7 Comparison of experimental results and calculated results for CH_4-Ar